Low-Level Mesoscale Wind Field Generation from Cloud Track Winds Using GOES-8 Imagery

by
Mark O. Yeisley

Department of Atmospheric Science
Colorado State University
Fort Collins, Colorado

Colorado State University

Department of Atmospheric Science

Paper No. 622

LOW-LEVEL MESOSCALE WIND FIELD GENERATION FROM CLOUD-TRACK WINGS USING GOES-8 IMAGERY

Submitted by

Mark O. Yeisley

Department of Atmospheric Sciences

Spring 1996

ABSTRACT OF THESIS

LOW-LEVEL MESOSCALE WIND FIELD GENERATION FROM CLOUD-TRACK WINDS DERIVED USING GOES-8 IMAGERY

During the period 4-31 May 1995 special imagery sequences were captured using the GOES-8 geostationary satellite in support of VORTEX (Verifications of the Origin of Rotation in Tornadoes EXperiment) and DoD-sponsored Geosciences projects. These image sets covered the American midwest and Gulf coast states, and consisted of visible image data of temporal intervals varying from one to thirty minutes.

Low-level wind fields derived from satellite-tracked cumulus velocities have been generated for more than two decades. Studies have shown that cumulus turrets with 0.5 to 3 km horizontal dimensions are of the correct size to best infer winds within the subcloud layer (Fujita and Pearl, 1973). Previous studies have been restricted by the temporal and spatial resolution of the observing platform, with minimum time intervals of 3-5 minutes used to track cumulus targets. "Rapidscan" or one-minute interval imagery is currently available from GOES-8 during specially scheduled events. The McIDAS (Man-computer Interactive Data Access System: Suomi, 1983) was used to navigate image sets and track small-scale cumulus in areas of weakly forced flow and near regions of dynamic mesoscale activity. Wind fields were derived using image intervals of one, five, fifteen, and thirty minutes.

Wind fields derived using each interval type are compared with each other and with surface observing platforms (National Weather Service observing sites, profiler stations). Winds derived using five-minute image intervals are found to be most representative of flow at cloud base. The use of rapidscan image data greatly improves target

continuity when manually tracking clouds; using five minutes of rapidscan imagery to follow a cloud element produces the most accurate wind vector describing cloud movement within that five-minute period.

Two techniques are used to infer mesoscale convergence/divergence fields from wind fields derived using five and fifteen minute interval imagery. Low-level convergence is computed along the length of an outflow boundary in central Texas using a McIDAS algorithm. Resulting values suggested convergence-enhanced convection would occur in a localized section of the boundary; images taken over the next several hours confirms this. Similar results were obtained using an irregular polygon method to compute low-level convergence in the vicinity of the thunderstorm.

ACKNOWLEDGEMENTS

This research was supported by Task 4 of the Department of Defense Geosciences, project, funded under DoD grant AAH04-94-G-0402.

TABLE OF CONTENTS

LIST OF FIGURES

1.0 Introduction

The launch of a new geosynchronous satellite in the mid-1960's (ATS-1) first enabled scientists to continuously observe atmospheric motions over areas where traditional data collection was either sparse or unavailable. Satellite imagery has since been used to track cloud motions and construct wind fields, especially at upper levels, enhancing model initialization processes and providing valuable wind information to pilots and other users. The accuracy of these wind fields is a function of satellite spatial/temporal resolution, accurate image navigation and registration, precise cloud height determination, and cloud tracking technique. Development of better satellites over the past three decades has made this process very reliable for upper-level wind field generation, where clouds are generally long-lived and stable.

Accurate low-level wind fields have proven more difficult to generate; the relatively short life span and small size of cumulus clouds that best infer low-level winds make it more difficult to accurately track them. But imagery sensors have improved over time, allowing greater resolution and enabling users to observe movements of individual thunderstorm cells, such as was possible on the Synchronous Meteorological and Geostationary Operational Environmental Satellites (SMS/GOES), which began service in 1974.

In May 1994 the National Atmospheric and Oceanic Administration (NOAA) launched GOES-8, the first in a series of next-generation satellites designed to provide both improved observational capabilities

and more reliable satellite platform characteristics. This new system combines better resolution with more accurate navigation, registration, and temperature determination, allowing more precise identification and tracking of small-scale cumuliform clouds. Improved temporal resolution (as short as one minute between consecutive images) should improve the ability to track individual cloud elements, allowing more accurate generation of low-level wind fields.

This study of low-level mesoscale wind field generation was conducted using visible imagery data from GOES-8 at varying temporal intervals, from 30 minutes to the highest frequency satellite data available at this time, one-minute rapidscan data. These data were recorded during May 1995 as part of VORTEX and Geoscience experiments conducted by NOAA/NESDIS (National Environmental Satellite Data and Information Service) as well as other organizations. The purpose of this thesis is threefold: to determine the effectiveness of GOES-8 imagery in generating mesoscale cloud-track wind fields in areas of both strongly- and weakly-forced flows, to better understand how cumulus level motion corresponds to surface and boundary layer flows, and to research the effectiveness of low-level cloud-track winds using GOES-8 imagery as a forecasting tool.

The cases chosen for this thesis occurred in three general areas: Texas, central Oklahoma, and Louisiana. Each case involved events both mesoscale and synoptic in nature, producing high winds, hail and/or tornadoes. Thunderstorm outflows were tracked, as were flow fields outside the thunderstorm influence region. These events were selected for two reasons: the availability of differing temporal interval imagery captured and the inclusion of rapidscan imagery in the data sets.

Individual cumulus cloud elements showing little vertical development over the course of each imagery sequence were identified and heights determined using several techniques to ensure proper target identification. Imagery was renavigated when necessary (except in the Louisiana case) such that subsequent images in a sequence lined up as precisely as possible with a chosen baseline image; errors due to faulty satellite navigation were then eliminated to the greatest extent possible. Clouds were tracked using visible imagery at intervals of thirty, fifteen, five, and one minute; wind fields were then generated using each of these interval types. Tracking was accomplished using the WIND program on the Man-computer Interactive Data Access System (McIDAS, Suomi et al., 1983) terminal.

Because each event had a wide range of temporal coverage, a comparison study was possible showing error differences among wind fields generated using differing time interval imagery. A comparison of the accuracy of the derived wind fields with surface-based observations versus profiler data is also presented. Areas of convergence/divergence are plotted using both an irregular trapezoid method and McIDAS wind vector differencing scheme. Limitations involved with winds generated using each interval type are discussed. Opportunities for further research are also presented.

2.0 CASE STUDIES

2.1 Synoptic Situation, 04 May 1995

Figure 2-1 shows the surface analysis at 18Z (1300 LST). A weak longwave trough extended over much of the central U.S throughout the day with the interest area just south of the right entrance region of a weak jet streak aloft at 200 and 300mb. This trough was also evident at 850mb, and kept winds at this level generally southwesterly over Louisiana (see Figure 2-2).

On the surface at 00Z a weak warm frontal boundary had extended from central Texas into southern Louisiana, at which time the boundary became more of a weak stationary front. Surface circulation brought warm moist air into the region, keeping skies overcast. Fog formed in the early morning hours throughout most of the interest area, keeping temperatures in the low 70's until daytime heating broke through the inversion and convection began.

As the day progressed a weak surface trough moved into western Louisiana, interacting with the stationary front and triggering convective activity along the northern edge of the Louisiana boot. The first storms appeared NNW of Baton Rouge at approximately 16Z, moving easterly along the frontal boundary as new storms continue to form NNW of Baton Rouge near the interaction of the surface trough and the frontal boundary. Figure 2-3 shows surface observations of wind at 19Z; with the exception of New Orleans all stations in southern LA reported southwesterly surface flow.

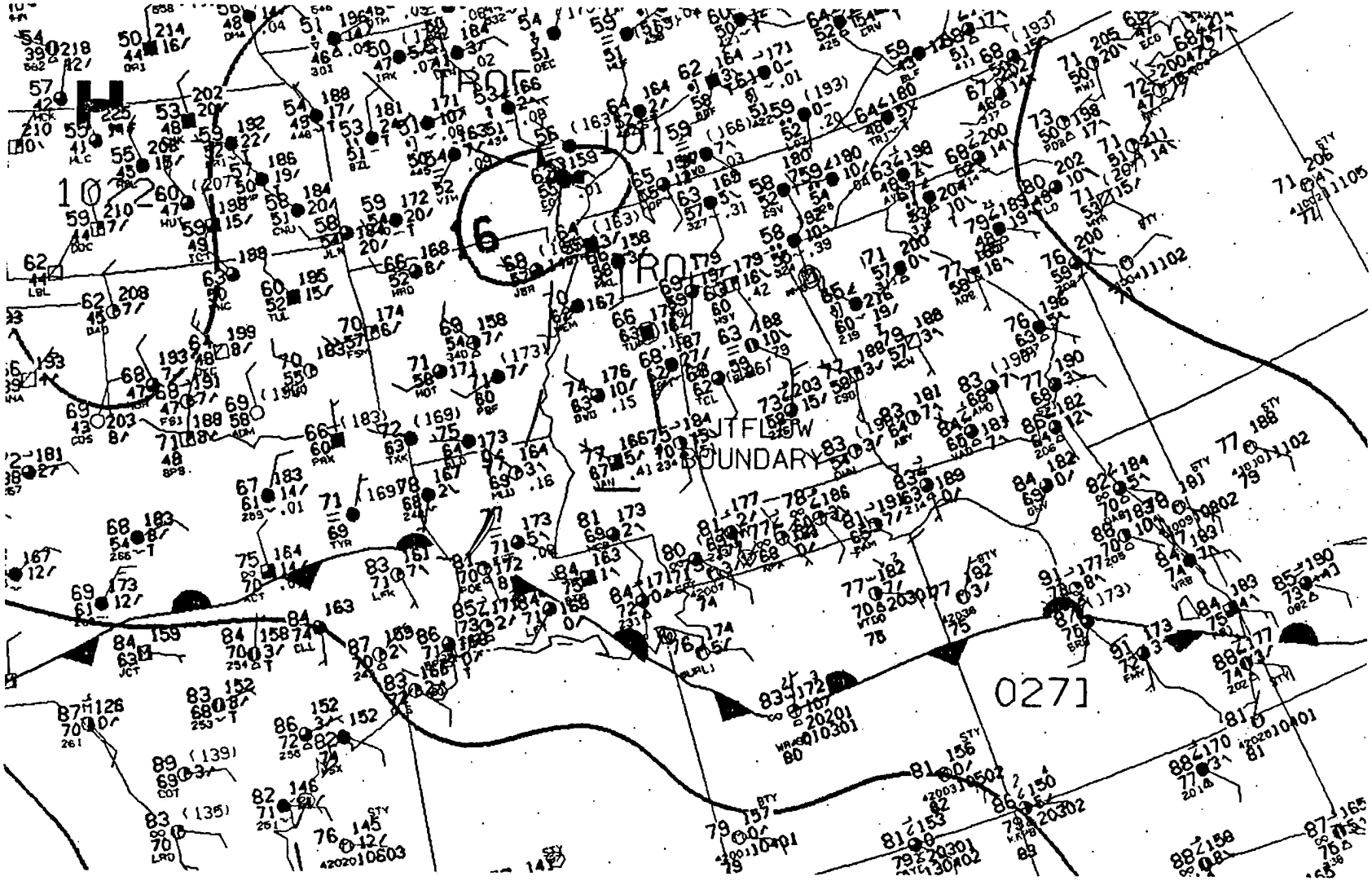

Figure 2-1 NMC surface analysis, 4 May 1995 1800Z.

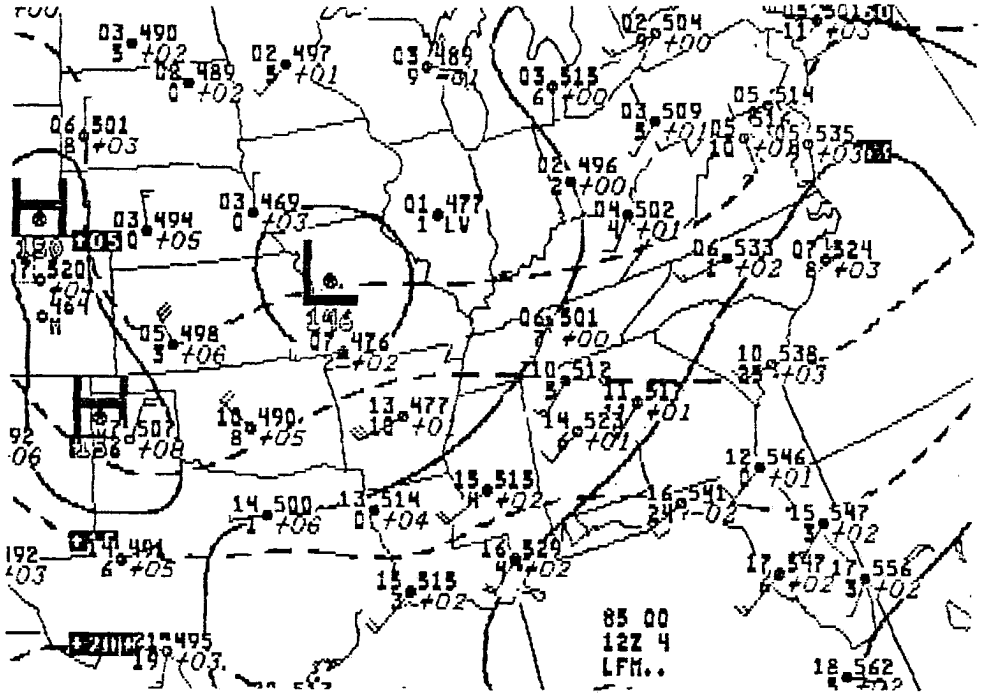

Figure 2-2 NMC 850 mb analysis, 4 May 1995 1200Z.

Figure 2-3 Surface wind observations, 4 May 1995 1900Z.

2.2 Synoptic situation, 17 May 1995

As the day began a longwave trough was situated over the four corners area of the southwestern U.S., extending into Mexico and apparent at all levels including 700 mb. A relatively weak cold frontal boundary was moving into northern Kansas, and a mesoscale surface low was located over the northwest corner of Texas with a weak trough extending southward. By 12Z the front had moved into northern Oklahoma while the low had tracked across the Texas panhandle to the Oklahoma border. Showers were triggered along the frontal boundary, and thunderstorms developed across much of northern Oklahoma. The low continued to track eastward, and by 18Z was interacting with the cold front, which had become quasi-stationary (See Figure 2-4). Most low-level features visible from satellite were obscured during this period by mid-level cloud and developing cirrus shields.

Figure 2-5 shows the surface analysis at 21Z (1600 LST). The low over southern Oklahoma has moved to the panhandle and deepened, while a dryline has pushed into eastern Oklahoma. Winds at the 850 mb level at 12Z were southwesterly and strong at 65 kts (Figure 2-6). Surface winds behind the dryline in southeastern Oklahoma were also southwesterly, as seen in Figure 2-7.

Winds for this case were derived in and around the Oklahoma City area, where low-level cumuli were moving rapidly to the northeast. Both surface observations from OKC and wind profiler data from Purcell, OK (approximately 30 km south of Oklahoma City) were available and were used for validation purposes.

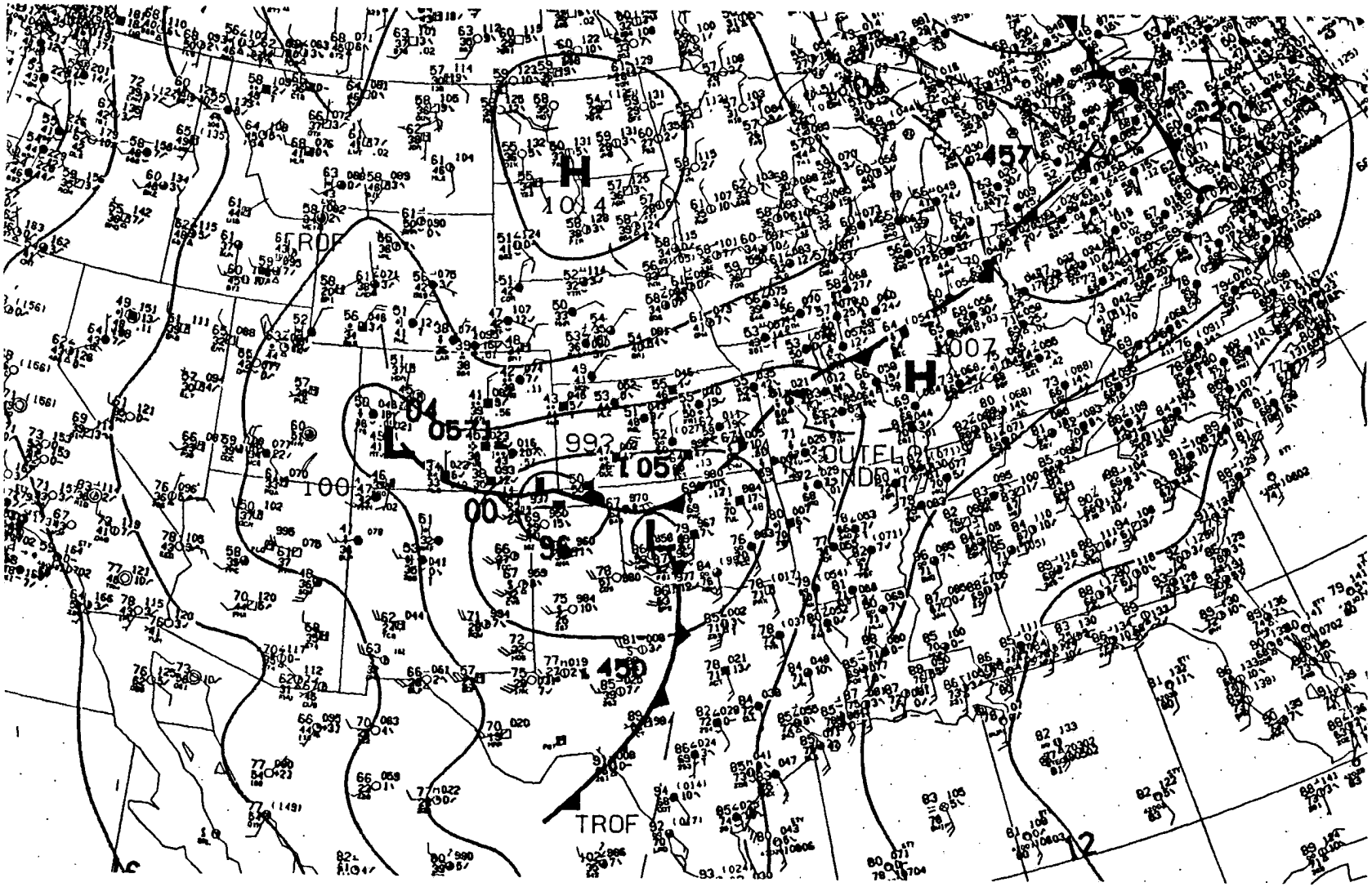

Figure 2-4 NMC surface analysis, 17 May 1995 1800Z.

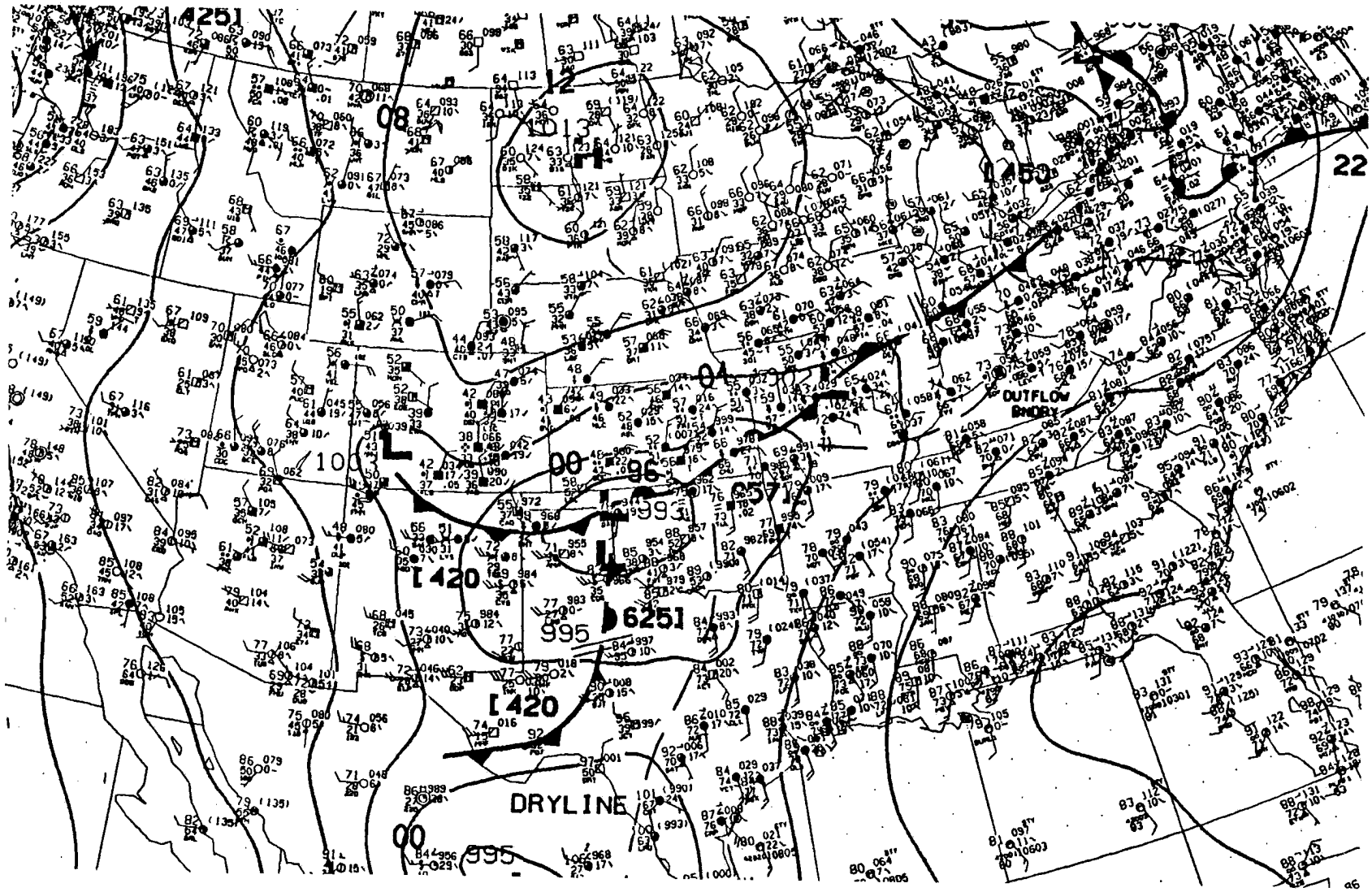

Figure 2-5 NMC surface analysis, 17 May 1995 2100Z.

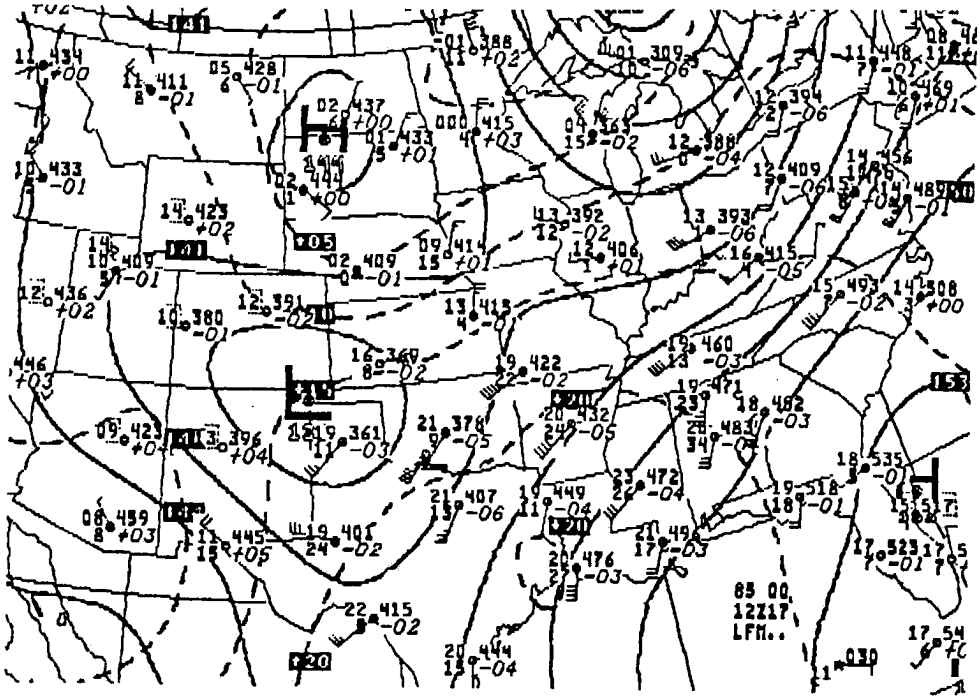

Figure 2-6 NMC 850 mb analysis, 17 May 1995 1200Z.

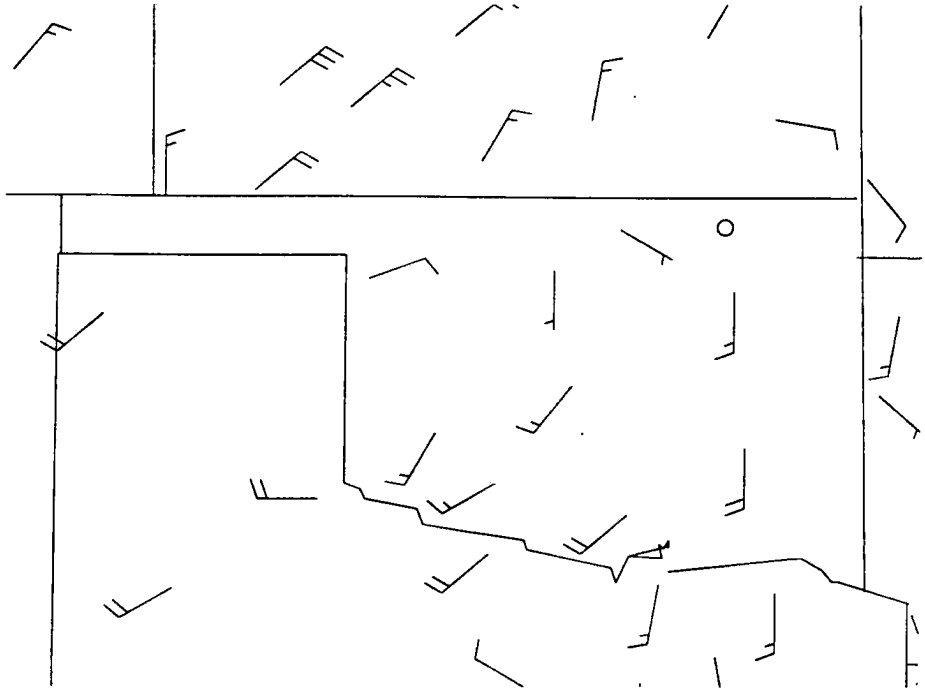

Figure 2-7 Surface wind observations, 17 May 1995 2000Z.

2.3 Synoptic situation, 23 May 1995

A longwave trough was situated over the southwestern U.S., extending southward from central New Mexico. At 12Z a surface low was located over the Oklahoma panhandle, with a cold front extending to the southwest. Surface flow was southerly over the entire Texas region, bringing moist air into contact with both the frontal zone and a fairly intense dryline extending from southeastern Utah into Mexico. Upper level flow over north central Texas was southwesterly at midlevels, then westerly near 300mb.

As the day progressed, the low tracked eastward and by 18Z was located north of Ft. Sill, Oklahoma (See Figure 2-8). The front had just passed Childress, Texas by this time and strong convection was being triggered along the frontal zone. Radar began detecting significant development as early as 1035Z, and by late afternoon a weather watch was put into effect. The thunderstorm studied in this case formed near Guthrie, Texas at approximately 20Z. As the storm moved northeast it created an outflow boundary along its trailing edge. The boundary propagated rapidly to the southeast at speeds reaching 50 knots. This outflow was able to be tracked for approximately thirty-five minutes, until it was obscured by a dense cirrus shield from a thunderstorm to the south.

For verification purposes, winds were also tracked around the Ft. Worth area at 20Z, as well as over the Palestine, Texas profiler located 200 km southeast of Ft. Worth. The flow in both of these areas was part of the same southerly flow field which extended throughout most of southeastern Texas. Figure 2-9 shows southerly flow was also present at 850 mb; 20Z surface observations are shown in Figure 2-10.

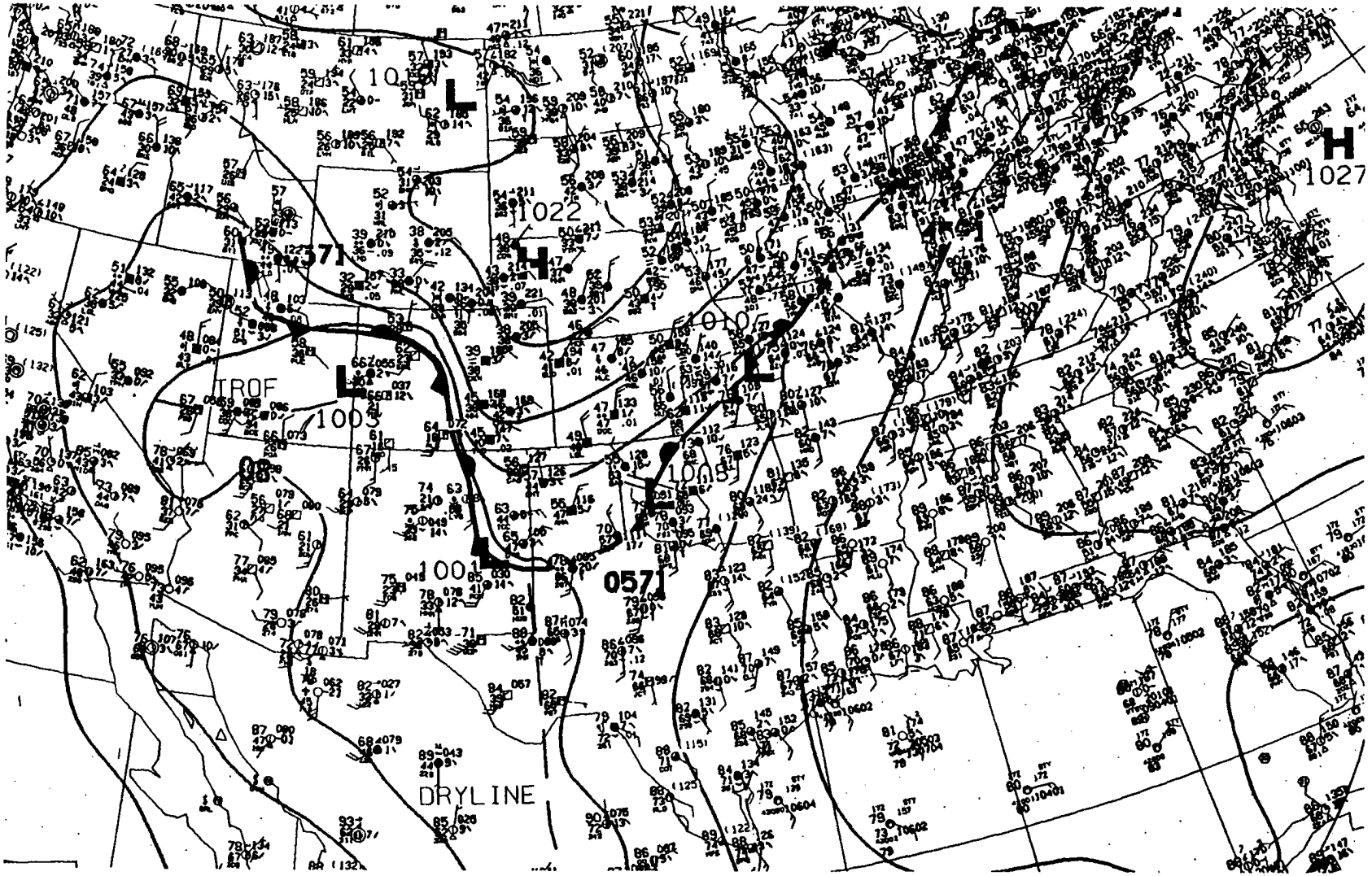

Figure 2-8 NMC surface analysis, 23 May 1995 1800Z.

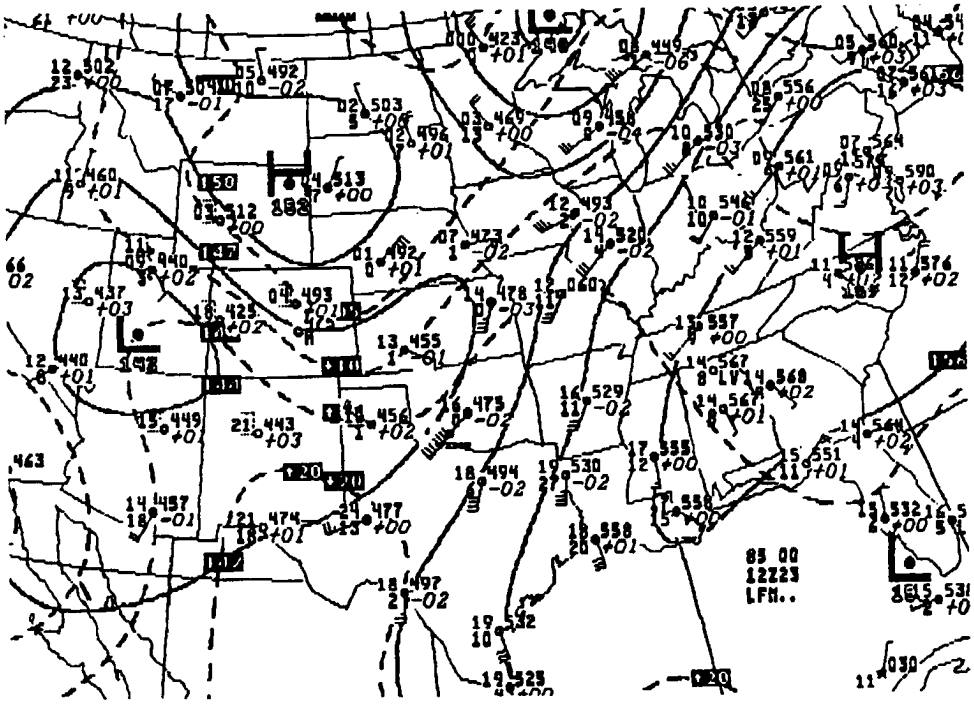

Figure 2-9 NMC 850 mb analysis, 23 May 1995 1200Z.

Figure 2-10 Surface wind observations, 23 May 1995 2000Z.

2.4 Synoptic situation, 31 May 1995

At 18Z a weak stationary front was located north of the Texas border with Oklahoma. A weak surface low over the northwest Texas panhandle was at the northern end of an intense dryline that extended southward into Mexico (See Figure 2-11). An upper-level low was located over Nebraska with a moderate trough extending southward. Surface flow was generally southeasterly throughout central Texas, becoming more westerly with height. Winds were generally weak to moderate at all levels above the region, a maximum of 40 kts is indicated on Figure 2-12 at 850mb. Between 18-19Z a large thunderstorm formed in north central Texas and traveled eastward to the Dallas area, generating hail and producing a large outflow boundary. It is along this boundary that a series of outflow interactions take place, including one thunderstorm that produced a tornado near Abilene.

Winds were tracked for this case along the southern edge of the old outflow boundary in the warm sector. Winds were also plotted to the immediate west and south of the Abilene thunderstorm. No vectors were possible along the boundary's northern edge; strong subsidence prevented the development of small cumulus that could be used as targets. Surface winds were erratic over central Texas as indicated in Figure 2-13, but flow to the south of the boundary was roughly southerly in nature. No surface reporting stations were within the region just south of the boundary. Observations at San Angelo (SJT), located approximately 100km south of the boundary, were used for comparison with winds plotted in that vicinity. Profiler data from Jayton, TX was unusable as the storm was located directly above the profiler during this period and no winds representative of the flow to the south of the storm are available.

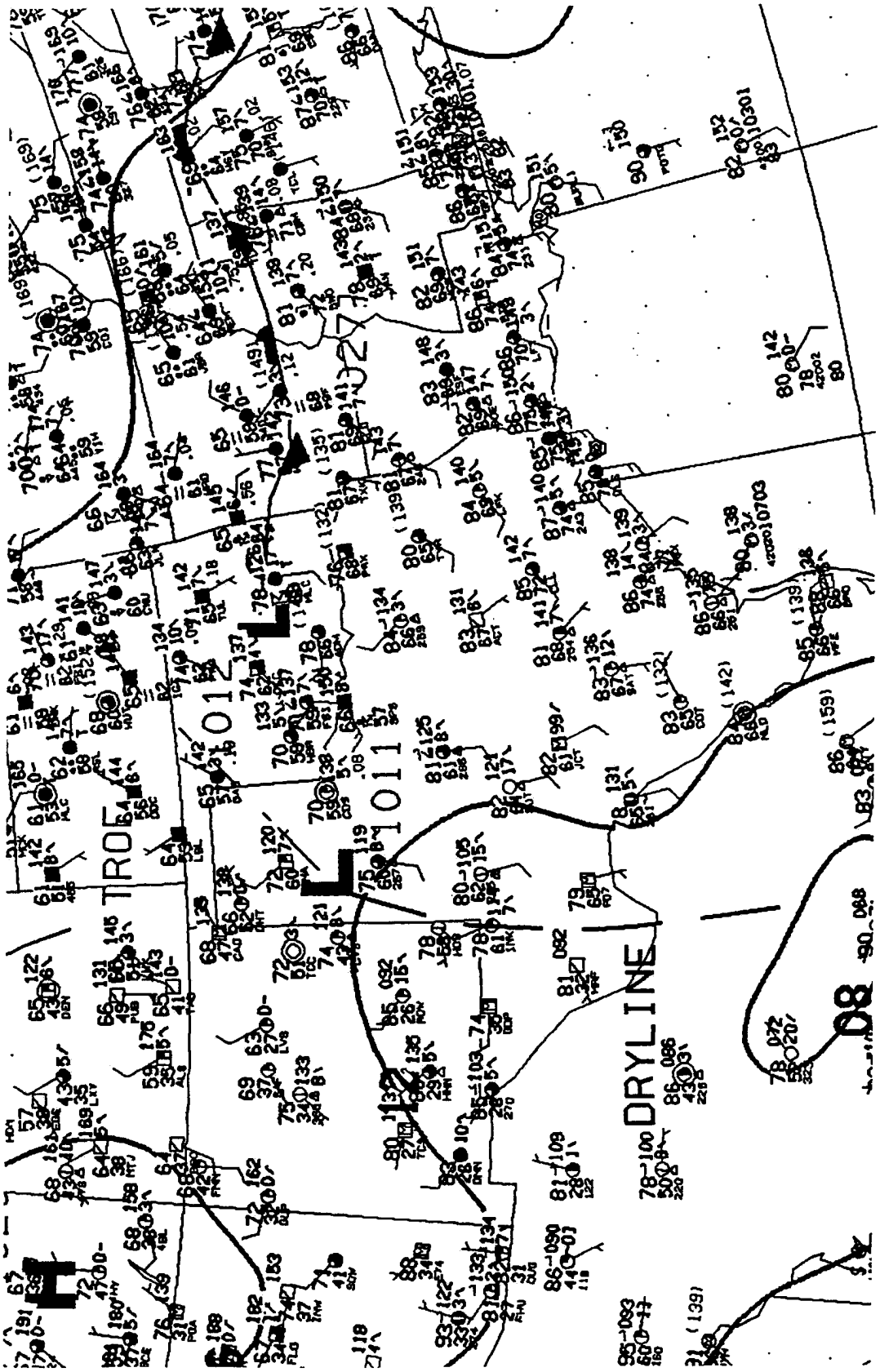

Figure 2-11 NMC surface analysis, 31 May 1995 1800Z.

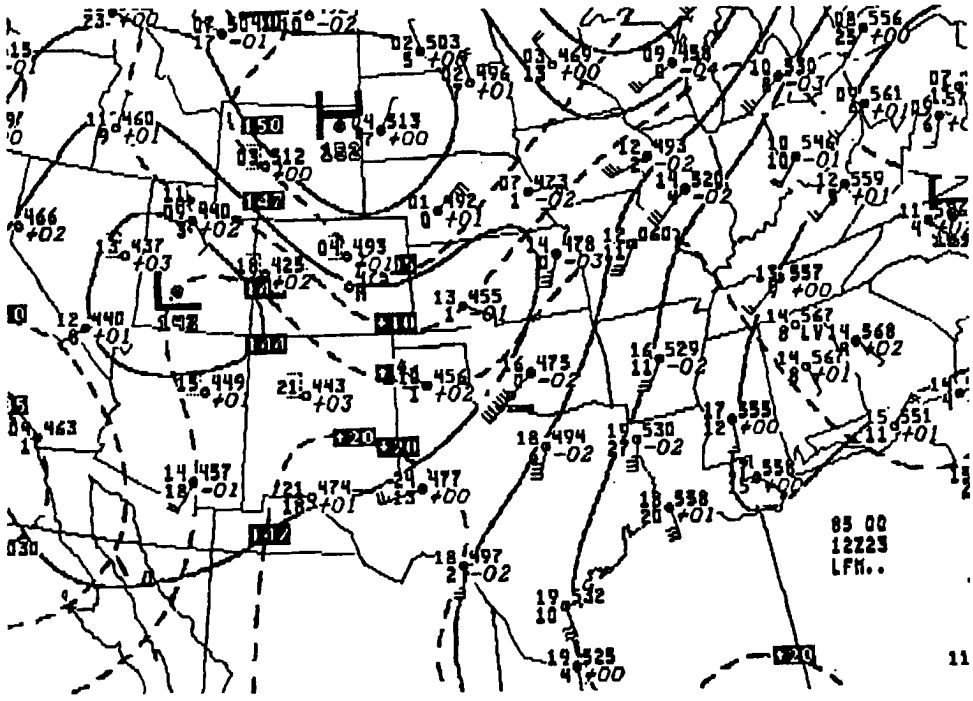

Figure 2-12 NMC 850 mb analysis, 31 May 1995 1200Z.

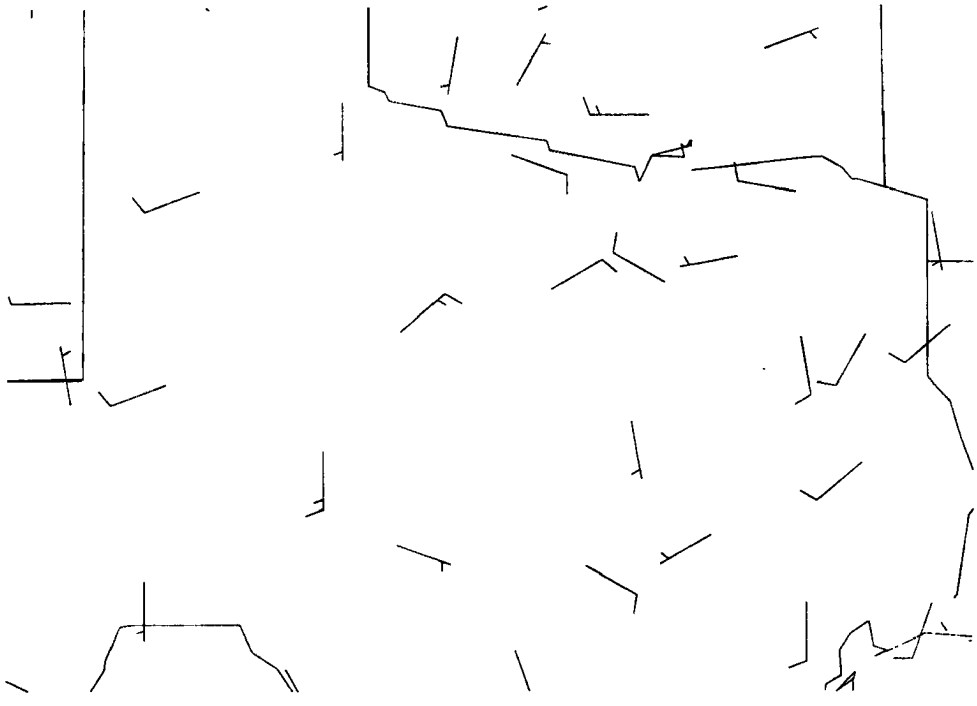

Figure 2-13 Surface wind observations, 31 May 1995 2000Z.

3.0 Low-level Wind Field Derivation

3.1 The GOES-8 Geostationary Satellite Platform

In May 1994 the National Atmospheric and Oceanic Administration (NOAA) launched GOES-8, the first in a series of next-generation geostationary satellites. All major components of the satellite are either new or greatly improved over previous geostationary platforms, enabling more accurate detection and tracking of small and mesoscale weather phenomena (Menzel, et al., 1994).

The satellite sensor is now earth-oriented, so it is able to view the surface nearly continuously. This is a major improvement over previous GOES/VAS satellites, which, employing a spin-scan radiometer, were only able to view the earth five percent of the time. The new scanning system works in a boustrophedron fashion, slewing from east to west and then back again. The sensor has higher spatial resolution (1 km in the visible, 4 km in the infrared), a stable linear response, and a new 10-bit data resolution capability. This is an improvement over previous GOES satellites, which had a nonlinear 6-bit capability, and provides 1024 brightness levels versus sixty-four. This allows more detail within the imagery and provides better use of low-light visible imagery.

Data sampling has been improved, with the new platform oversampling the 1km visible imagery by a factor of 1.75, versus no oversampling of the visible by the previous satellite. This allows better detection of cloud tops/edges and improves the ability to derive

low-level winds from them. Noise levels have been reduced 2 to 3 times compared to GOES-7, yielding a better signal-to-noise ratio.

Image navigation is also improved, using landmarks, range and stellar positioning; resulting in a more accurate location of each pixel within an image. Geographic landmarks of known latitude and longitude are located within image data (usually visible imagery is used). The line and pixel in the imager corresponding to that landmark is sent to the Orbit and Attitude Tracking System (OATS), where it is processed for use in orbit determination. Range is determined by measuring the period of time elapsed between the up- and downlink signal of the retransmitted data.

Stellar positioning is accomplished through an onboard sensor, which is pointed east of a star's predicted position and tracks the star as it crosses the sensor field of view. The star's position is processed on the ground and is then relayed to the OATS, which calculates the exact position of the satellite. Navigation accuracy at nadir is now within 4 km (within eight hours of noon), compared to 10 km available on GOES-7.

Registration, in which the sensor is controlled such that each pixel defines the same earth location on successive images over a 24-hour period, has also been improved. Since the attitude of the satellite is affected by its slewing motion and by thermal exposure, accurate registration is essential. Two onboard systems work to keep the registration within the specified error range; the image motion compensator (IMC) and the mirror motion compensator (MMC).

The OATS generates coefficients describing orbit and attitude contribution to pixel shift based on a "perfect" GOES projection

(defined by satellite subpoint), then transmits them to the satellite. The IMC applies these in an orbit and attitude model, which then computes correction signals and sends them to the servomotors controlling azimuth and elevation. The motors compensate for predicted attitude and orbit motion, producing an image with no apparent motion. These images are earth-located and registered by the IMC to the standard grid, which is generated once every 24 hours. Each subsequent image is then registered to the one before, keeping within established error limits.

The scan mirrors for the imager and sounder operate independently; while one is scanning the other can be slewed for stellar sensing or for blackbody calibrations. This slewing affects the attitude of the satellite and is corrected for by the MMC. As scan motion in one instrument is sensed by the MMC, a compensating signal is generated and sent to the servomotor of the other instrument. These corrections are made continuously and further increase the registration accuracy of the satellite. Registration accuracy is within 1.5 km between successive images 15 minutes apart.

Calibration of visible and infrared data is done in separate fashion, with visible channels calibrated in the testing lab. Because the satellite carries no calibrated sources of visible data on board, visible channels cannot be calibrated after launch. Normalization of visible data, however, is accomplished in real time after the satellite is launched. The imager has eight silicon photodiode detectors in its focal plane, producing image data simultaneously for eight lines as the mirror scans. Raw radiance outputs are normalized at Wallops Island, VA in real time using 10-bit conversion tables to compensate for gain

differences between detector channels. One channel is designated as a reference channel; the other channels are subsequently modified so their intensity distributions match that of the reference.

Since the new satellite is three-axes stabilized and not spinning like its predecessor, diurnal temperature fluctuations are on the order of tens of degrees Kelvin. As such, infrared calibrations must be made frequently enough to compensate for this phenomenon. The infrared channels are calibrated in flight as the sensors view space and an onboard blackbody. Since the blackbody fills the aperture of the sensor when viewed, a full-system calibration is possible (versus partial calibration on GOES-7). The imager views the blackbody every ten minutes, unless in doing so an image already being collected is interrupted. A calibration equation, which relates sensor output in digital counts to scene radiance (R) is given by:

$$R = qx^2 + mx + b$$

where the coefficients m and b are the slope and intercept, respectively, and are determined when the imager views space and the onboard blackbody. The coefficient q corrects for nonlinearities in sensor response, and is determined in the laboratory prior to launch. Calibration slopes and intercepts are computed in real time at Wallops Island. Brightness temperature accuracy and precision have been improved over GOES-7 (within 1.0 K and 0.3 K, respectively) allowing better cloud edge resolution and more precise target identification.

3.2 McIDAS Wind Tracking Software

All cloud tracking was accomplished using the University of Wisconsin's McIDAS WIND program, with improvements made by Patrick Dills at CIRA (Cooperative Institute for Research in the Atmosphere). While this program has the ability to track winds automatically, for this study the manual (single pixel) method was used to derive wind fields.

The primary equipment consists of the McIDAS terminal, a UNIX workstation, and a mouse. The user controls an electronic cursor which is placed on a selected cloud target to track. The coordinates at the cursor center define the displacements used in calculating the wind vector components. The user clicks on the target; this is the initial position coordinate. The target is then followed through a specified time interval and the user locates the target again, defining the final position coordinate. The difference between the two points defines the motion vector. The vector is graphically displayed as a wind barb on the screen; the vector components and wind speed/direction are also displayed on the McIDAS terminal (McIDAS-OS2 Users Guide, 1994). The user is responsible for accurately following the cloud feature; care must be taken when tracking the cloud or erroneous winds will result.

3.3 Methodology

For this study imagery intervals of 30, 15, 5 and 1 minute were used to derive wind fields in situations involving both strong mesoscale and weak synoptic scale forcing mechanisms. Small cumulus clouds were tracked using GOES-8 visible imagery with 1 km resolution to derive low-level wind fields. The interest area was halved in each case with each data point digitally repeated to give the impression of increased resolution, enabling better target tracking and continuity.

3.3.1 Image Navigation

Before a series of images can be used to derive cloud-track winds, each image in the series must be precisely navigated to reduce the wind vector error caused by improperly navigated imagery. This is done using a McIDAS navigation algorithm. The user first identifies a specific landmark on a reference image. The landmark must be visible and unobscured during the desired image sequence in order to use it for this process. Once the landmark is chosen, its exact latitude and longitude is computed by the algorithm. The user then enlarges the image, centering on the landmark. At this point an enhancement scheme is used to define the landmark as well as possible.

Subsequent images are then loaded individually, centering on the landmark and enlarging to match the reference image. If the landmarks do not match exactly on the images, the user can "shift" the image to match that of the reference. This process is then repeated for all subsequent images in the sequence and the renavigated images are saved as a loop for subsequent analysis.

3.3.2 Target Identification/Tracking

The best targets for inferring low-level winds are cumulus turrets 0.5 to 3 km in diameter (Fujita, et al., 1975). Larger clouds were avoided during this study, as they are more likely to be affected by shearing forces, vertical development, and entrainment. To be a valid tracer of the wind, the target must be a quasi-passive, shallow cloud element drifting with the wind during the time of the image series being used (Stewart, et al., 1985). Once a target is selected for tracking, the cursor is placed at the upshear edge of the cloud whenever possible to minimize contamination of the motion vector by the above mentioned

processes (Negri et al., 1980). The target is followed for a specified time period and marked again, as closely as possible to the original spot marked on the cloud. Tracking in this study was done using the image correlation method, which states that an image is discarded if the vector difference between consecutive vectors is greater than 5 ms^{-1}. This method was not employed when using rapidscan data sets; round-off errors routinely cause vectors to exceed this parameter.

3.3.3 Cloud Height Assignment

Errors in cloud height have been identified as the largest source of error when computing cloud-track winds (Lee, 1979). Clouds tracked for this study were of small horizontal extent; as such accurate vertical vector placement is quite difficult. Infrared imagery corresponding to the visual is too coarse in resolution to be of any practical use. To ensure that clouds tracked were as close to the same height as possible, several checks were made during target selection. Cloud morphology and operator experience were used to initially select targets for tracking. A cloud identified as a possible target was selected as long as the shadow it projected was similar in size to the cloud itself, indicating its proximity to the ground. Other targets were then chosen that displayed similar characteristics. The shadow technique to estimate cloud height was not used in this study, as cloud height errors using this technique are greatest around 20Z, when nearly all of the events in this study took place. Cloud heights were estimated by using the surface observation of the nearest reporting station at the time of the event. When available, upper-air sounding data was also used to verify cloud height.

3.3.4 Wind Field Generation

The 4 May 1995 Louisiana case was the first studied and the only case where image navigation techniques were not employed. This was done to compare the errors using different time intervals when accurate image navigation is not employed. Rapidscan data were not used in this case because of the very large errors that would be generated due to the lack of proper navigation.

Winds tracked during the remaining cases were all navigated prior to wind field generation. In each case wind fields were derived using each imagery interval type, as near to normal National Weather Service (NWS) reporting times as possible. When possible, winds were tracked near surface reporting stations and/or wind profiler sites to provide a source of validation data for this study.

3.3.5 Verification Procedures

Derived wind fields were compared with observations made by NWS surface reporting stations, wind profiler data from representative sites, and upper-air sounding data. Profiler data was preferred when available because of the high number of reporting levels throughout the lower atmosphere. Each of the wind fields were derived using events occurring between 18-20Z. The 00Z upper-air soundings from the following day were generally recognized as being the most representative of the atmosphere at the time of the events, although in one case the 12Z sounding was a better indicator of conditions at the later time.

4.0 Wind Field Comparison Studies

4.1 04 May Unnavigated Case

During the period 1845-1915Z winds were derived along the length of the "boot" of Louisiana, from Lake Charles (LCH) to New Orleans (MSY), as well as over the central portion of the state. Winds were derived in a weakly-forced environment south and west of a decaying frontal zone. These winds were derived from non-navigated imagery, intended only as a comparison with those derived from imagery precisely navigated in the lab after satellite capture.

Six surface reporting stations were used as a comparison: MSY, LCH, Lafayette (LFT), Baton Rouge (BTR), and Alexandria (ESF). Data from the wind profiler at Winnfield (WNF), roughly 80 km north of Alexandria, was also used. Winds plotted within a 10-20 km radius of a reporting station are considered representative of that station and are averaged to give a mean wind speed and direction.

At 19Z most stations along the boot reported southerly to southwesterly winds. Scattered conditions were reported with cloud bases from 2800-3700 ft (850-1125 m). Upper-air data (5 May/00Z) from Slidell (just north of MSY) and Lake Charles showed southerly and southwesterly flow, respectively, within the boundary layer. Alexandria, in central Louisiana, reported winds of 4 kts/300° at 19Z, with cloud base at 2000 ft (~600 m). This correlates well with the 5 May/00Z Shreveport sounding (200 km WNW of Alexandria) which reported cloud base at approximately 940 mb (~600 m).

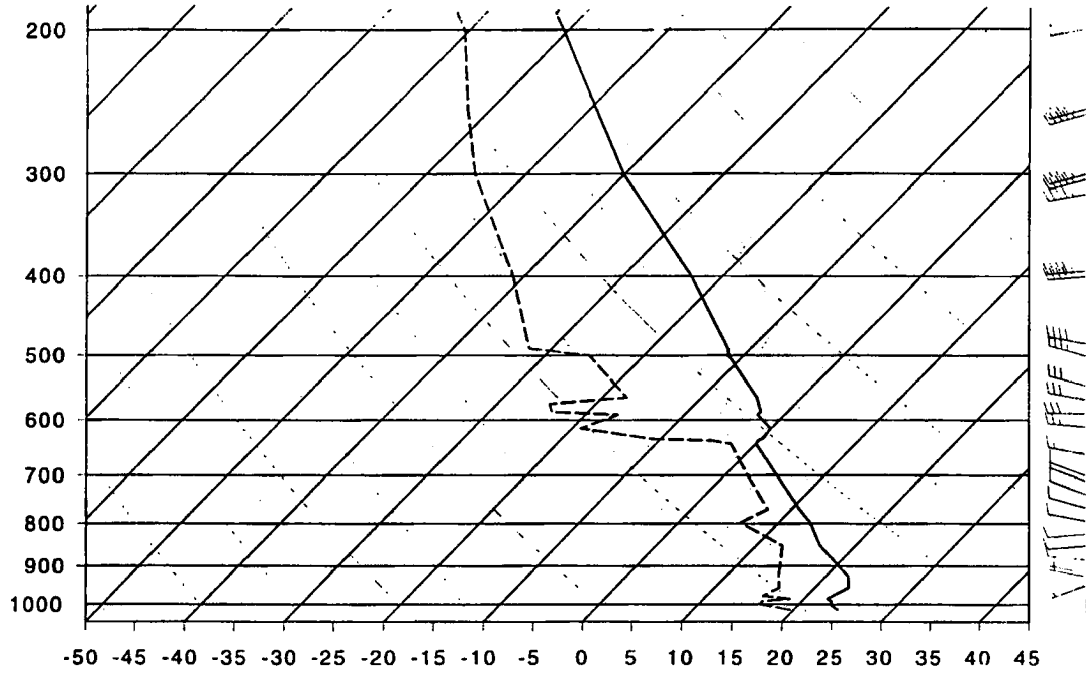

Figure 4-1 Slidell, LA upper-air sounding, 5 May 1995 00Z.

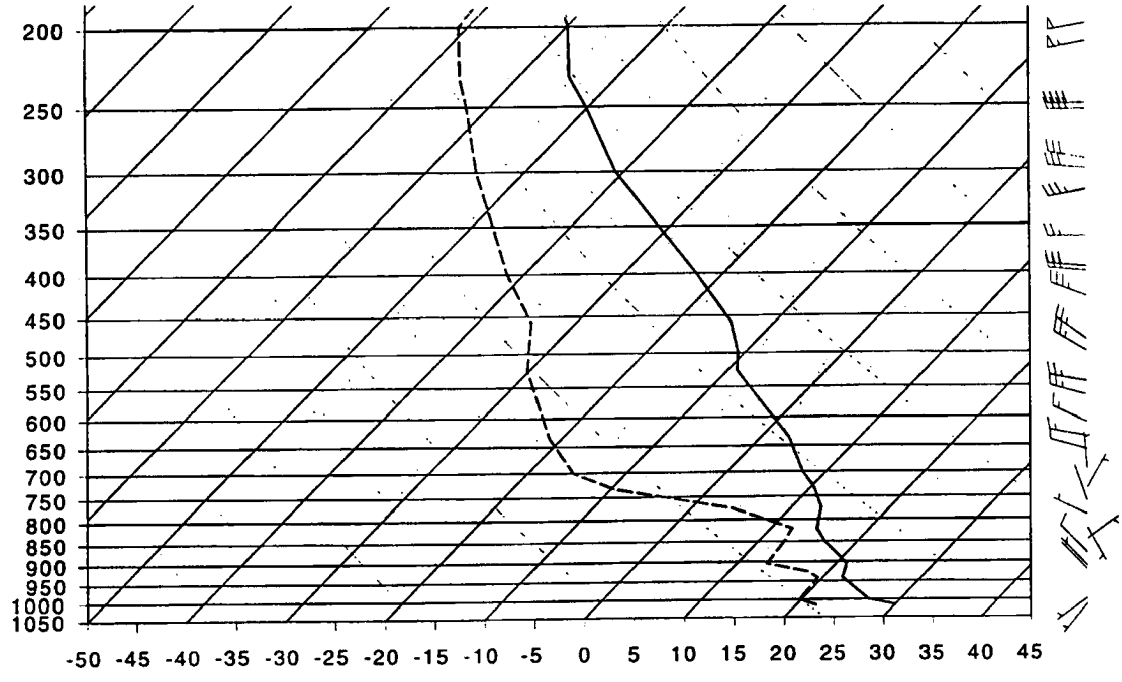

Figure 4-2 Lake Charles, LA sounding, 5 May 1995 00Z.

Figure 4-3 shows winds derived using 30-minute interval imagery from 1845-1915Z. While target continuity was maintained using 5-minute interval imagery for this case, few clouds remained extant during the thirty minute period. Derived wind speeds were similar to reported surface wind observations, differing by 1-3 knots.

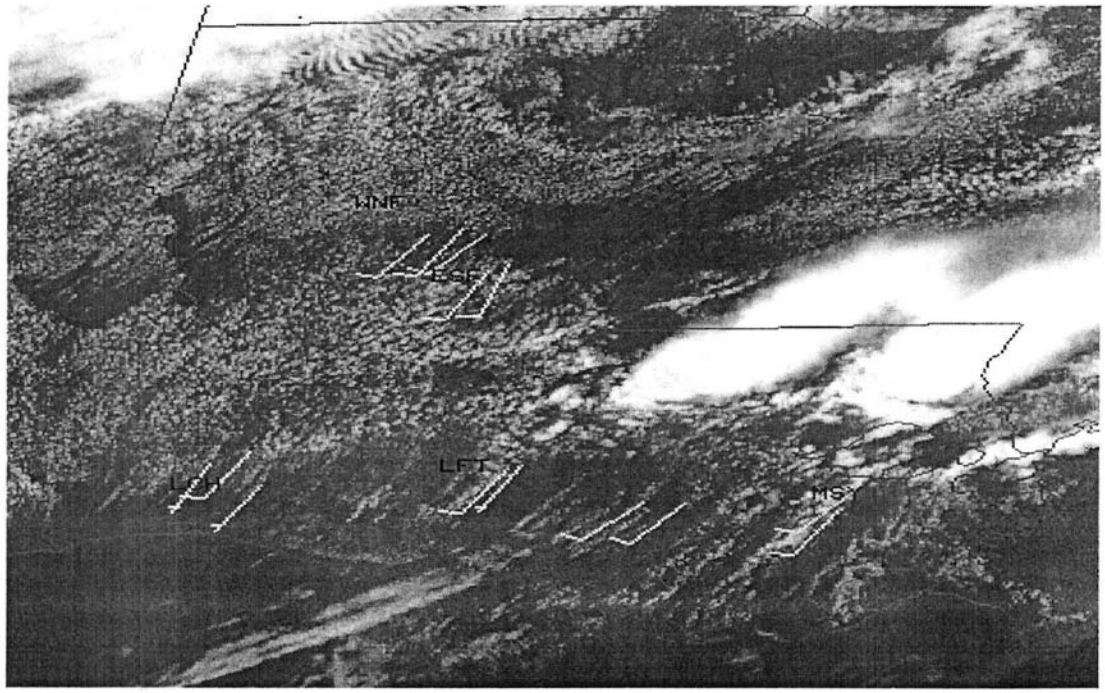

Figure 4-3 Derived 30-minute winds, 4 May 1995 (1845-1915Z).

However, large differences were noted in direction; most derived winds were oriented in a more southerly fashion than observed values. These large differences are illustrated graphically in Figure 4-4. Figure 4-5 shows a large difference in direction was also noted, though not as large, when derived winds in the vicinity of the profiler were compared to the average wind reported within the 500-750 m layer.

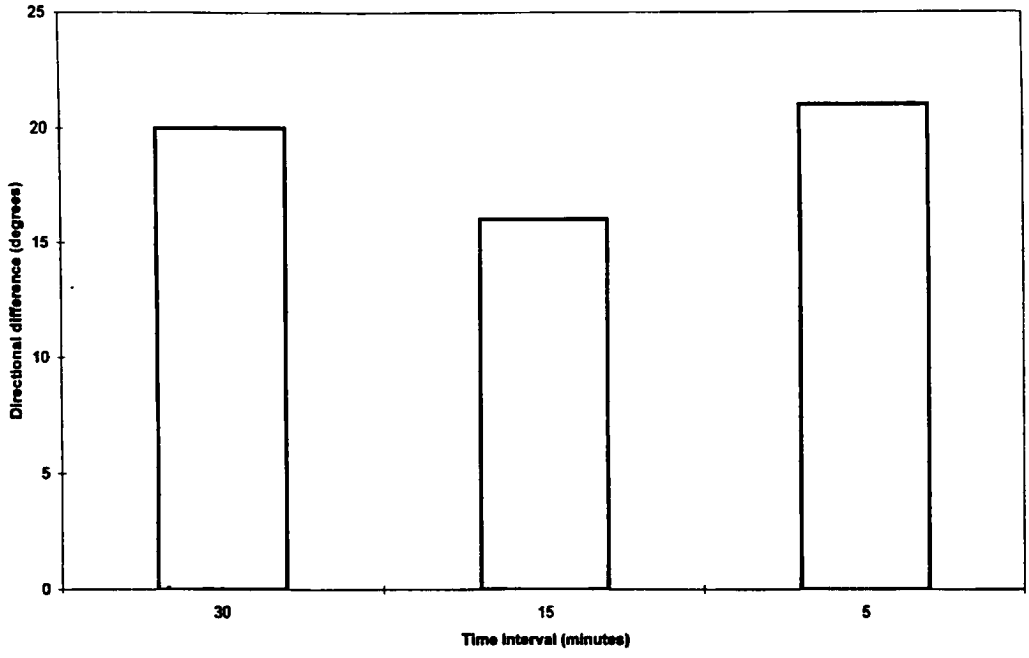

Figure 4-4 Average directional difference, compared to 19Z surface observations, of winds derived from imagery of differing temporal intervals.

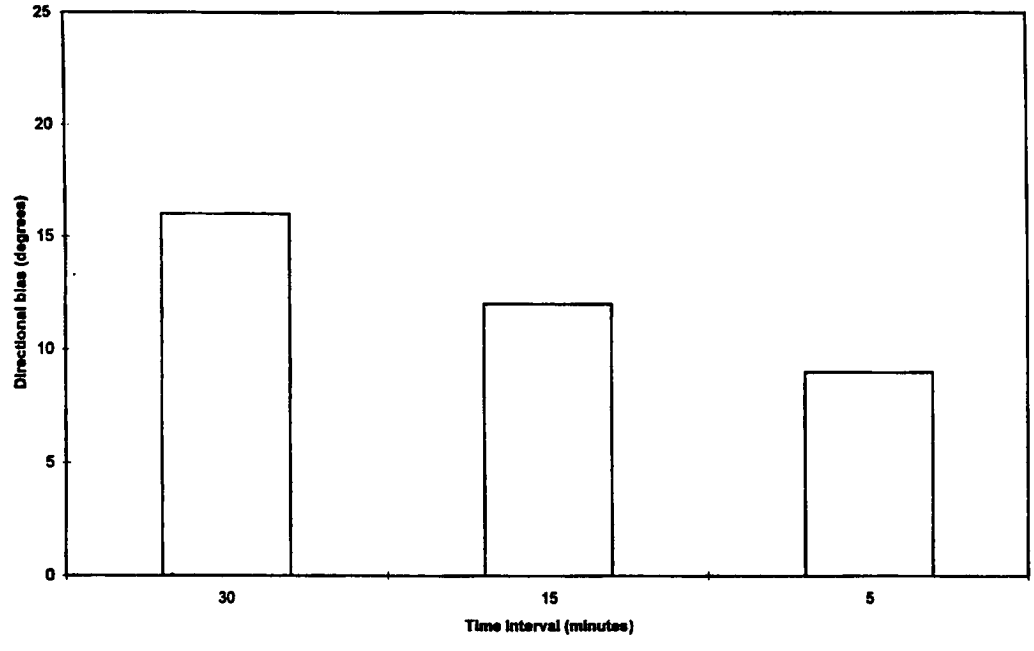

Figure 4-5 As above, except compared to 19Z Winnfield, LA profiler data.

Winds derived using 15-minute intervals, averaged over three time periods from 1845-1915Z, revealed similar results (See Figure 4-6). Directional differences remained evident in roughly the same magnitude observed earlier. Target continuity was maintained as before; because of the shorter time interval, a larger number of targets were available for tracking. Accuracy of winds derived in the vicinity of the profiler improved nearly 25% in both speed and direction using the shorter image interval.

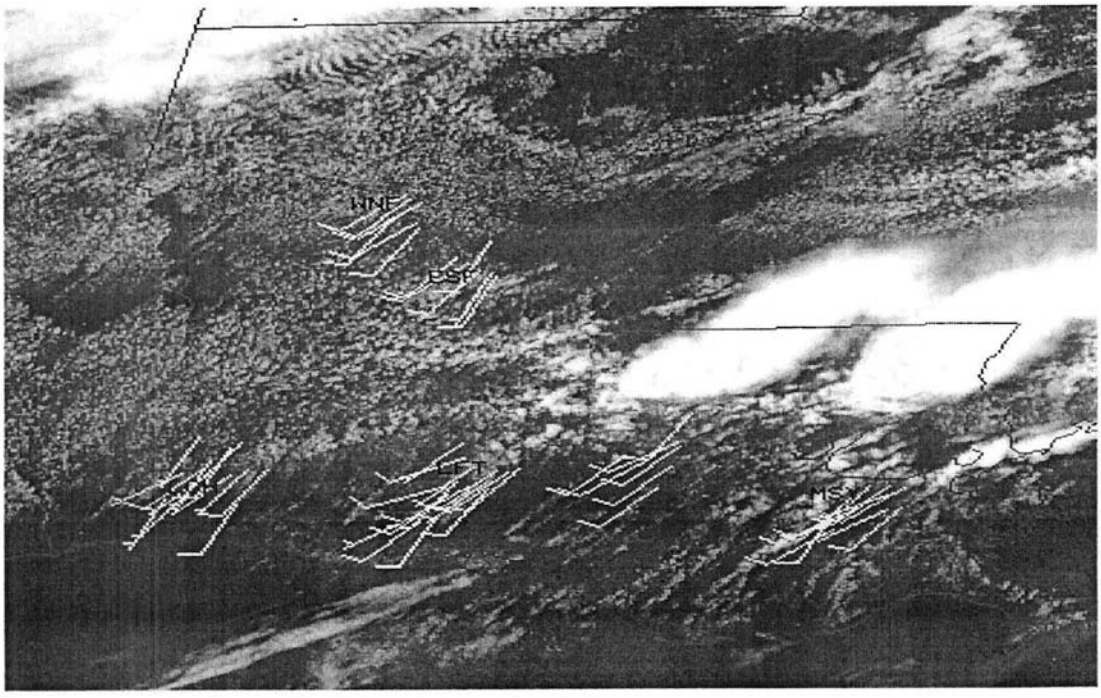

Figure 4-6 Derived 15-minute winds, 4 May 1995 (1855-1910Z).

Figure 4-7 shows winds derived using 5-minute interval imagery. Large directional differences similar in magnitude to longer interval imagery remained evident, although winds derived near the profiler improved. Speed differences compared with surface observations and profiler data are listed by interval type in Figures 4-8 and 4-9.

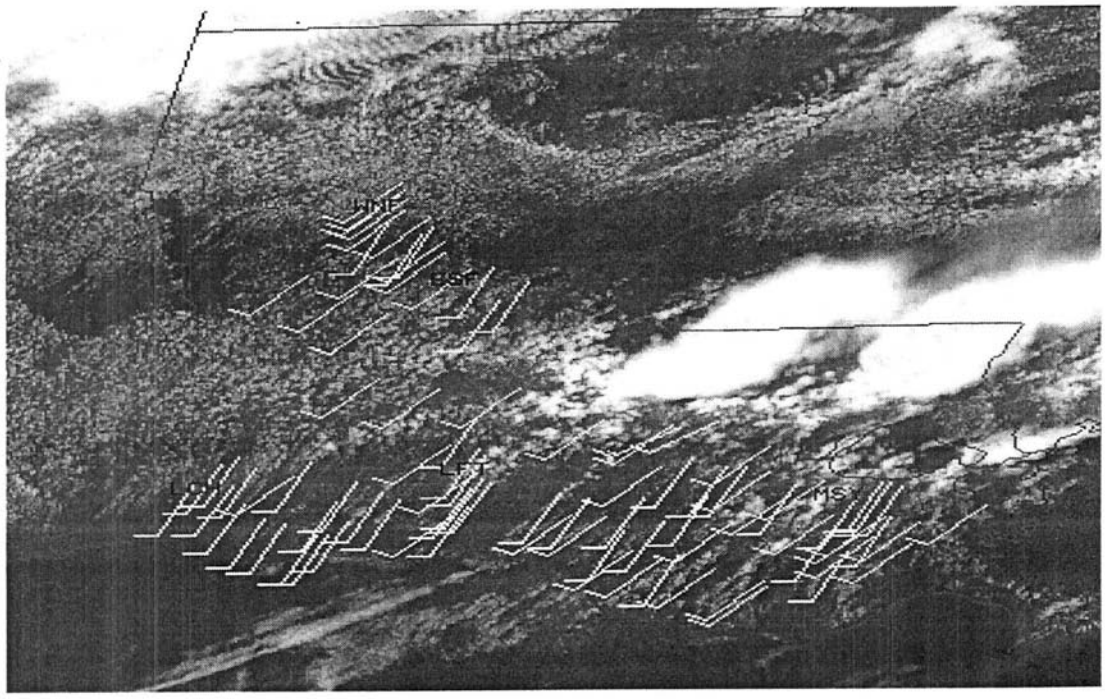

Figure 4-7 Derived 5-minute winds, 4 May 1995 (1855-1900Z).

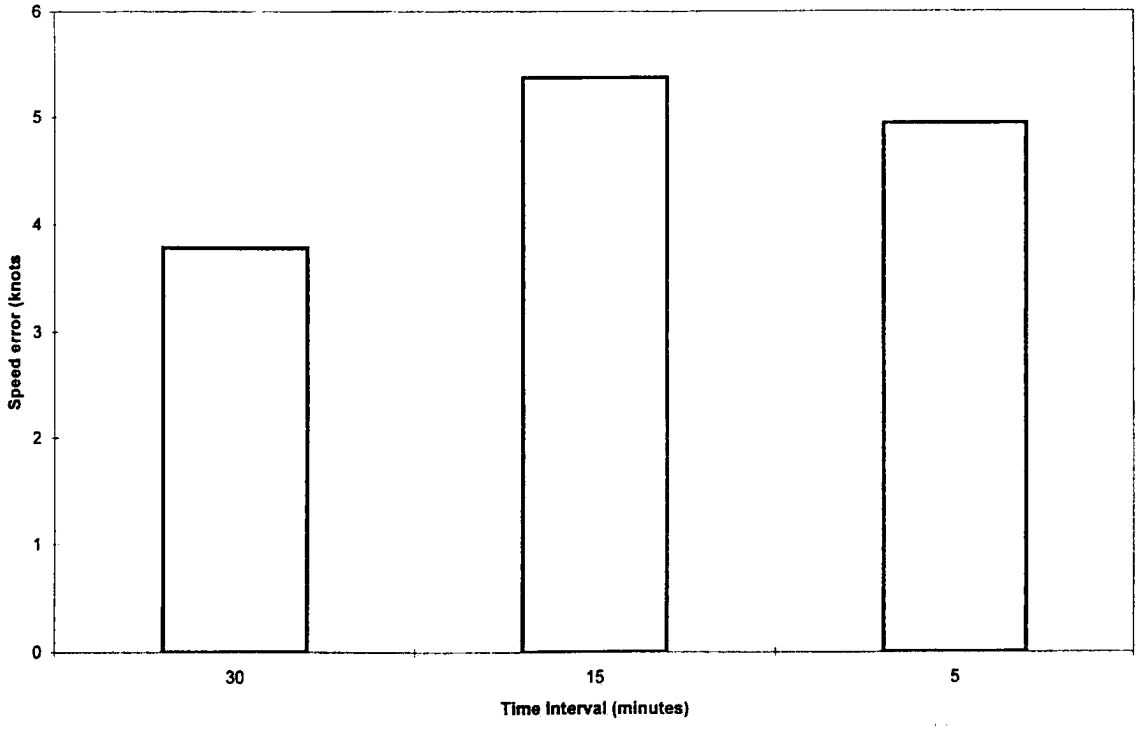

Figure 4-8 Average speed difference, compared to 19Z surface observations, of winds derived from imagery of differing temporal intervals.

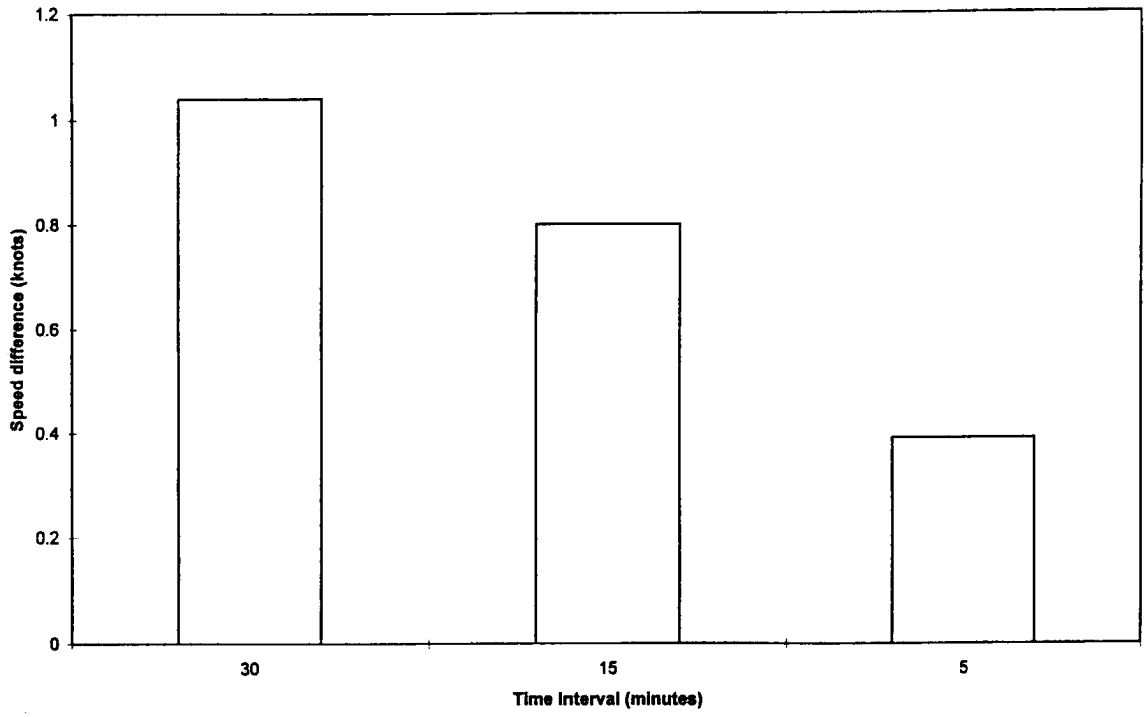

Figure 4-9 Average speed difference, compared to 19Z Winnfield, LA profiler data, of winds derived from imagery of differing temporal intervals.

The large directional difference in each case is partly due to image shifts caused by improper satellite navigation and/or registration. While normally scheduled imagery intervals (every fifteen minutes over the continental U.S.) appear to be well navigated, shorter interval imagery specially scheduled for the study of severe/unusual weather seems more poorly navigated (Dr. Garrett Campbell, personal communication). New navigation software was installed in mid-late 1995; future studies may show these problems with satellite navigation and registration to be diminished. It is imperative, however, that studies using short interval imagery include precise renavigation algorithms before image sequences are analyzed. As will be made evident later in this paper, accurate wind field derivation depends greatly upon precise image navigation and registration.

4.2 17 May Oklahoma Case

Winds were derived over central and southern Oklahoma from north of Oklahoma City (OKC) to just south of the Purcell (PRC) wind profiler, thirty miles south of OKC. Wind fields were derived for the period 1945-2015Z, to coincide with 20Z NWS reporting times. A small area of moderate convective activity was occurring north and east of OKC, with clearing conditions behind. Small non-developing cumulus cells in the vicinity of both locations were used for this study.

At 20Z OKC reported scattered clouds at 6000 ft (1825 m) above ground level (AGL), with winds of 16-23 kts/220°. Purcell reported winds at 1750 m AGL of 24.3kts/240°. The 12Z sounding from Norman, south of Oklahoma City, indicated cloud base at approximately 1500 m. Cloud base remained low until 18Z, when the clouds dissipated as a dryline approached. The 00Z sounding was also not indicative of 20Z atmospheric conditions; by then the dryline was east of Norman and no clouds were present. However, both soundings (see Figures 4-10,11) showed strong (30-45 kts) southwesterly flow at the 6000 ft level.

Figure 4-12 shows winds derived using thirty-minute interval imagery; winds averaged 22.9 kts/236°. Fifteen-minute interval imagery for the same period, shown in Figure 4-13, yielded an average of 22.83 kts/237°. Each of these wind sets were derived using five-minute interval data for target continuity. Both sets coincide closely with reported profiler winds, but not surface observations, suggesting low-level cloud-track winds are more representative of flow at cloud base rather than that at the surface. This coincides with previous studies conducted using other satellite platforms and wind measurement techniques.

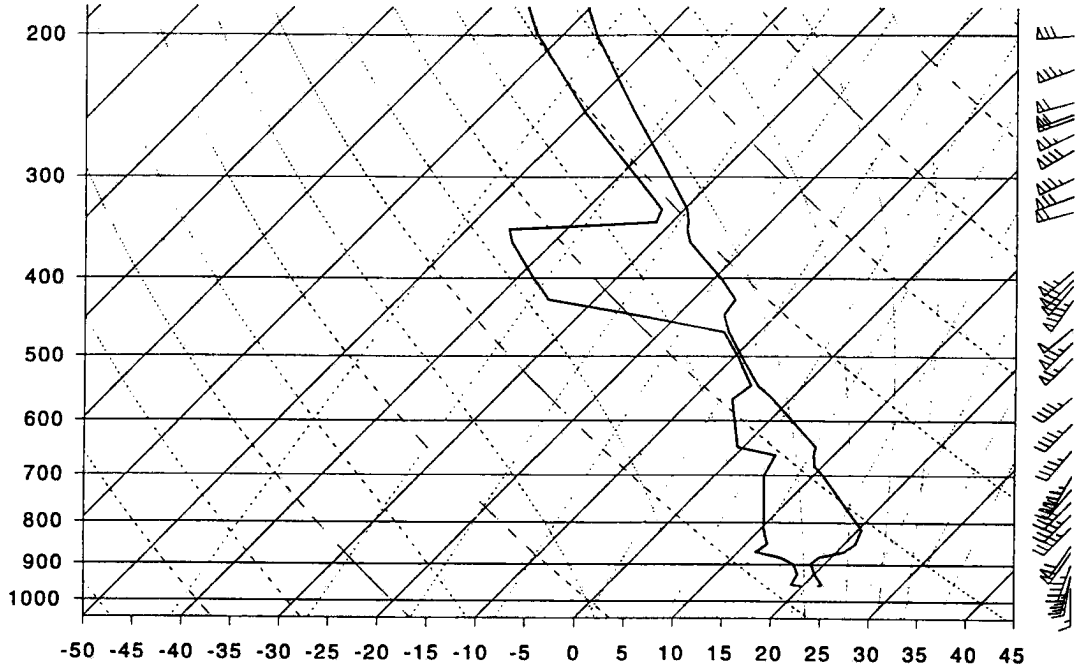

Figure 4-10 Norman, OK upper-air sounding, 17 May 1995 12Z.

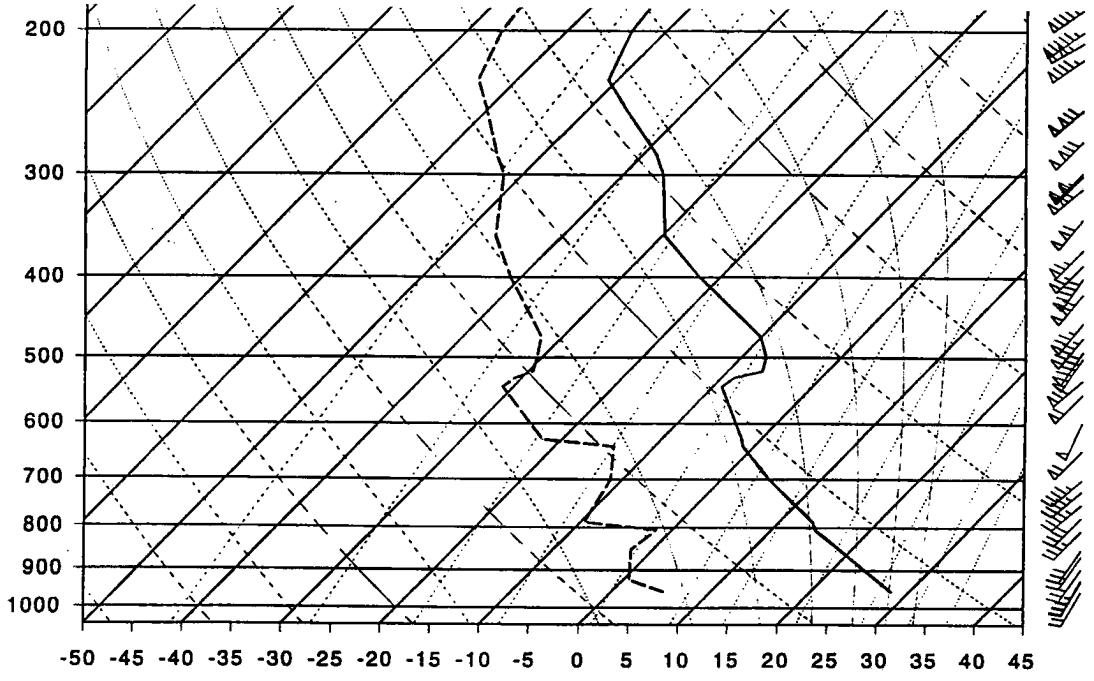

Figure 4-11 Norman, OK upper-air sounding, 18 May 1995 00Z.

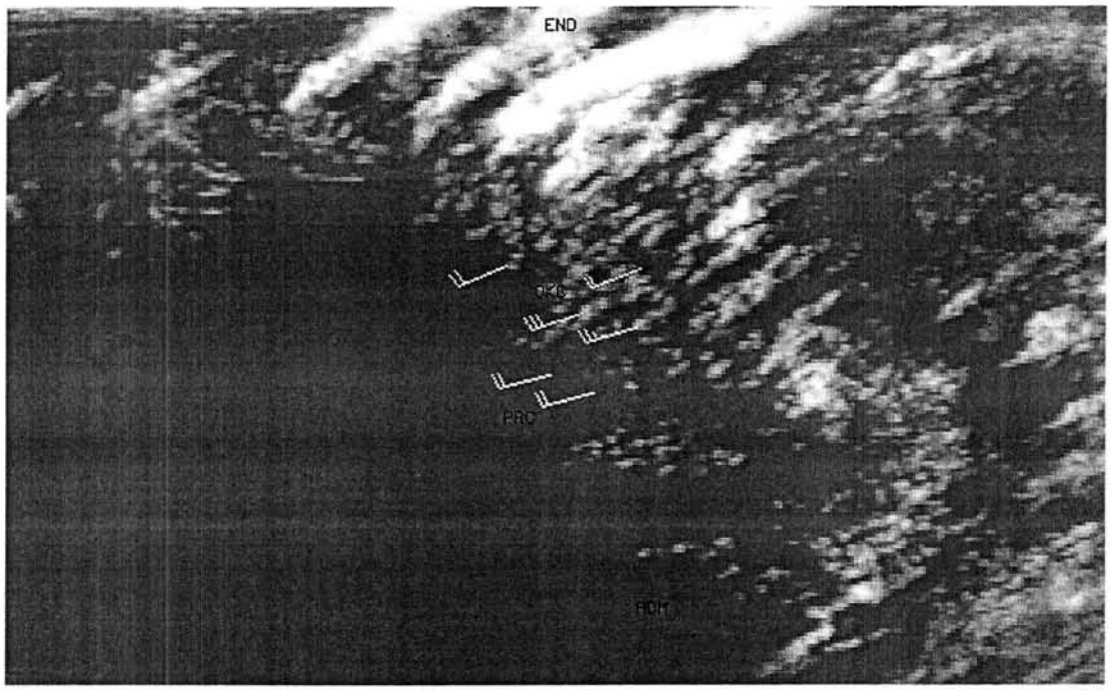

Figure 4-12 Derived 30-minute winds, 17 May 1995 (1945-2015Z).

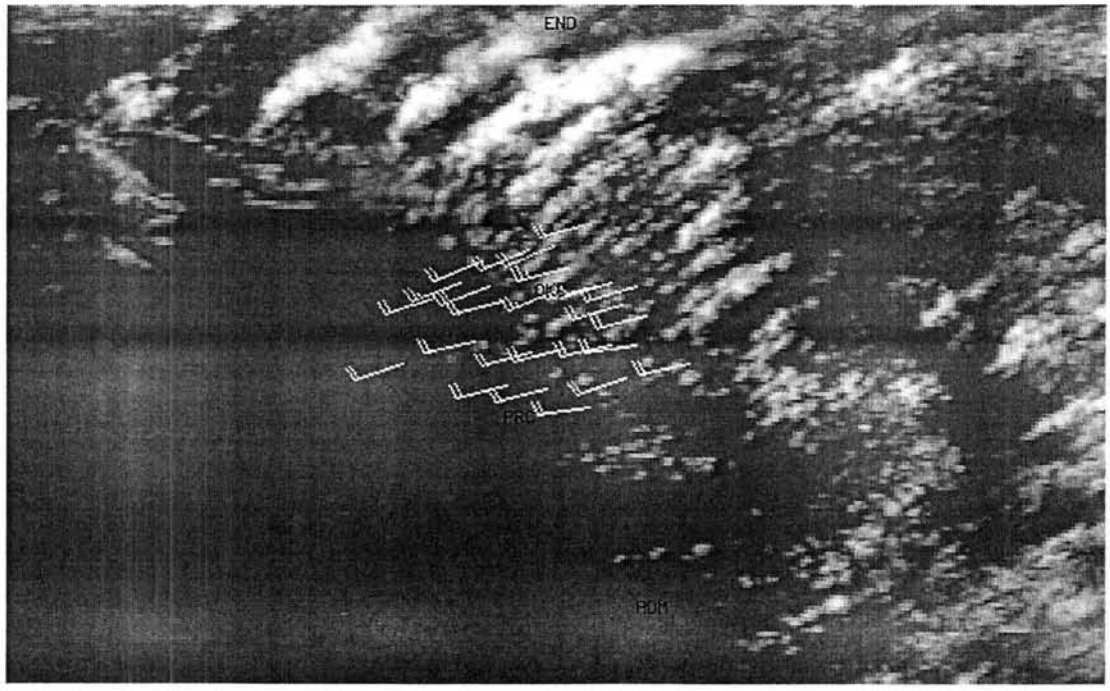

Figure 4-13 Derived 15-minute winds, 17 May 1995 (1955-2010Z).

An example of winds derived using five-minute interval imagery is shown in Figure 4-14. Averaged winds derived using several five-minute intervals from 1955-2010Z produced larger direction differences than those derived from longer intervals. The surface observations help explain this discrepancy: Oklahoma City reported gusty conditions as early as 1825Z; these continued through the following two observation times. The larger difference is most likely due to environmental variability of the wind field.

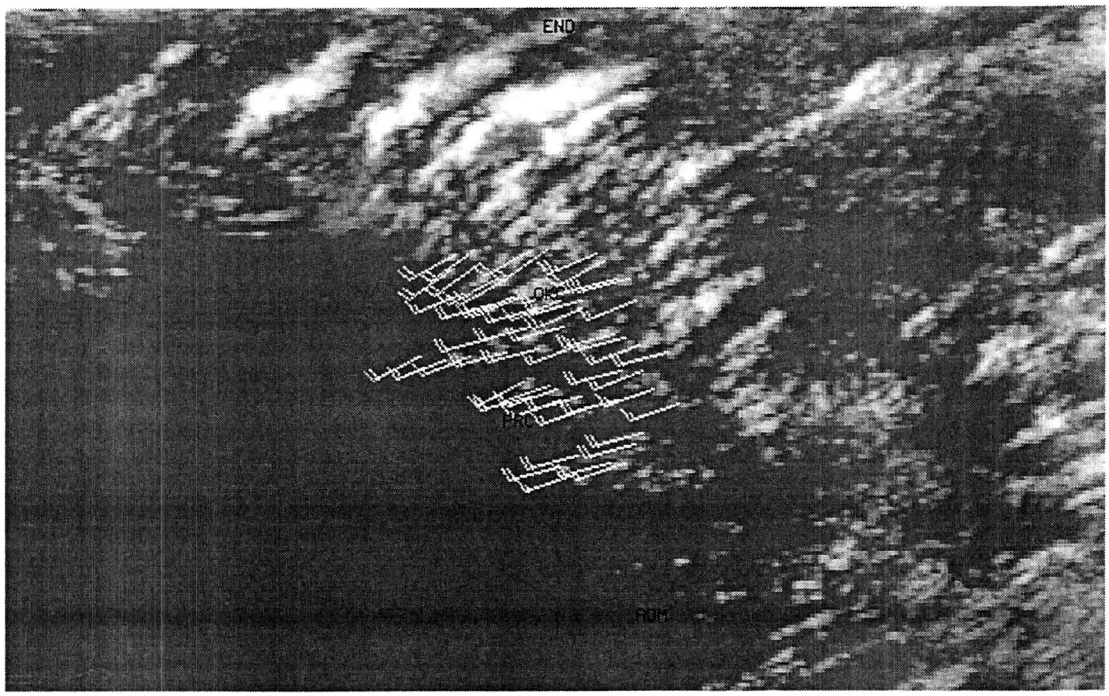

Figure 4-14 Derived 5-minute winds, 17 May 1995 (1959-2004Z).

Hourly profiler data was used for comparison in this study; these are 1-hour averages derived from 6-minute radial velocity samples taken over the preceding hour (Schlatter and Zbar, 1994). A process known as consensus averaging is used in which data within a certain threshold (sampled horizontal velocities must be within 2 ms^{-1}) are averaged. At

least four of the measurements made must agree to form a consensus average, or the hourly average is reported as missing. Isolated spikes in the data are excluded, thus variability is smoothed out. Six-minute data may prove better for comparison in variable wind conditions.

One-minute imagery was obtained in the following fashion: A target was selected that remained visible over the tracking period (2004-2011Z). Targets were tracked using a time-step method, yielding a set of seven winds, derived using increasing intervals of one to seven minutes. This method ensures precise continuity is maintained throughout the tracking process. As seen in Figure 4-15, winds were not similar in speed or direction during each interval; errors due to imperfect navigation and resolution produced vectors that tended to "oscillate" about their true magnitude and direction until a sufficient time interval (usually 4-5 minutes) had elapsed.

In this case wind vectors initially showed a purely westerly component, then adopted a more representative southwesterly component as the number of intervals used to calculate the wind was increased. Comparisons of differences in speed and direction of derived winds versus surface observations and profiler data is given in Figures 4-16 through 4-19. At first glance it appears that the average wind using five-minute data does not agree with values found after five one-minute intervals. But the five-minute winds are *average* values over the 1955-2009Z period. When compared to five-minute winds derived from 2004-09Z, vector differences are minimal (Figures 4-20,21). The small differences are likely due to more accurate tracking; cursor placement at exactly the same point on the cloud element was easier using rapidscan imagery.

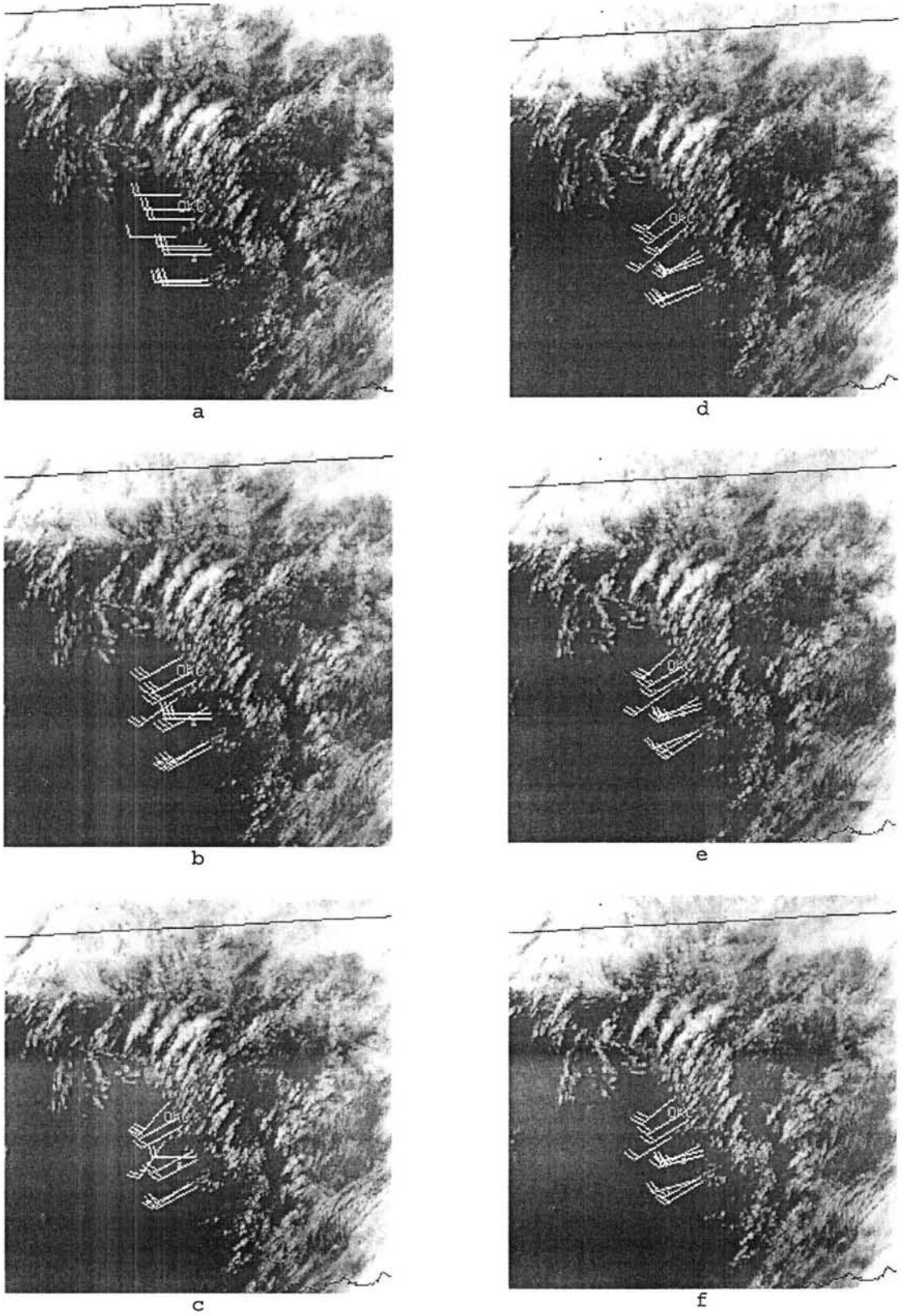

Figure 4-15 Wind series plotted at 1-minute intervals from 2005-2011Z.

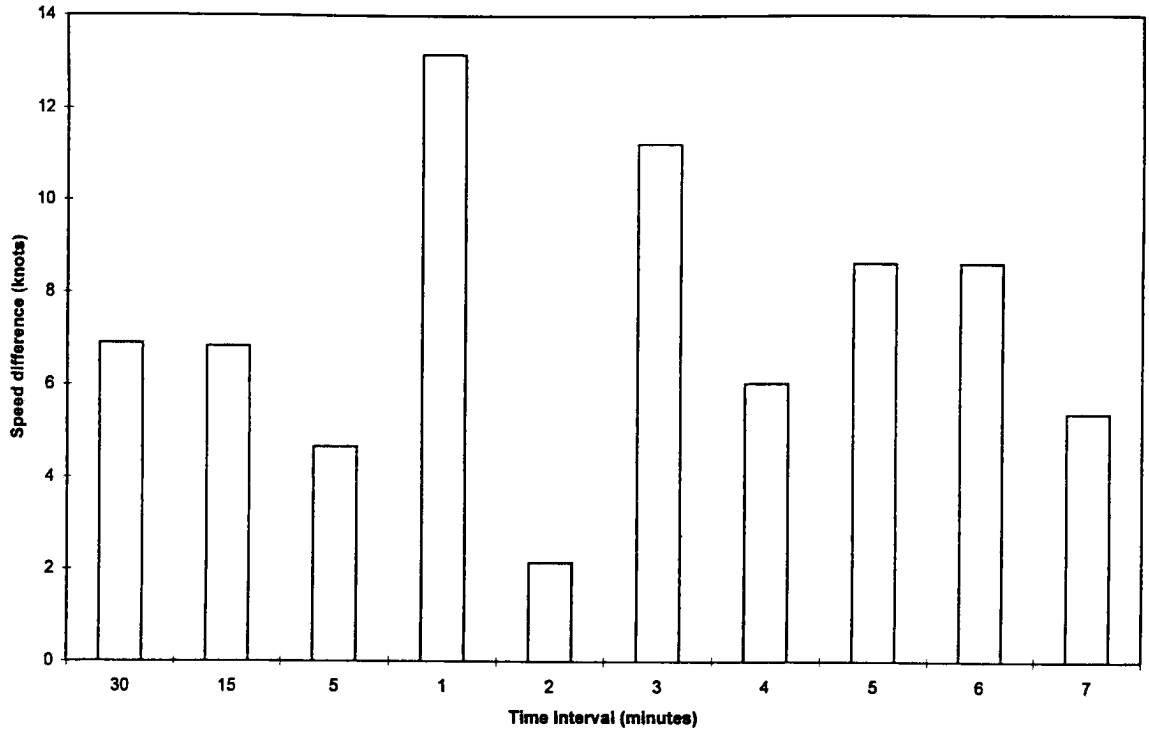

Figure 4-16 Average speed difference compared to 20Z OKC surface observations. Time intervals labeled 1-7 refer to winds derived using an increasing number of one-minute intervals, from 2005-11Z.

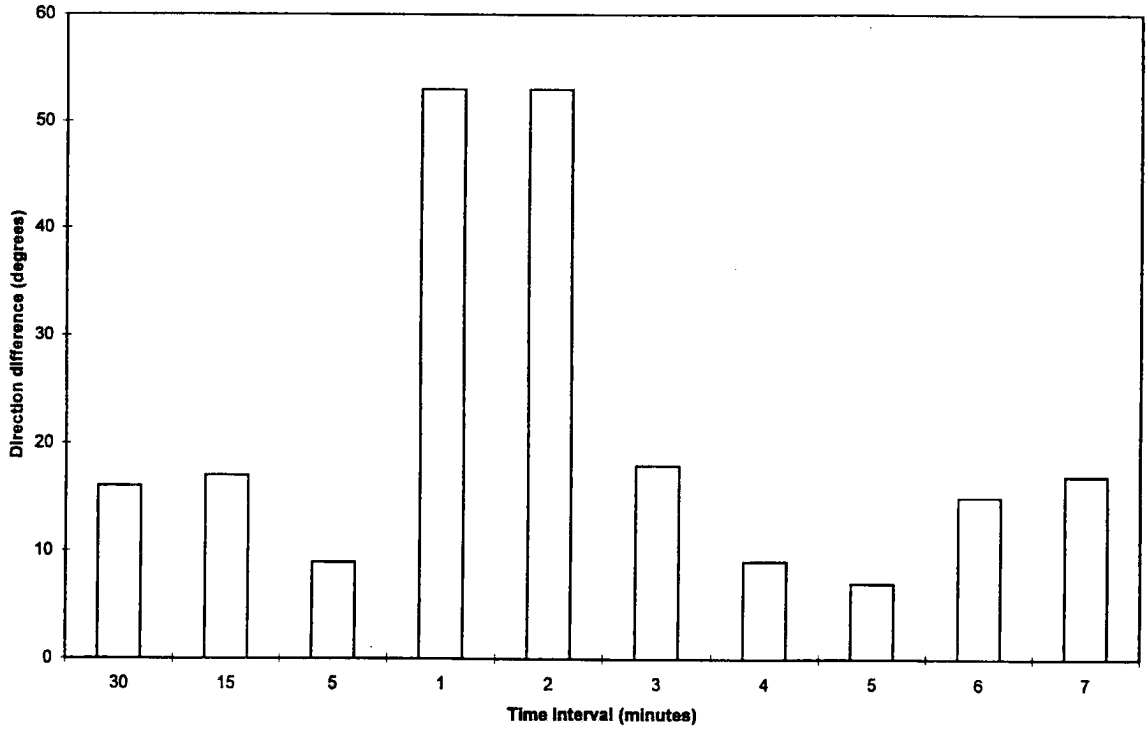

Figure 4-17 Average direction difference compared to 20Z OKC surface observations (same format as above).

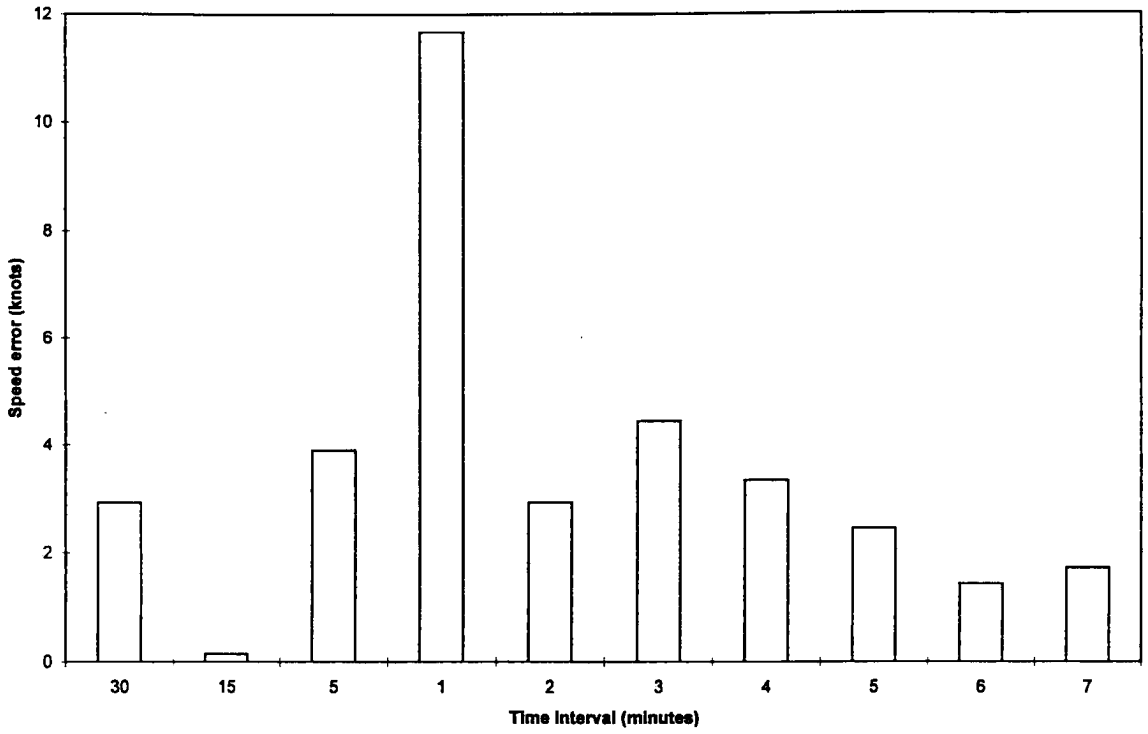

Figure 4-18 Average speed difference compared to 20Z PRC profiler data. Time intervals labeled 1-7 refer to winds derived using an increasing number of one-minute intervals, from 2005-11Z.

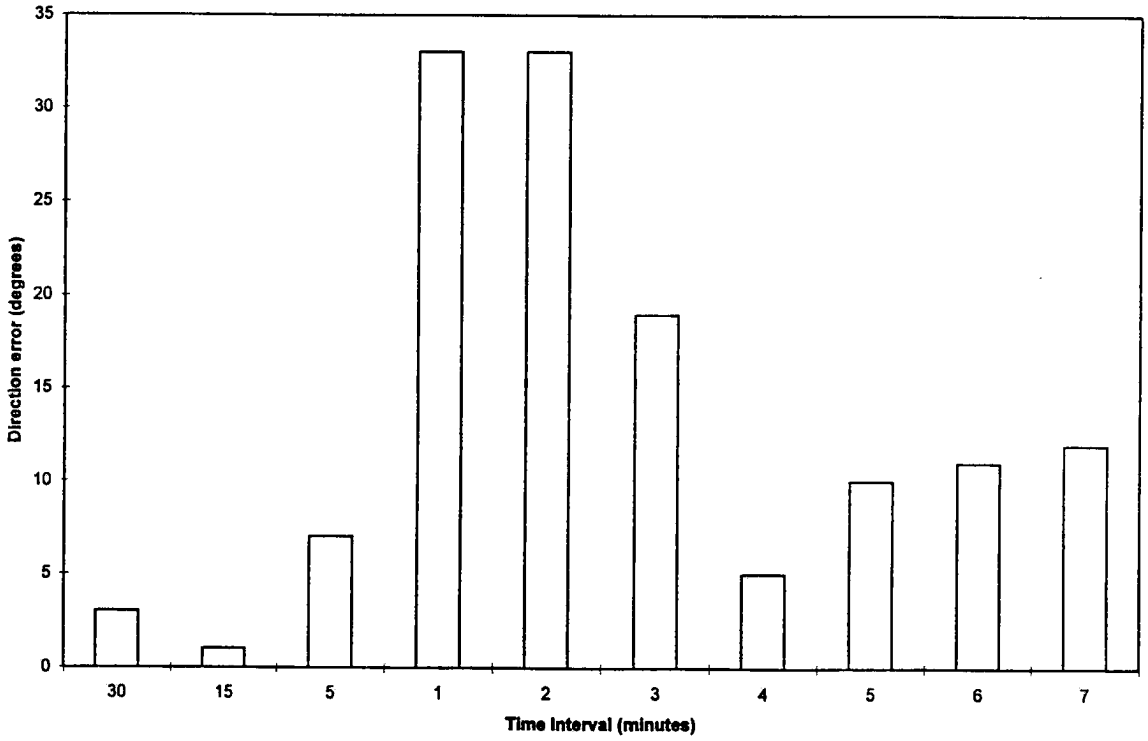

Figure 4-19 Average direction difference compared to 20Z PRC profiler data (same format as above).

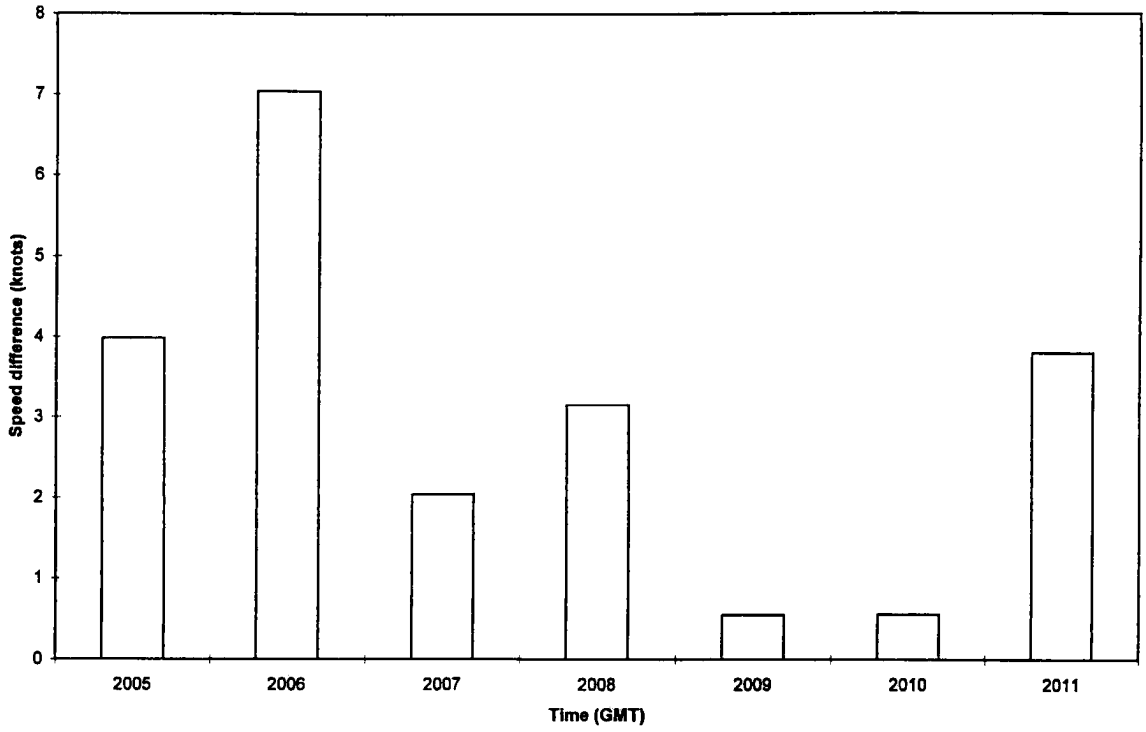

Figure 4-20 Average speed difference of winds derived from an increasing number of 1-minute intervals (2005-11Z) when compared to winds derived using 5-minute data from the same time period (2004-09Z).

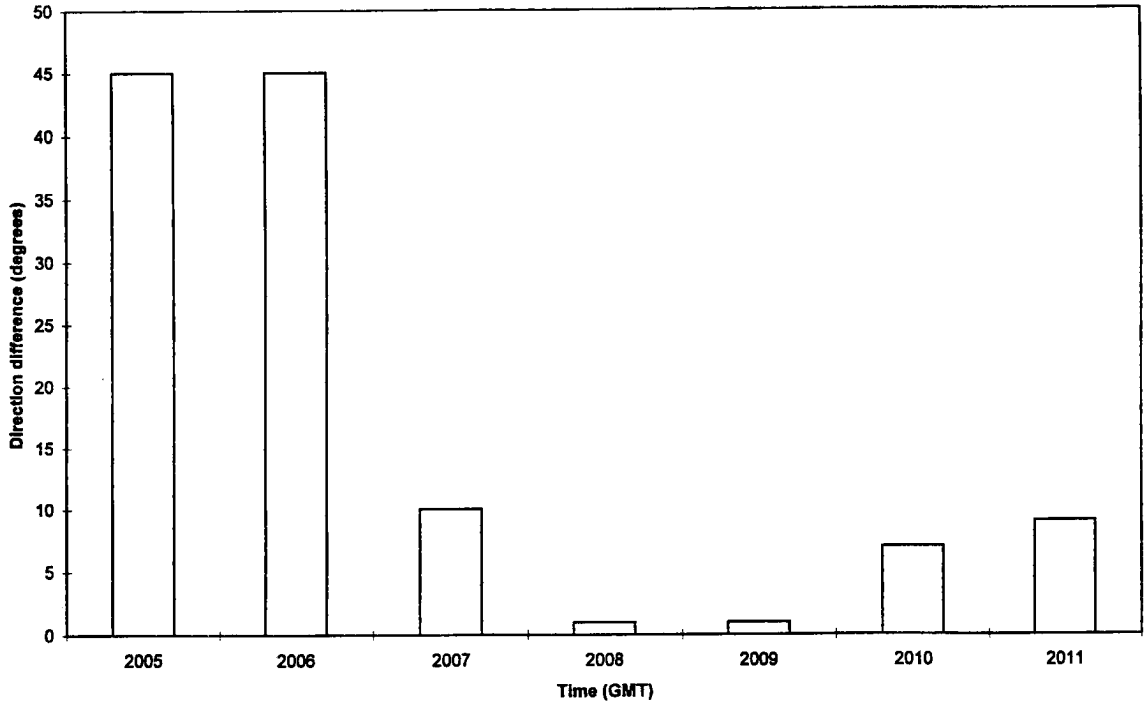

Figure 4-21 Average direction difference (same format as above).

4.3 23 May Ft. Worth Study

On 23 May 1995 a large area of eastern Texas was under the influence of a large-scale southerly flow field characterized by small cumuliform clouds. Winds were plotted around the Ft. Worth area between 1945-2045Z to compare with surface observations. At 20Z Ft. Worth (FTW) reported 18kts /170° (taken at Meacham International Airport). Meacham also reported scattered cloud conditions at 4000 ft (1219 m) AGL at this time. The Palestine, TX wind profiler (roughly 200 km ESE of FTW) was also used for verification. Both locations are under the influence of the same flow field, at least in the lower levels. Figure 4-22 shows Ft. Worth sounding data from 24 May/00Z. Cloud base was approximately 4500 ft (850 mb); winds were southwesterly within the cloud layer, becoming southeasterly below. The same wind distribution was noted at the profiler at that time: southwesterly within the cloud layer, southeasterly below.

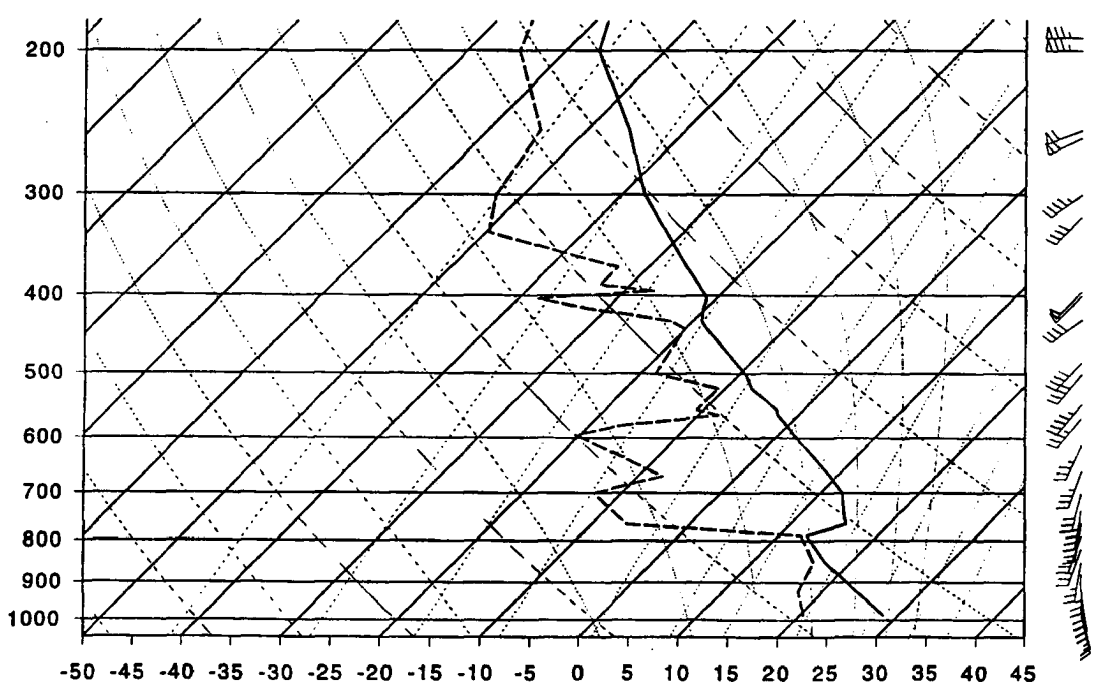

Figure 4-22 Ft. Worth upper-air sounding, 24 May 1995 00Z.

Average winds derived around FTW using 30-minute interval imagery (1945-2015Z) were slow at 16 kts, but identical in direction. Continuity in both 30-minute and 15-minute intervals was maintained as before. Fifteen-minute winds generated for several intervals between 1945-2015Z averaged 16 kts/171°, 2 knots slower than observed but within a degree in direction. Average 5-minute winds derived using several sets from 1955-2010Z showed an increase in speed accuracy, with an average measured wind around FTW of 17.33 kts/174.33°. Winds derived from rapidscan imagery correlated less well with surface observations; winds averaged 25.37 kts/172° for the period 2004-2011Z. Differences in wind speed and direction are given in Figures 4-23,24. No discernible cloud movement was detected during the first interval; therefore no differences were plotted for it.

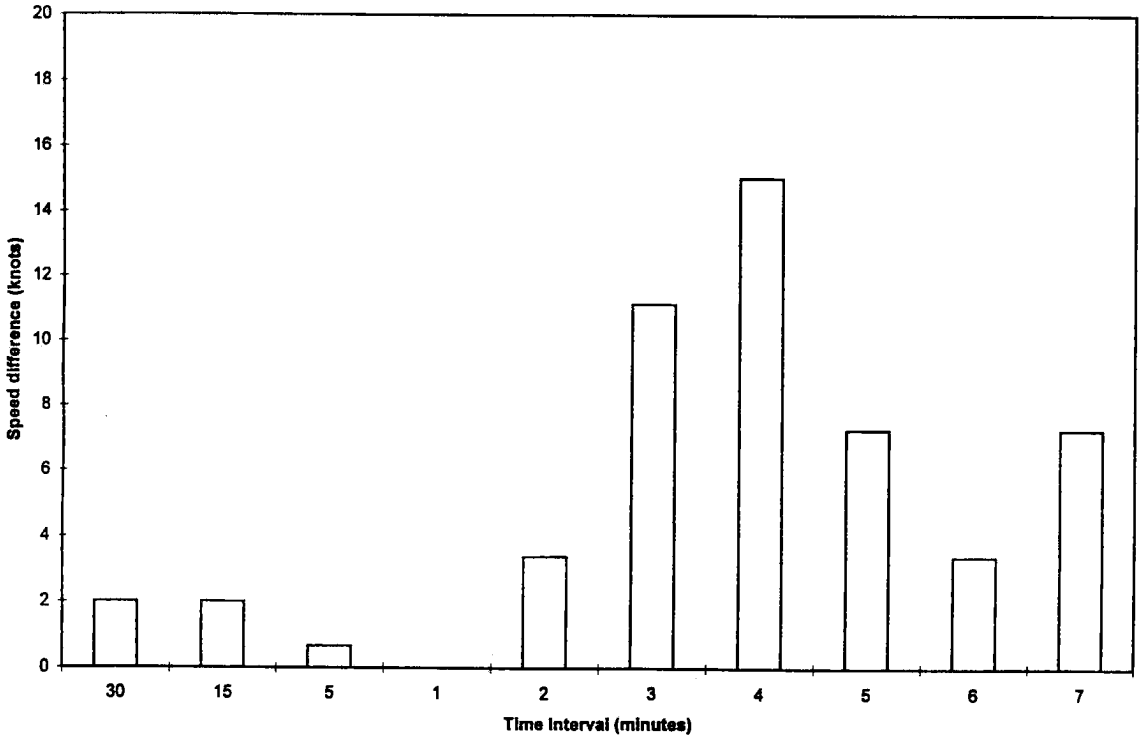

Figure 4-23 Average speed difference compared to 20Z FTW surface observations. Time intervals labeled 1-7 refer to winds derived using increasing an increasing number of one-minute intervals from 2005-11Z. No cloud movement was discerned during the first 1-minute interval.

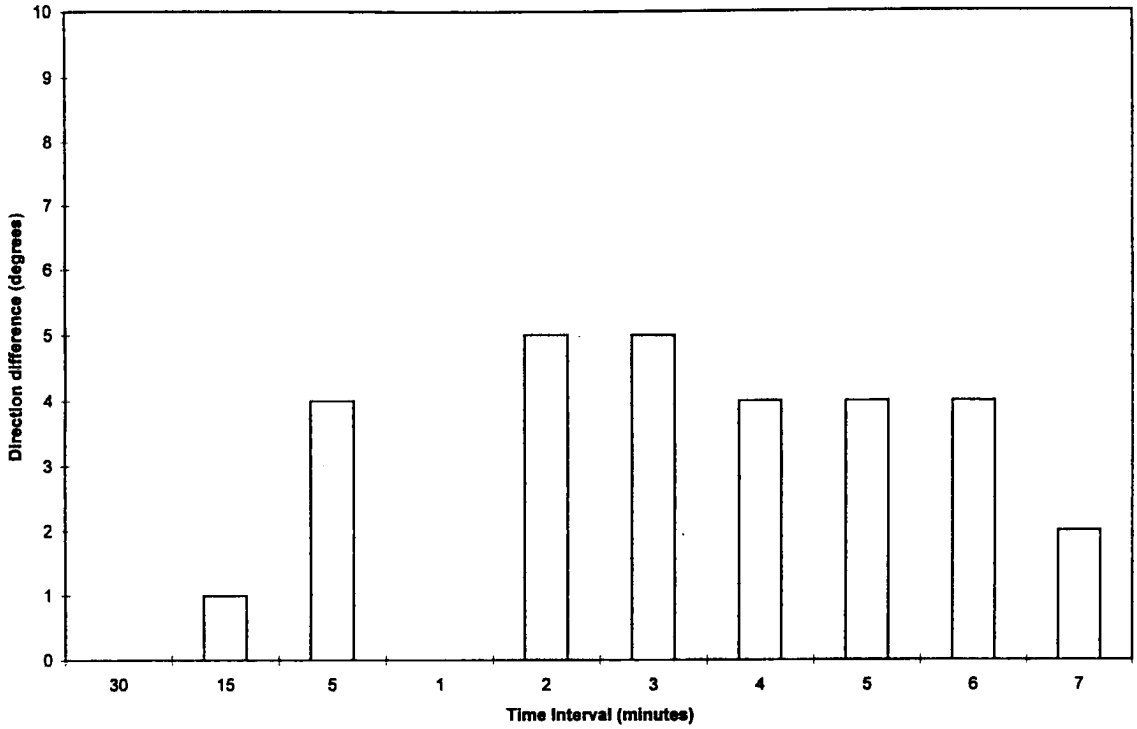

Figure 4-24 Average direction difference compared to 20Z FTW surface observations (same format as above).

Winds were also plotted in the vicinity of the Palestine profiler during the same time period, using all four interval lengths. Derived winds were compared with winds reported at 1250 m AGL (17.49 kts/177°). Average 30-minute winds were computed at 14 kts/162°, while 15-minute derived winds averaged 16 kts/162°. Average five-minute winds were closest to those observed at 14.61 kts/161°, while rapidscan imagery yielded winds from 2004-09Z of 18.14 kts/167°. Figures 4-25 to 4-28 show winds near the profiler derived using each temporal interval. Difference comparisons for each interval type are shown in Figures 4-29,30. Rapidscan data after five one-minute intervals had elapsed yielded the most accurate winds. Wind speed/direction comparisons between winds derived from the first five rapidscan intervals and five-minute winds from the same time period are shown in Figures 4-31,32.

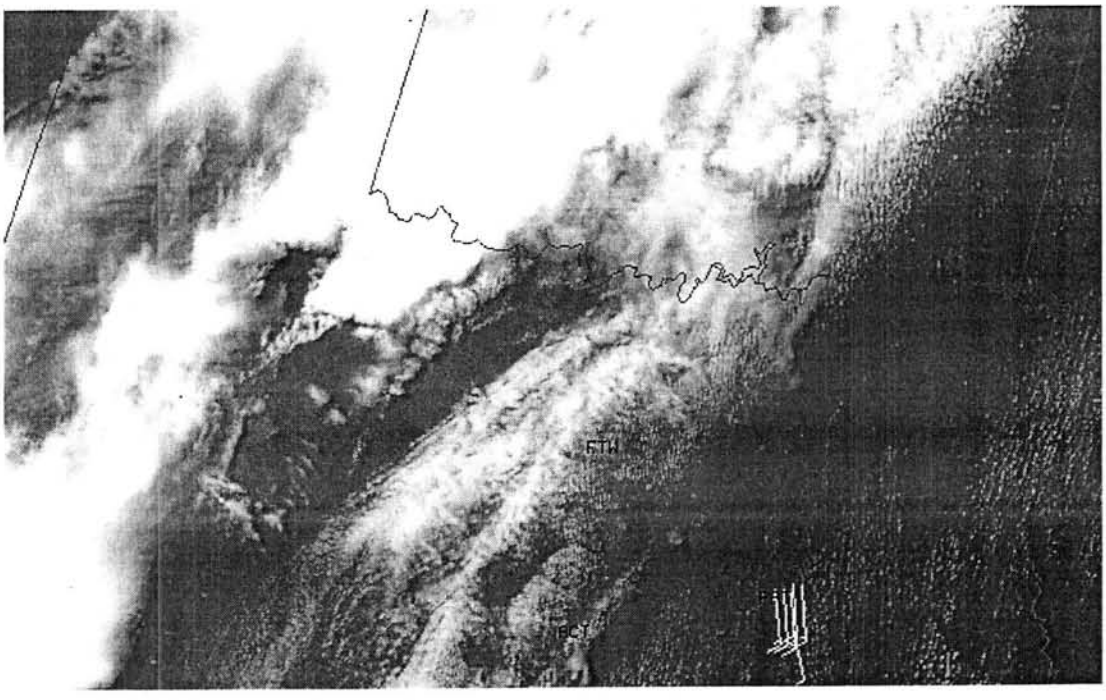

Figure 4-25 Derived 30-minute winds near the PAT profiler (1945-2015Z).

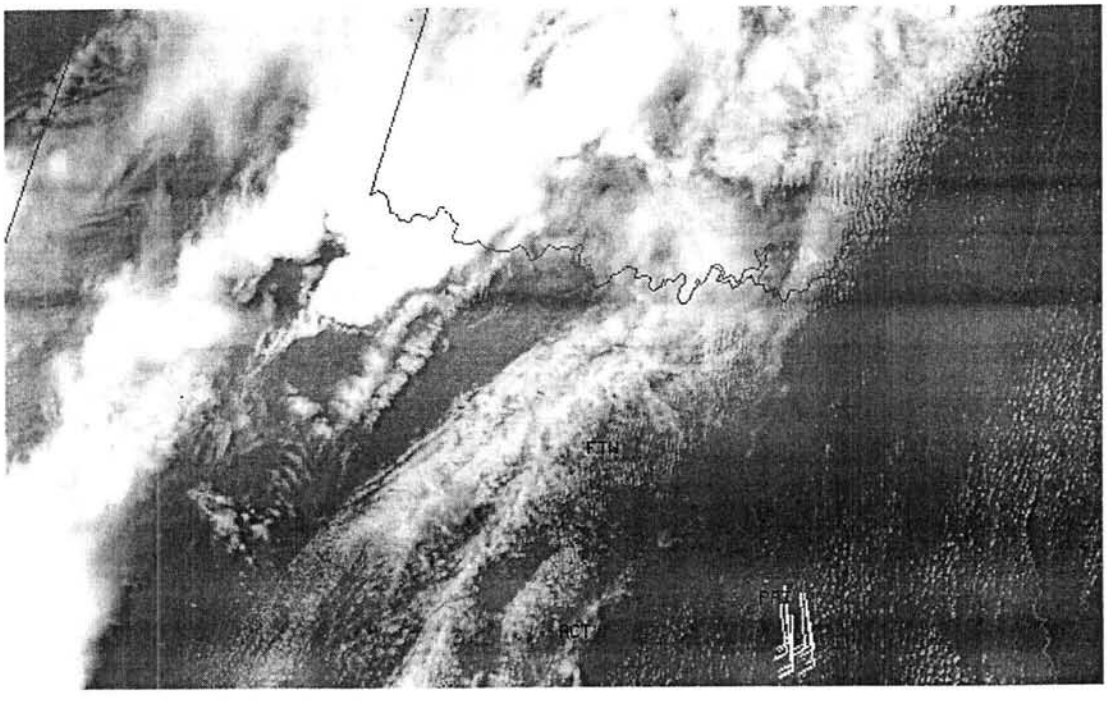

Figure 4-26 Derived 15-minute winds near the PAT profiler (1955-2010Z).

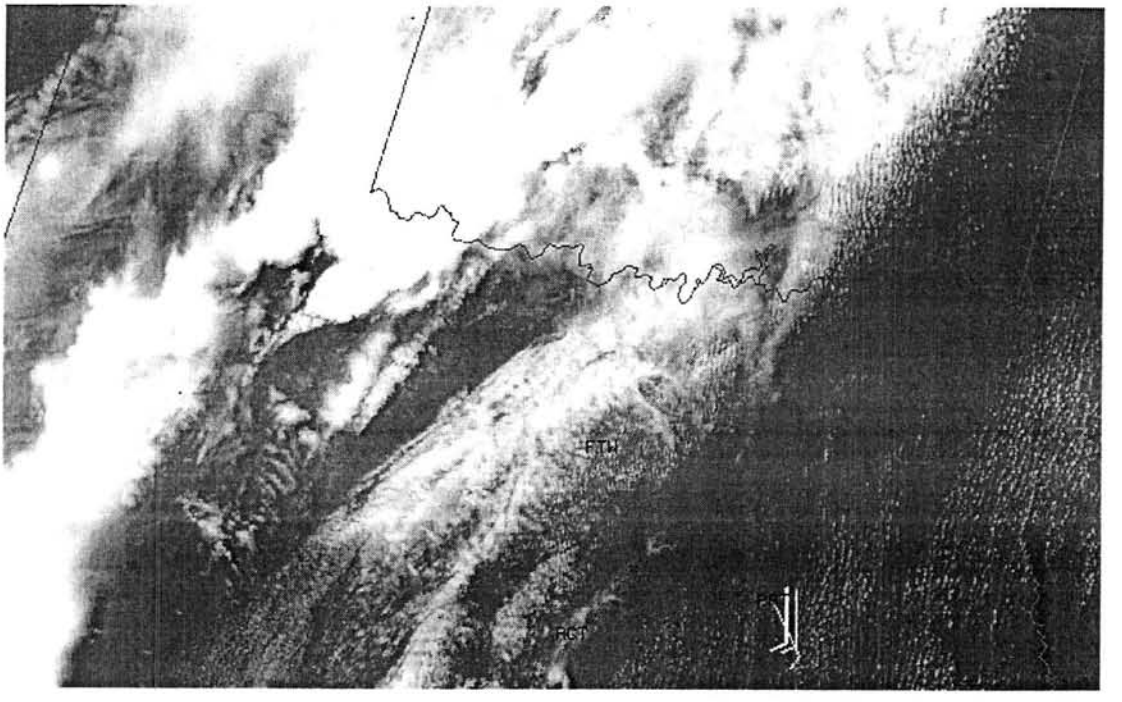

Figure 4-27 Derived 5-minute winds near the PAT profiler (1959-2004Z).

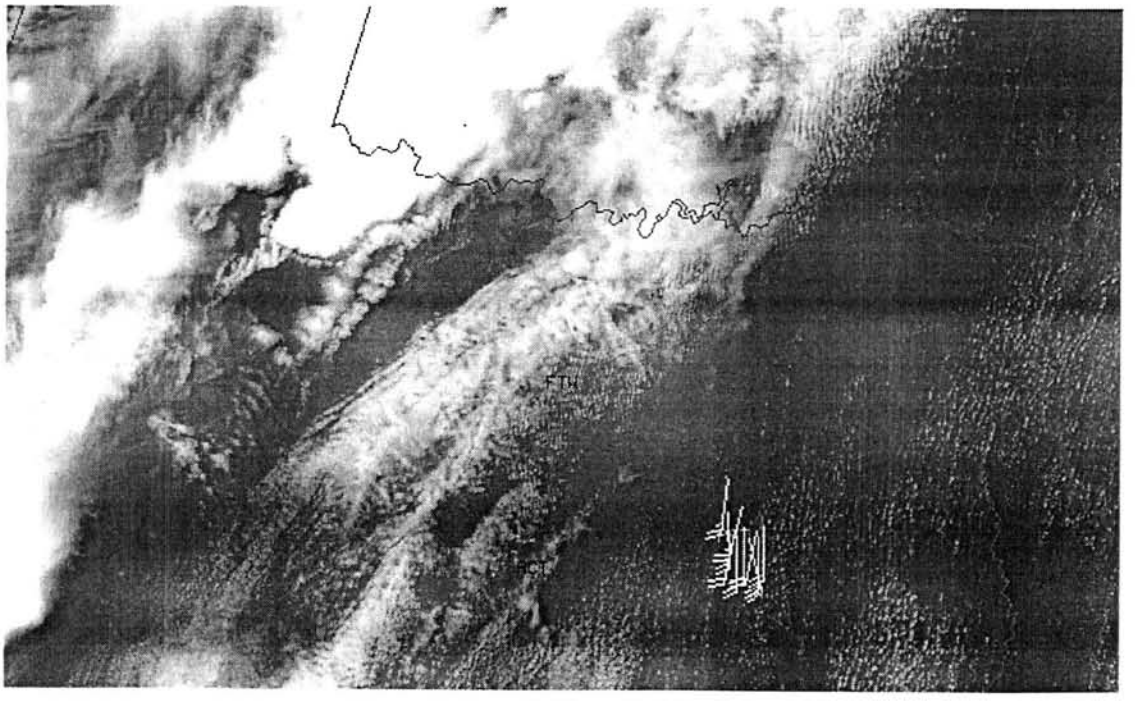

Figure 4-28 Derived 1-minute winds near the PAT profiler (2004-11Z).

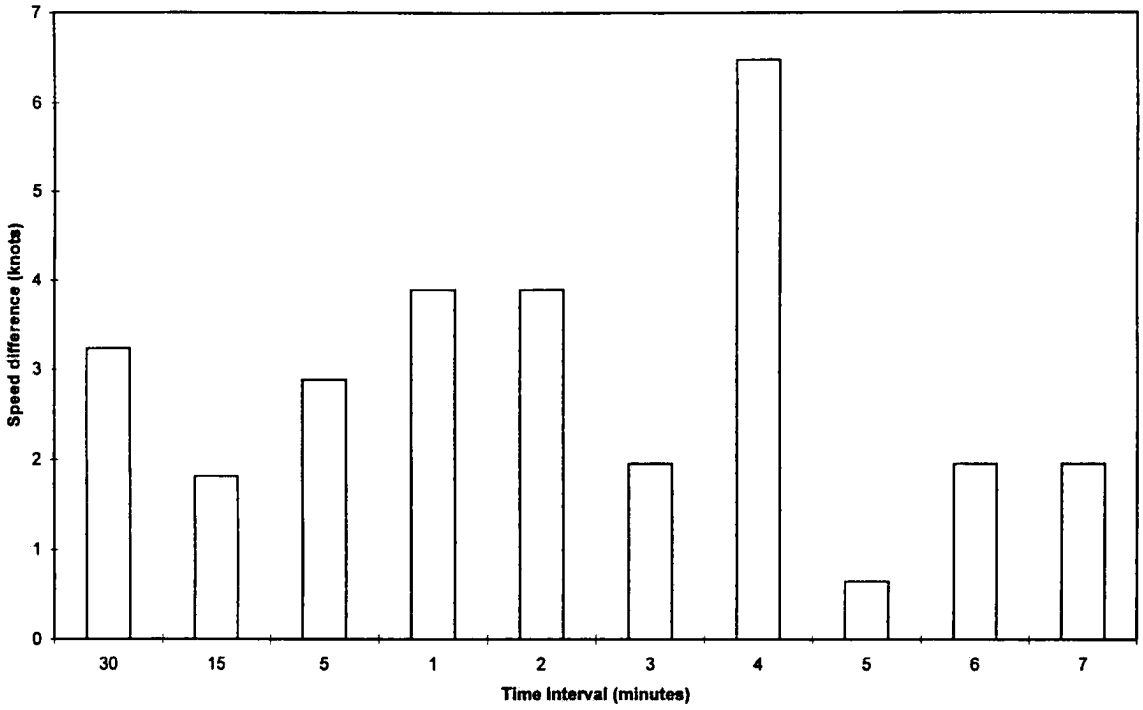

Figure 4-29 Average speed difference compared to 20Z PAT profiler data. Time intervals labeled 1-7 refer to winds derived using an increasing number of one-minute intervals, from 2005-11Z.

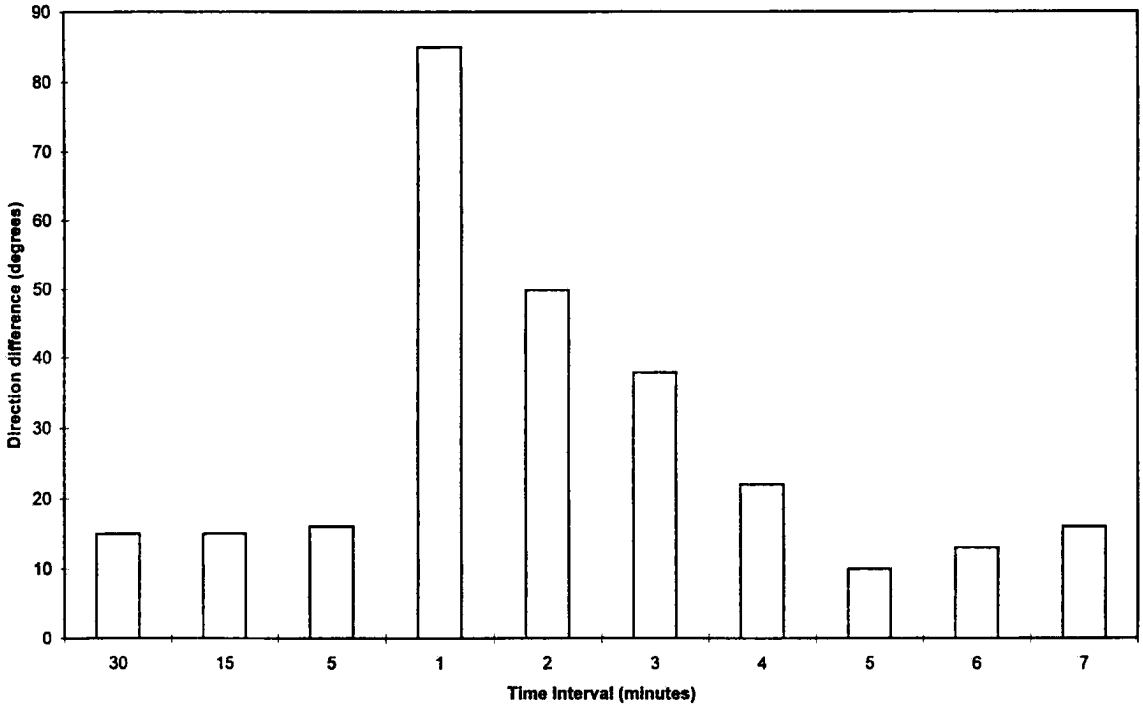

Figure 4-30 Average direction difference compared to 20Z PAT profiler data (same format as above).

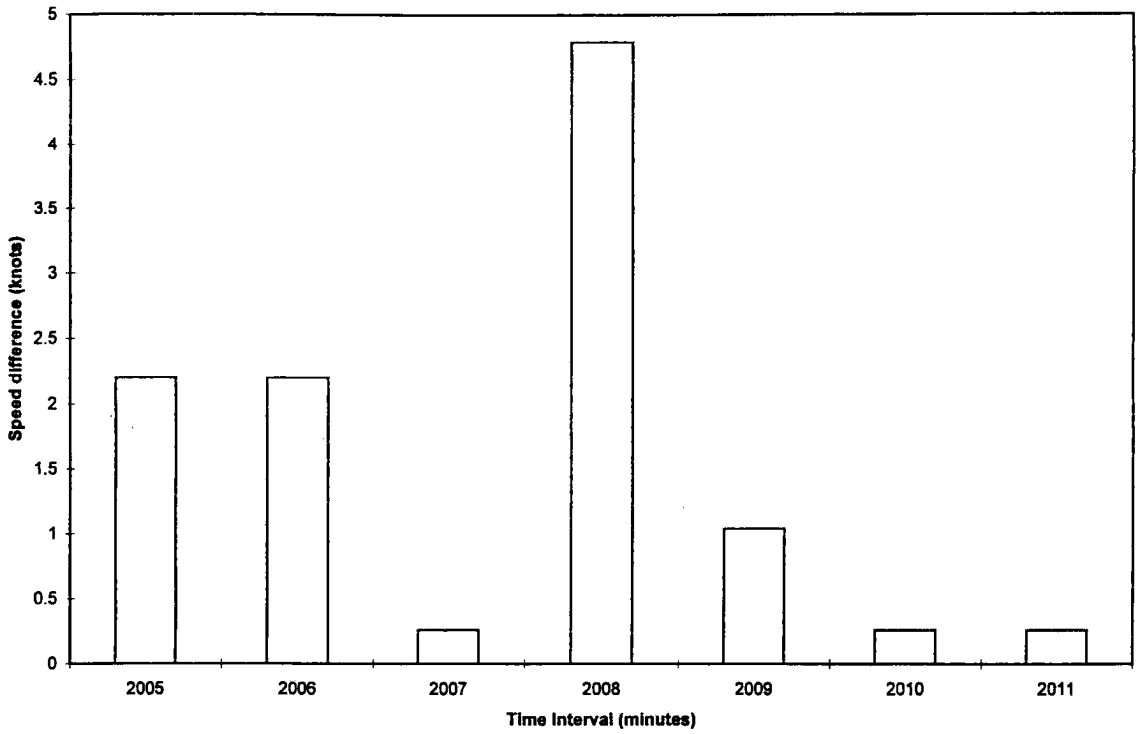

Figure 4-31 Average speed difference of winds derived from an increasing number of 1-minute intervals (2005-11Z) when compared to winds derived using 5-minute data from the same time period (2004-09Z).

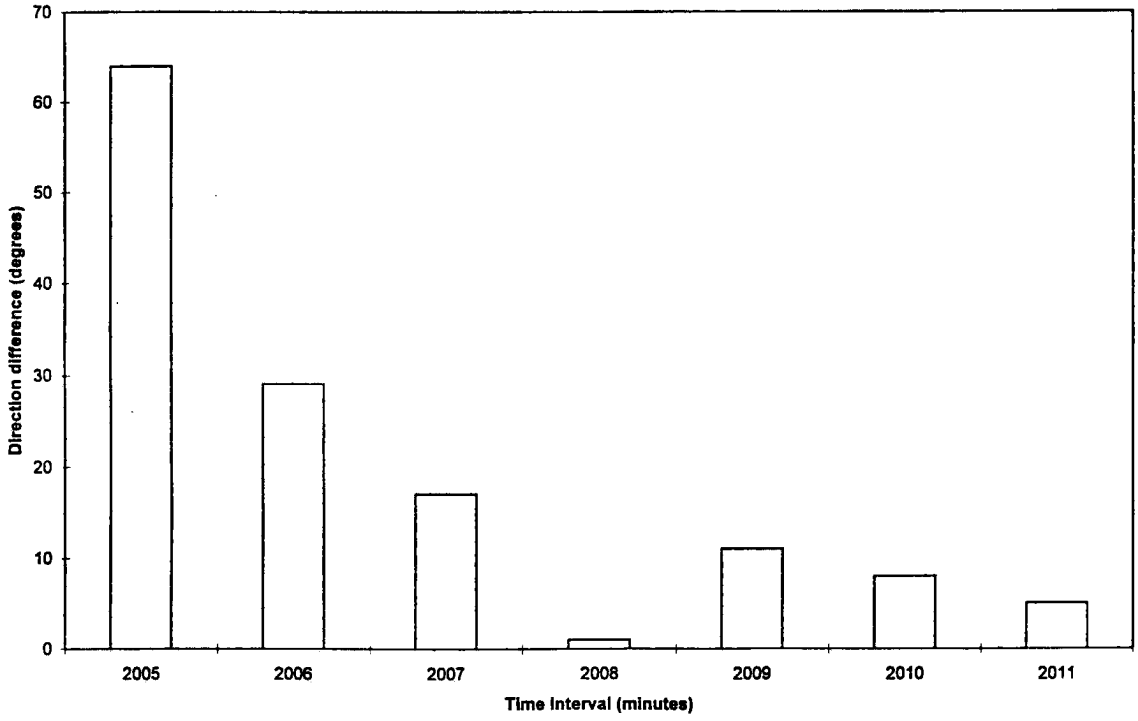

Figure 4-32 Average direction difference (same format as above).

4.4 23 May Outflow Boundary Case

On the same day a series of thunderstorms formed along the Texas-Oklahoma border; imagery detailing their development was taken as part of the VORTEX experiment. Between 2015 and 2045Z an outflow boundary formed south of a large thunderstorm cell near Guthrie, TX and was tracked as it propagated to the southeast. Because of the dynamic nature of this event, 30-minute wind analysis was not possible. Only one 15-minute sequence was tracked because of difficulties in maintaining target continuity, even when using shorter intervals. The boundary's progress was tracked using five-minute interval imagery from its inception at approximately 2015Z until 2045Z, when a cirrus deck from a thunderstorm to the southwest completely obscured the event. Rapidscan imagery was available from 2035-2042Z, and was used as well.

Targets using 15-minute intervals were tracked only during the initial phase (2010-25Z) of the outflow, when winds were slowest and good continuity was still possible. Winds along the length of the outflow boundary averaged 30.23 kts/308°. Five-minute winds within the same area averaged 30.58 kts/310° during that period. Average wind speed slowed to 20.2 kts/292° from 2030-40Z, then increased to 39.6 kts, 308° by 2045Z before the boundary was obscured. Winds along the boundary generally increased northward toward the parent thunderstorm. Just before the outflow boundary was obscured, winds at the southern (outermost) end averaged 33 kts; speeds greater than 50 kts were recorded in the vicinity of the main storm. Figure 4-32 shows the evolution of the flow and derived winds along the boundary as it propagated away from the parent thunderstorm from 2025-2045Z.

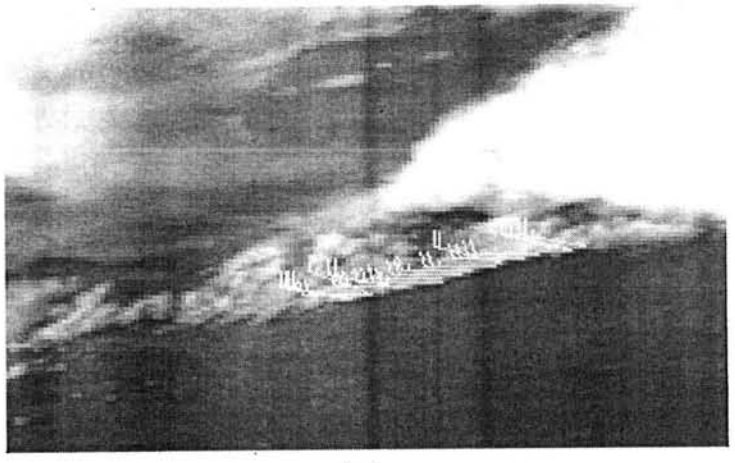

(a)

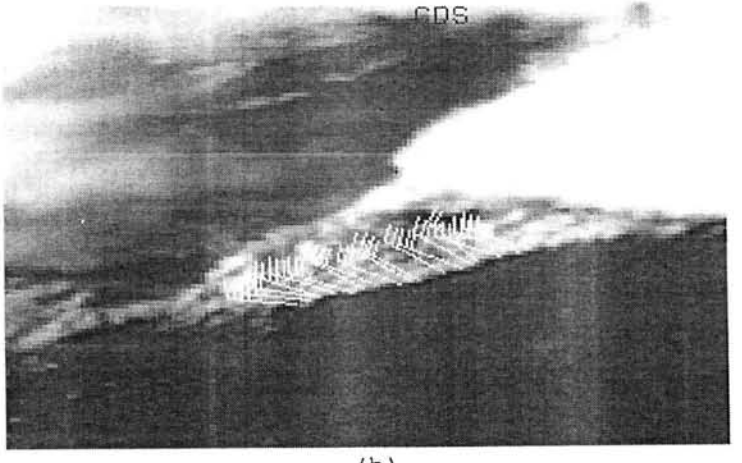

(b)

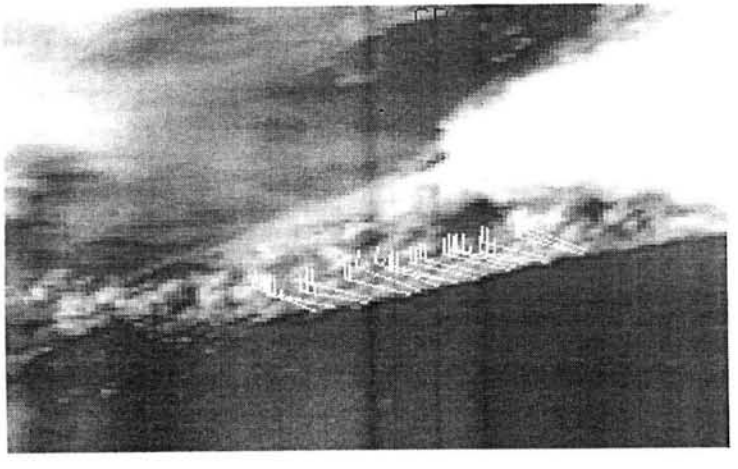

(c)

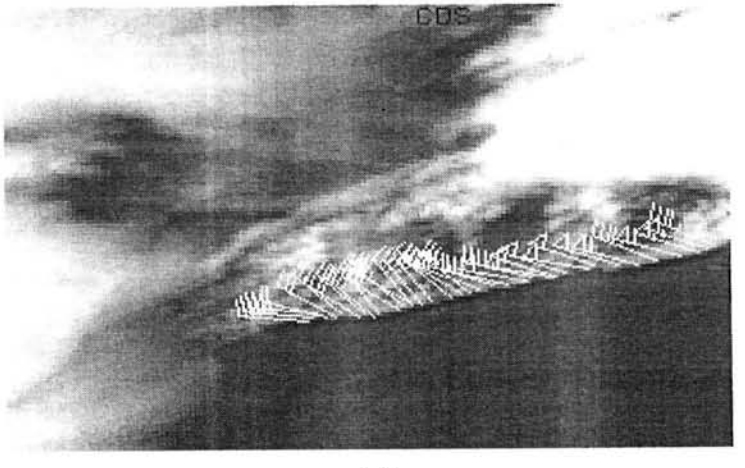

(d)

Figure 4-33 Time-lapse outflow progression, 2030-45Z.

Rapidscan imagery, available from 2035-2042Z, produced a purely westerly flow field; wind direction remained constant at 273°, with speeds ranging from 15-35 knots along the boundary. Average winds derived after five one-minute intervals was 28.52 kts/273°. When compared to average winds derived during the same time frame using five-minute interval imagery (20.74 kts/300°), rapidscan-derived winds were found to be faster and more westerly. As there is no corroborative data available with which to compare this localized mesoscale event, it is impossible to verify which winds are more accurate. It was difficult to maintain accurate continuity even with five minute data, as clouds were changing rapidly as the boundary propagated outward. In this dynamic flow scenario five-minute intervals may have been too long to maintain good target continuity and erroneous vectors were most likely generated. It is reasonable to assume, however, that better continuity was possible using rapidscan image intervals and that winds derived after five one-minute intervals had elapsed are most representative of the flow during that time period.

4.5 31 May 1995 Abilene Case

On this date a large thunderstorm formed over north Texas and moved westward toward Dallas, generating a long outflow boundary. A second thunderstorm later developed along this boundary between Lubbock and Abilene. Winds were tracked in the warm air mass south of the storm and the old outflow boundary as well as near the dynamic inflow area around the thunderstorm. Because of rapid vertical development in the immediate vicinity of the thunderstorm and the boundary, clouds were affected by upper-level flow and not representative. Continuity was maintained using shorter interval imagery as in previous cases.

Winds were plotted using 30-minute data from 1945-2015Z. Five-minute data was again used for continuity. The derived wind field is divided into two general areas, one area to the southeast of the storm, where the flow was generally southerly, and one to the west and southwest of the storm, in an area of more southwesterly flow. The nearest profiler (Jayton, TX) was directly under the thunderstorm for the duration of the event and was influenced by its local mesoscale circulation. Surface observations from San Angelo, TX (SJT), approximately 70 miles south of the storm, were the only corroborative data available for this case. SJT reported winds of 16 kts/180° at 20Z, with scattered clouds at 4000 ft. The 12Z sounding from Midland, 100 miles west of San Angelo, shows cloud base at approximately the same level. Thirty-minute winds are shown in Figure 4-34; near SJT they averaged 7.78 kts/196°. Figure 4-35 shows 15-minute winds during the same period; average winds derived near SJT were 9.88 kts/200°.

Three sets of five-minute winds were derived, using data from 1955-2010Z; an example is shown in Figure 4-36. Average winds around San Angelo were more representative of the reported flow at 15.02 kts/190°, differing by less than a knot. Rapidscan imagery was available from 2004-11Z; after five one-minute intervals, rapidscan data yielded winds in that area of 17.5 kts/193° (Figure 4-37). Figures 4-40 and 4-41 show a comparison of the differences in speed and direction of winds derived using each interval type with the SJT observation. Winds derived from five-minute imagery again showed the smallest difference in both speed and direction. Differences in speed and direction of one-minute winds compared to five-minute winds from the same time period are shown in Figures 4-38 and 4-39.

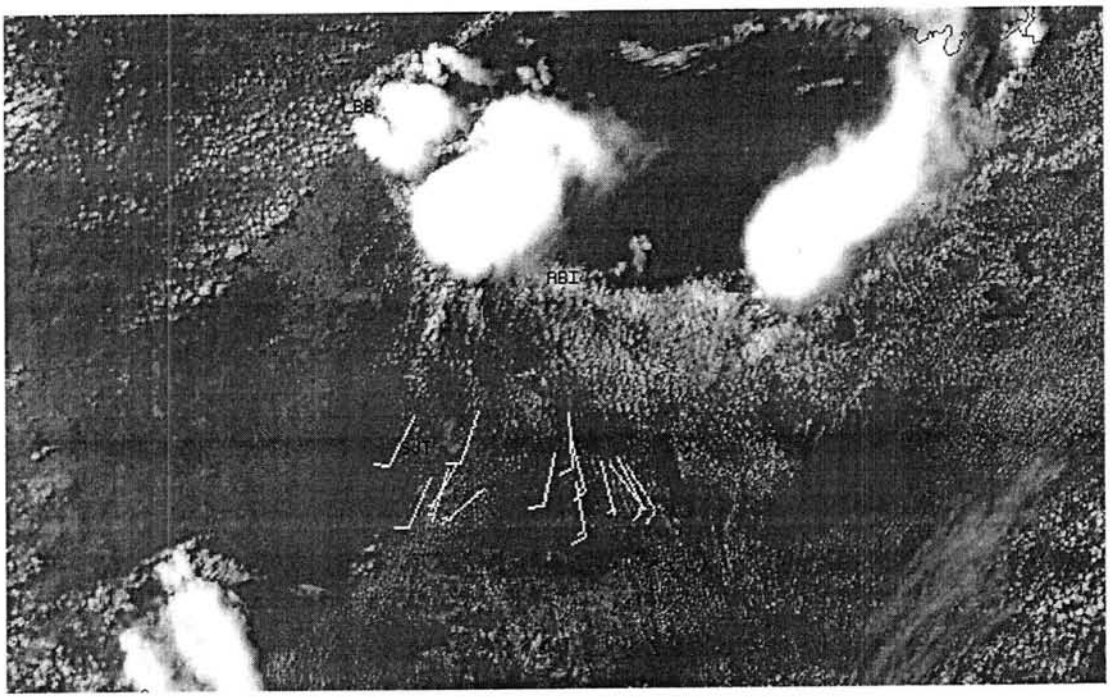

Figure 4-34 Derived 30-minute winds, 31 May 1995 (1945-2015Z).

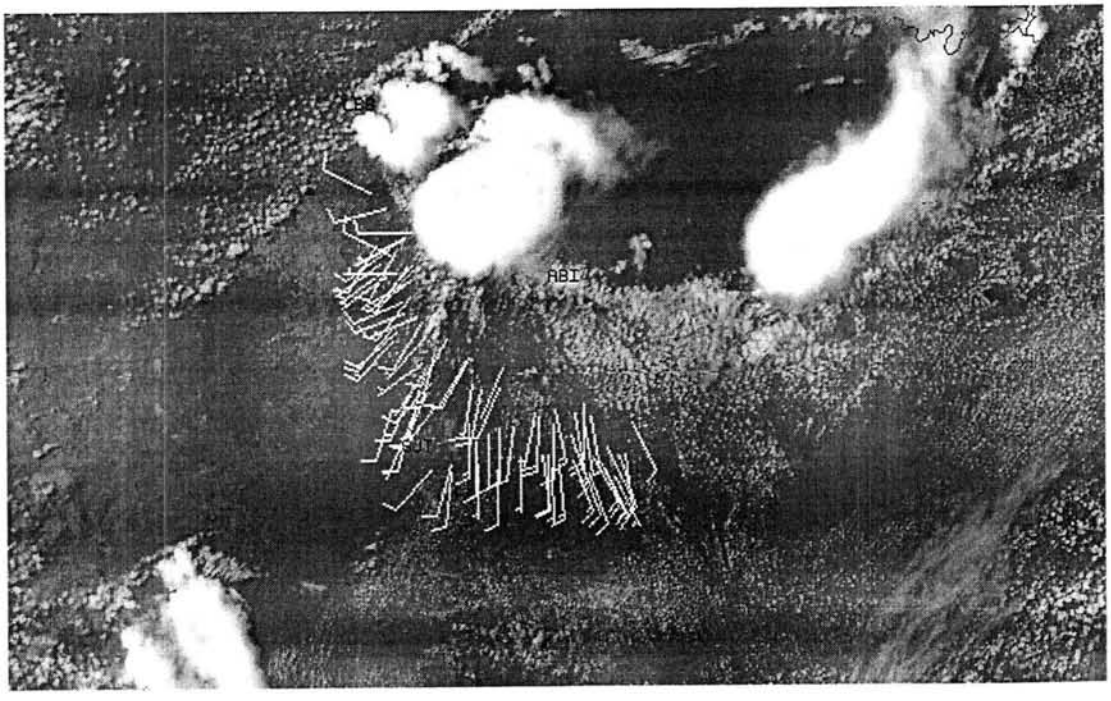

Figure 4-35 Derived 15-minute winds, 31 May 1995 (2000-2015Z).

Winds to the east of the storm (along the southern edge of the outflow boundary) were fairly homogeneous, averaging 8 kts/152° using 30-minute, 9.56 kts/160° with fifteen-minute, and 10.26 kts/166° using five-minute interval imagery. Rapidscan imagery yielded winds of 9.72 kts/165° after five one-minute intervals. Assuming the rapidscan derived winds as ground truth, vector differences using five-minute data are negligible. Low-level winds derived using intervals of five minutes again appear to be the best indicators of flow at that level. This is made more clear when looking at the span of wind speeds and directions derived using longer intervals, which varied from 4-16 knots and by as much as forty degrees within the same geographical area. If rapidscan imagery is available, the higher degree of target continuity made possible using this imagery would result in the best representation of the low-level flow.

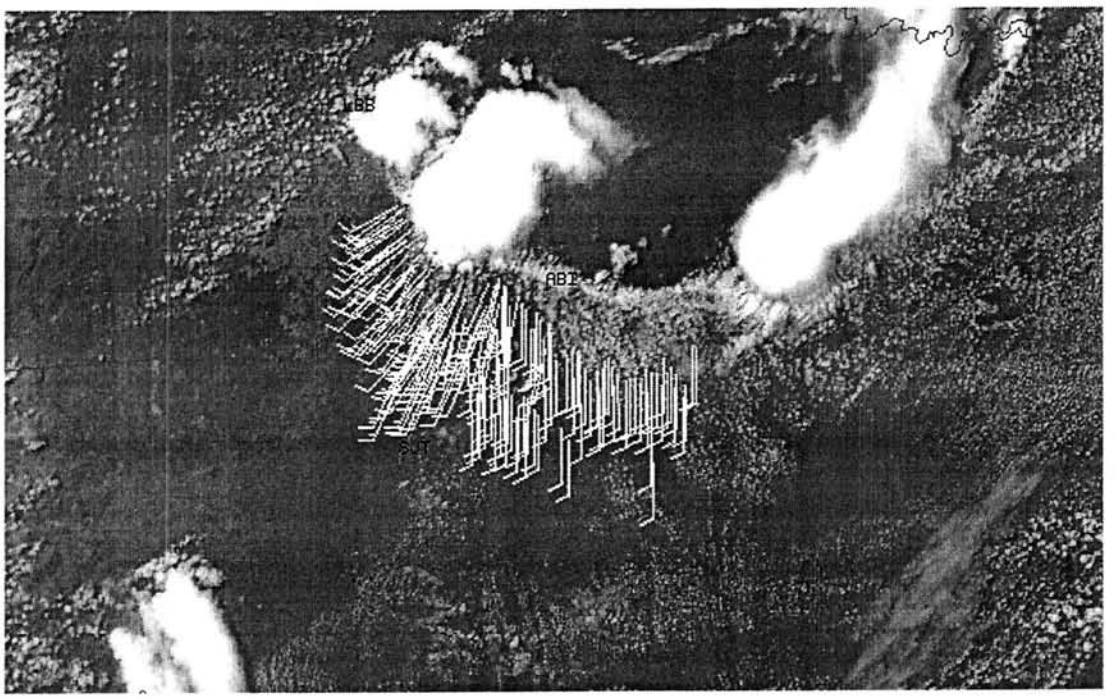

Figure 4-36 Derived 5-minute winds, 31 May 1995 (2000-05Z).

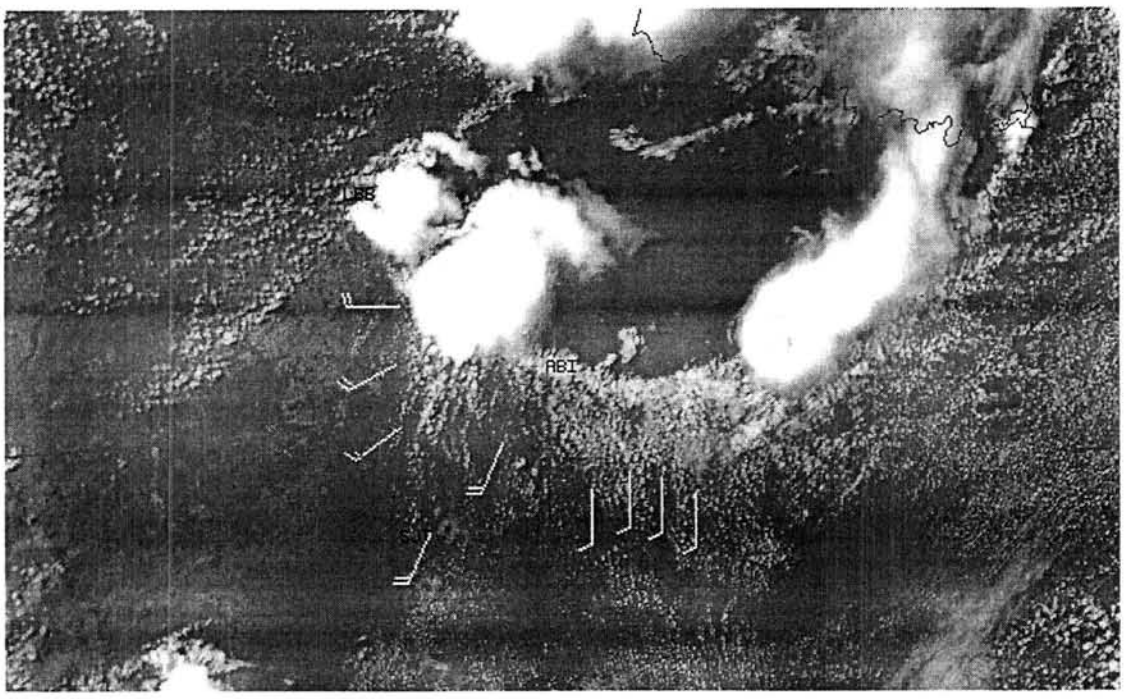

Figure 4-37 Derived 1-minute winds, 31 May 1995 (2004-11Z).

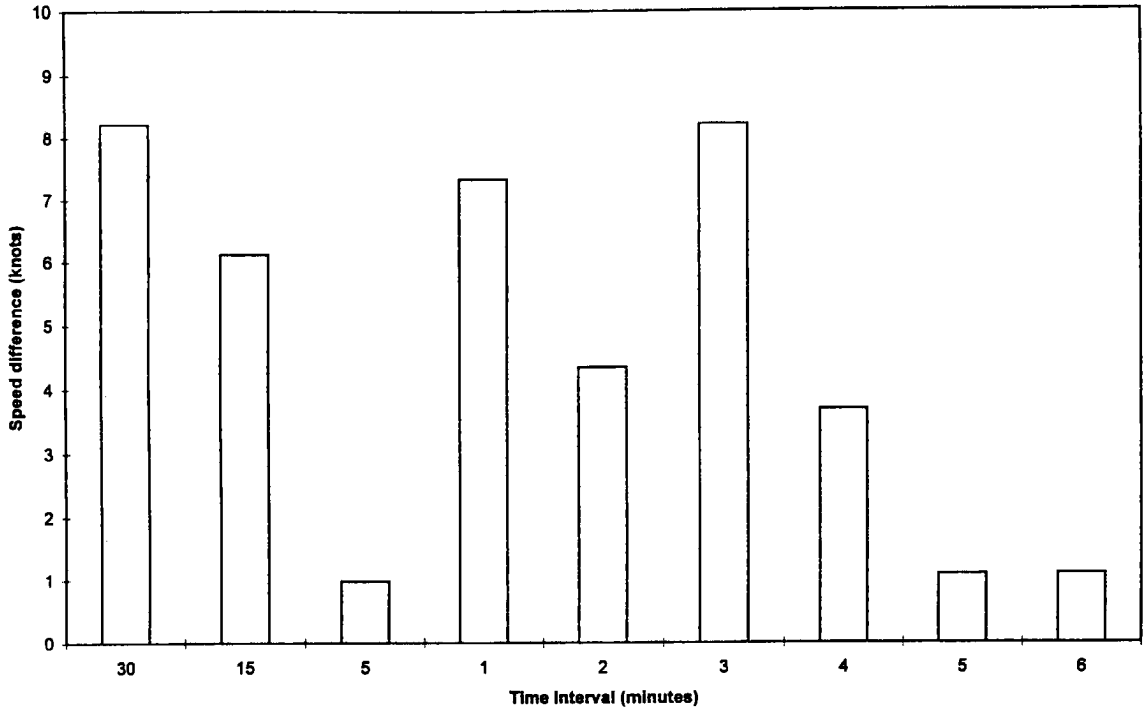

Figure 4-38 Average speed difference compared to 20Z SJT surface observations. Time intervals labeled 1-7 refer to winds derived using an increasing number of one-minute intervals, from 2005-11Z.

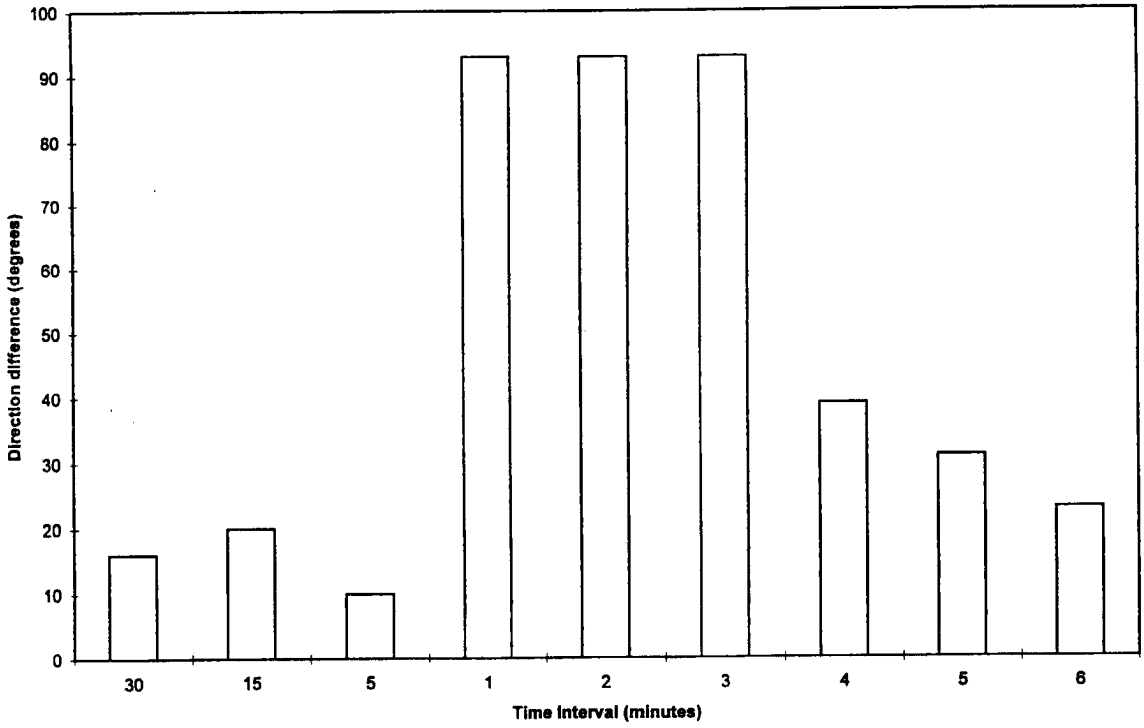

Figure 4-39 Average direction difference (same format as above).

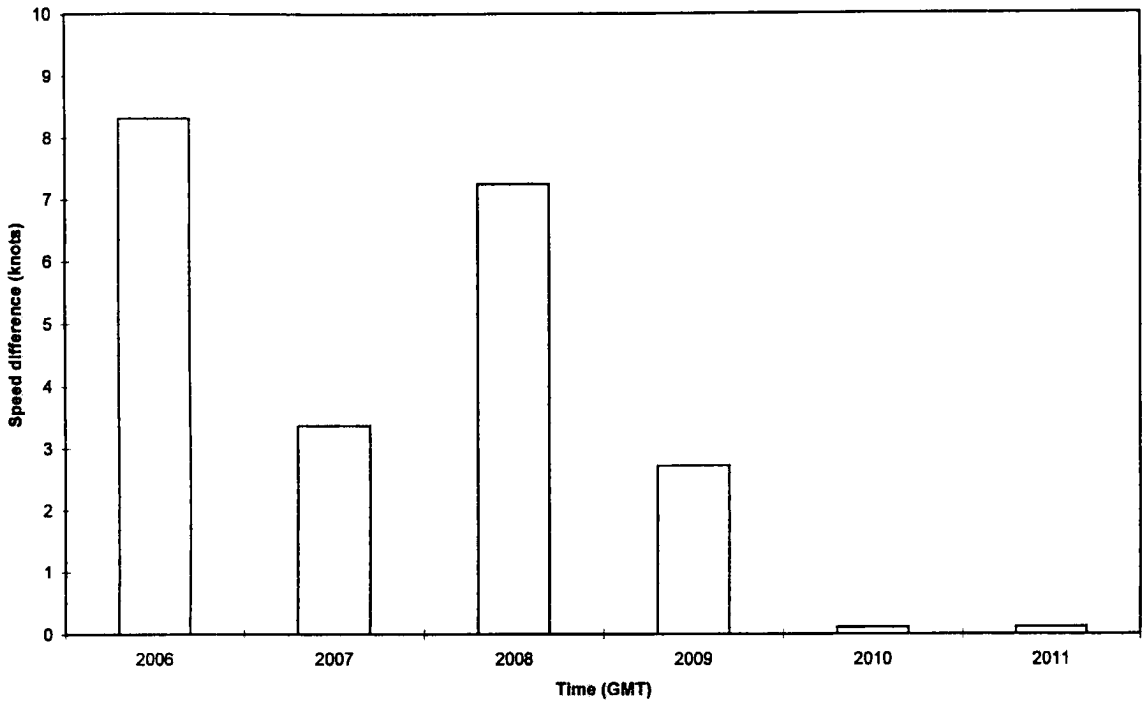

Figure 4-40 Average speed difference of winds derived from an increasing number of one-minute intervals (2005-11Z) when compared to winds derived using 5-minute data from the same time period (2005-10Z).

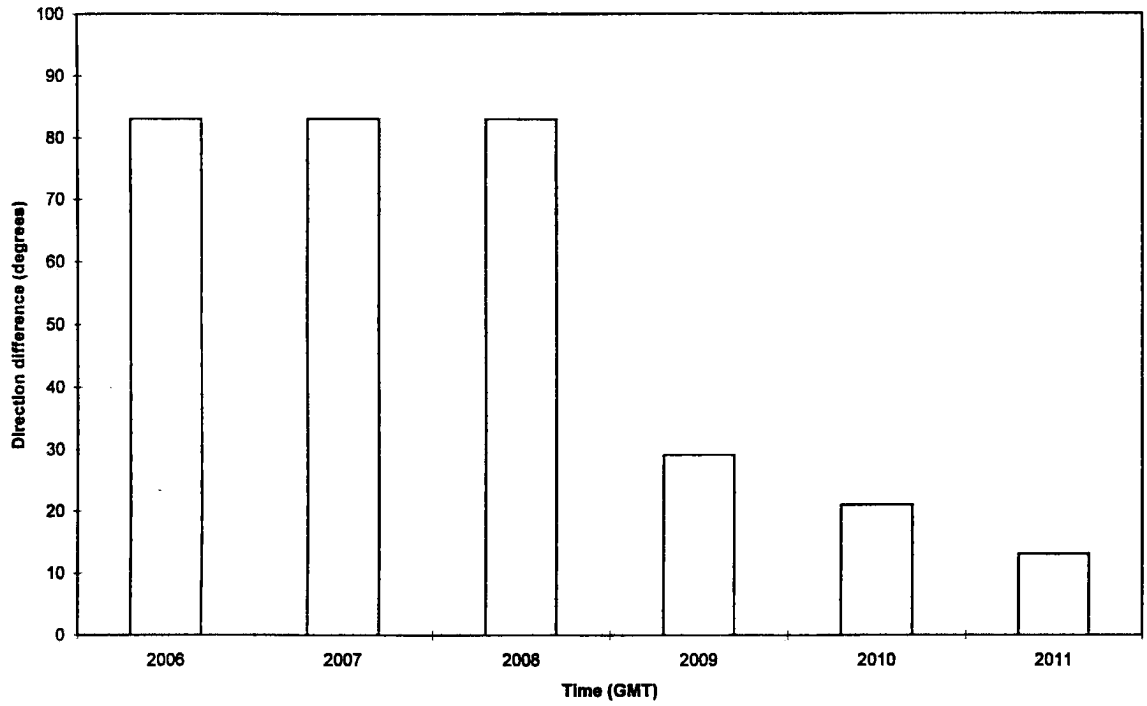

Figure 4-41 Average direction difference (same format as above).

4.6 Error Sources

There are several error sources that make a contribution to total error when plotting winds in the fashion described earlier. These sources include the satellite sensing, processing and transmitting process, the McIDAS WIND program, operator error, improper height assignment, errors in profiler data, and non-systematic cloud motions relative to the flow field (Maddox et al, 1979). Each of these contribute in varying degrees, and are discussed in detail below.

4.6.1 Satellite Error

Although the satellite is three-axes stabilized and has mechanisms designed to eliminate the majority of navigational error, image jogs due to daily attitude adjustments are still present, and are especially evident when rapidscan image sequences are used. These jogs are caused by imperfections in the earth sensor, in navigation software, and in operating procedures (GOES Tech Notes, 1976). Image shear due to east-west scanline assembly errors was also evident in several cases; these areas were avoided when tracking winds. Although the imagery was renavigated as closely as possible using the McIDAS navigation algorithm, image jitter was still present in most cases. Figure 4-42 shows the frequency distribution of speed error averaged over all sets of 1-minute interval derived winds. If the image jitter were oscillatory and non-biased, a normal distribution centered about zero would be expected. This does not appear to be the case. However, round-off error (discussed in the following section) is greatest in the wind derived from the first interval. Figure 4-43 shows a more normal distribution after the first interval is omitted; after smoothing a Gaussian distribution is readily distinguishable (Figure 4-44).

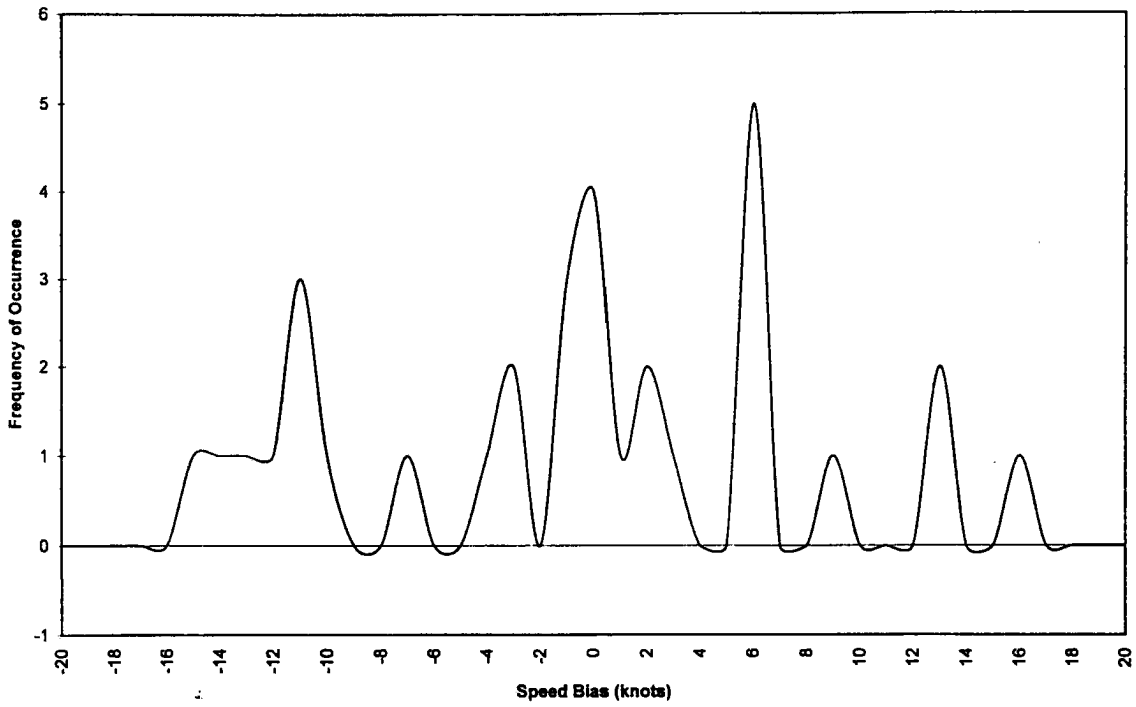

Figure 4-42 Frequency distribution of averaged speed differences from one-minute interval sets using all seven intervals.

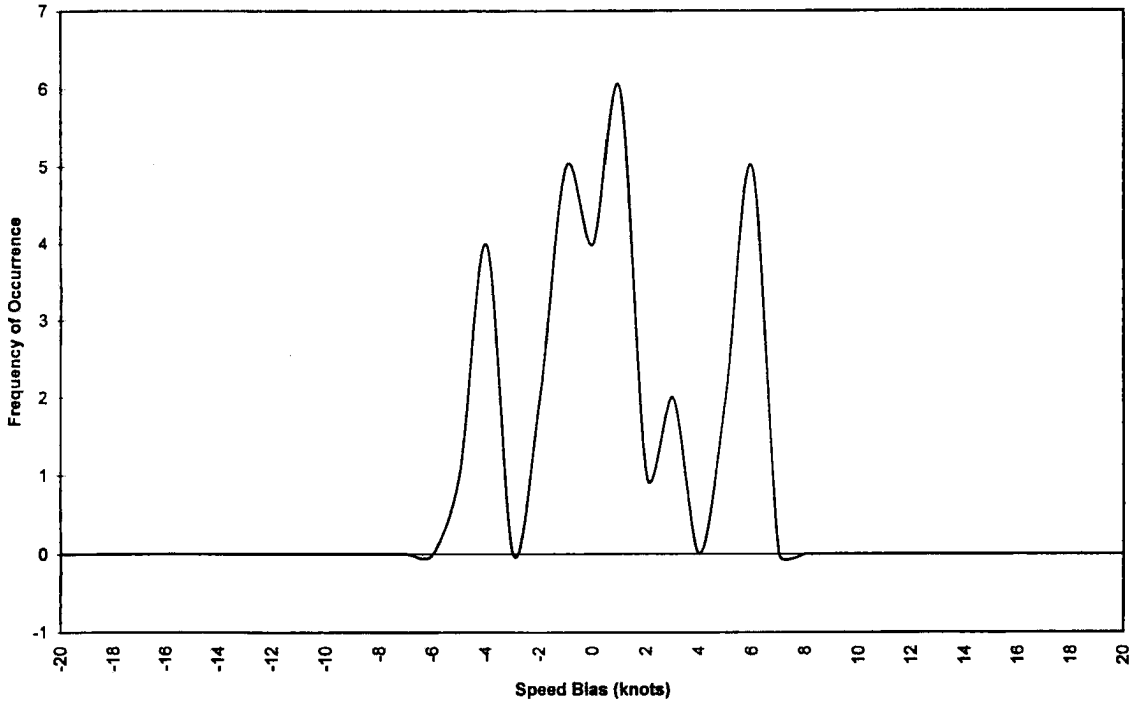

Figure 4-43 Frequency distribution when first interval is omitted.

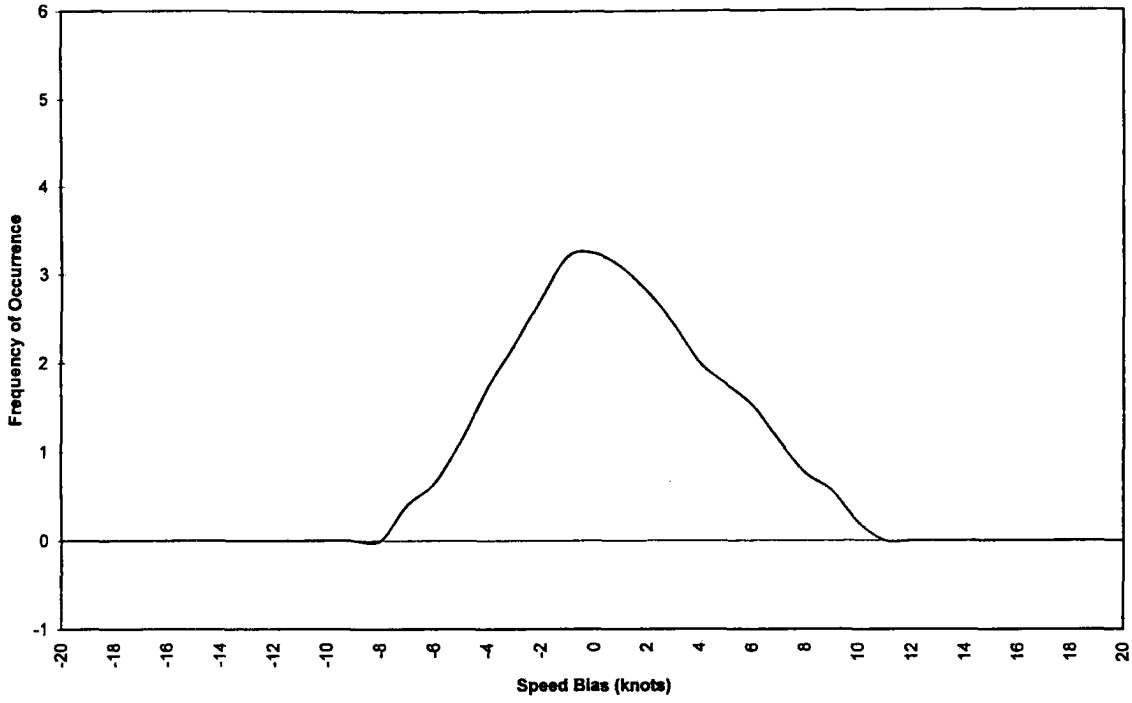

Figure 4-44 Frequency distribution after smoothing.

The error due to image jitter thus does not appear to introduce a noticeable bias. Errors due to this effect could be considered to at least partially cancel each other and behave as random error. Errors due to image jitter appear largest when plotting slow moving clouds using one-minute image intervals, as they can cause clouds to appear to move orthogonal to the actual flow from one image to the next.

4.6.2 McIDAS WIND Program Round-off Error

Round-off errors are introduced due to limitations of the WIND program, especially in slow-moving wind fields. If a cloud is moving such that its position is recorded as moving only one pixel between successive images, the program then has a maximum of eight possible pixels available to derive wind direction. As the temporal interval is increased, the number of possible pixels into which the cloud can move

increases as $(2n+1)^2$. Faster-moving clouds would be less affected by round-off errors; shorter intervals between images could be used and round-off error minimized.

4.6.3 Operator Error

The WIND program in manual mode is entirely within the control of the operator; errors can therefore be introduced due to operator inexperience in identifying appropriate targets and/or maintaining accurate target continuity. The best measure of operator error due to inaccurate continuity is to compare derived winds using five-minute interval imagery versus those derived from the same targets using five one-minute intervals over the same time period. Operator error due to inaccurate continuity using 5-minute data was measured at 0.6 kts. This is consistent with error estimates determined by Peslen (1980).

4.6.4 Errors Due to Improper Height Assignment

Errors in height assignment cause large problems, especially in more dynamic situations, because of vertical wind shear, which is greatest near regions of active weather (Merrill, et al., 1991). Since clouds tracked in this study were of limited horizontal extent, precise vertical location of resultant vectors was troublesome. Determination of cloud height with infrared techniques was not possible; infrared data resolution is too coarse to identify clouds of this size. As mentioned earlier, cloud targets were chosen based on the size of the shadow cast as well as the similarity of brightness values to other chosen cloud targets to minimize errors in height assessment. Cloud heights were inferred from nearby surface and upper-air observations; wind vectors were generally within the 850-900 mb level.

4.6.5 Non-Systematic Cloud Motion Error

This error concerns clouds whose movements may not approximate the mean flow. Targets were chosen which displayed little horizontal change or vertical growth during the tracking period; errors due to shear at differing levels was then minimized. Clouds believed affected by external mesoscale influences (proximity to a large storm, e.g.) or by topography were not used. Error measurements for this problem were not possible and as such their magnitude is unknown.

It should be noted that the last three error types have major random components and will often cancel each other. Even with all errors accounted for, resultant cloud-track winds are not truly a direct measurement of the wind field. Clouds are not always passive tracers, their location may be in areas not representative of the wind field, and their motion may represent a layer-mean flow rather than a wind vector at one specific level (Schmetz, et al., 1993). These considerations must be taken into account when assigning heights to derived wind fields.

4.6.6 Errors in Profiler Data

Profiler data used for this study were averaged hourly values taken from stations in the NOAA Wind Profiler Demonstration Network (WPDN), part of a 31-station network covering most of the central U.S. The profilers operated on a frequency of 404 MHz in low-altitude mode; winds are measured every 250 m beginning 500 m AGL to a maximum height of 9.25 km (Schlatter and Zbar, 1994). WPDN radars sense small fluctuations in atmospheric refractive index caused by turbulent mixing of air with different temperature and moisture contents using Doppler shift. The amount of shift is proportional to the air motion relative

to the radar. In the low-altitude mode, mean wind differences in u and v from radiosonde data obtained at the same location averaged -0.1 ms^{-1} and -0.45 ms^{-1}, respectively (Martner, et al., 1993). Most of this variability is likely due to real differences in the winds between the profiler sample area and the moving radiosonde. Studies have shown that more than 97% of profiler measurements accurately represent tropospheric winds (Schlatter and Zbar, 1994).

4.7 Temporal Interval Comparison

Speed and direction differences compared with surface observations for each case were averaged and the results shown in Figures 4-45 and 4-46. As expected, speed accuracy improves as the temporal interval decreases to five minutes. Directional accuracy was also greatest when five-minute imagery was used. Using rapidscan imagery for continuity and deriving wind vectors after five one-minute intervals have elapsed would likely yield the most representative low-level winds in situations of variable mesoscale flow. It can be seen that low-level derived wind vectors are somewhat useful in inferring the surface wind, to within 3 kts/10° when five-minute interval imagery is employed.

When compared to hourly profiler data (Figures 4-47,48), average speed difference is less for all image interval types, indicating again that low-level cloud-drift winds are more representative of flow at cloud base. Accuracy generally increased as shorter temporal intervals were used; the larger differences noted using five-minute data versus five one-minute data intervals is likely due to continuity errors and natural wind variability. The ability to place the pixel as close to the same point on the cloud after each image interval was greatly enhanced with rapidscan data.

Profiler data derived from six-minute radial velocity samples would likely be a better source of comparative data when plotting variable winds. However measurement errors due to spurious radar targets or other phenomena, which are flagged but not deleted, could produce erroneous verification. Overall, five-minute imagery appears to be well suited for determining accurate low-level winds in both dynamic and more static flow fields. The use of one-minute data for purposes of continuity would limit continuity errors and produce even more representative wind fields.

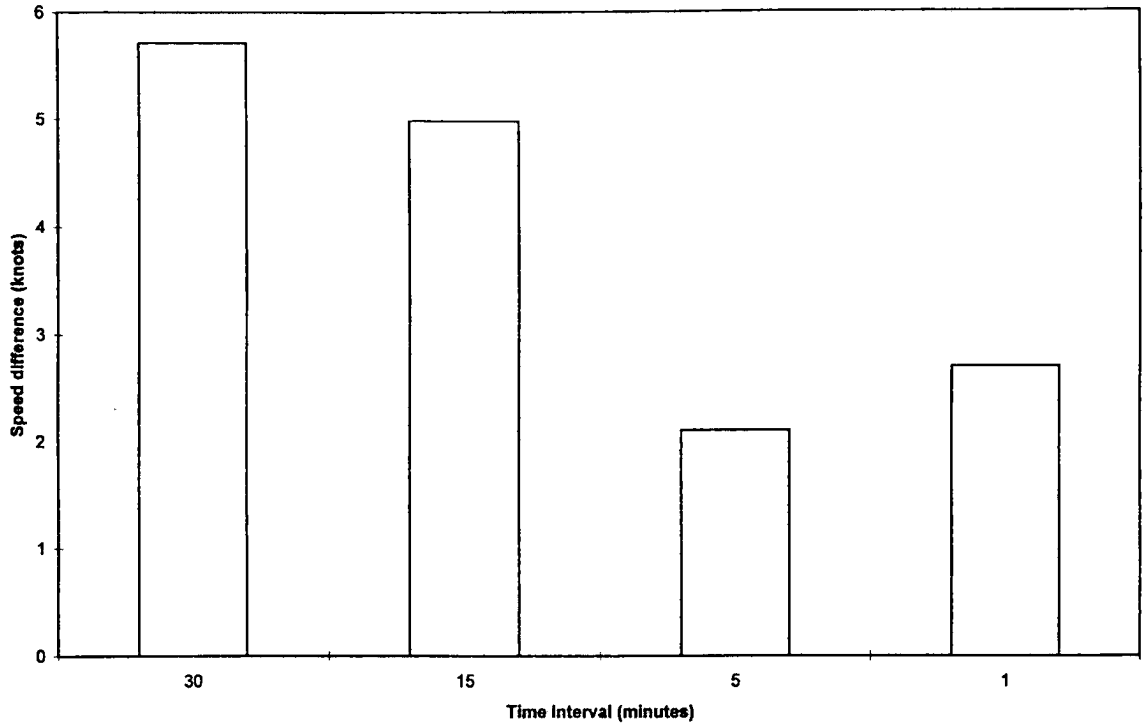

Figure 4-45 Average speed difference of all derived winds when compared to surface observations. Winds derived using 1-minute data are given after five one-minute intervals have elapsed.

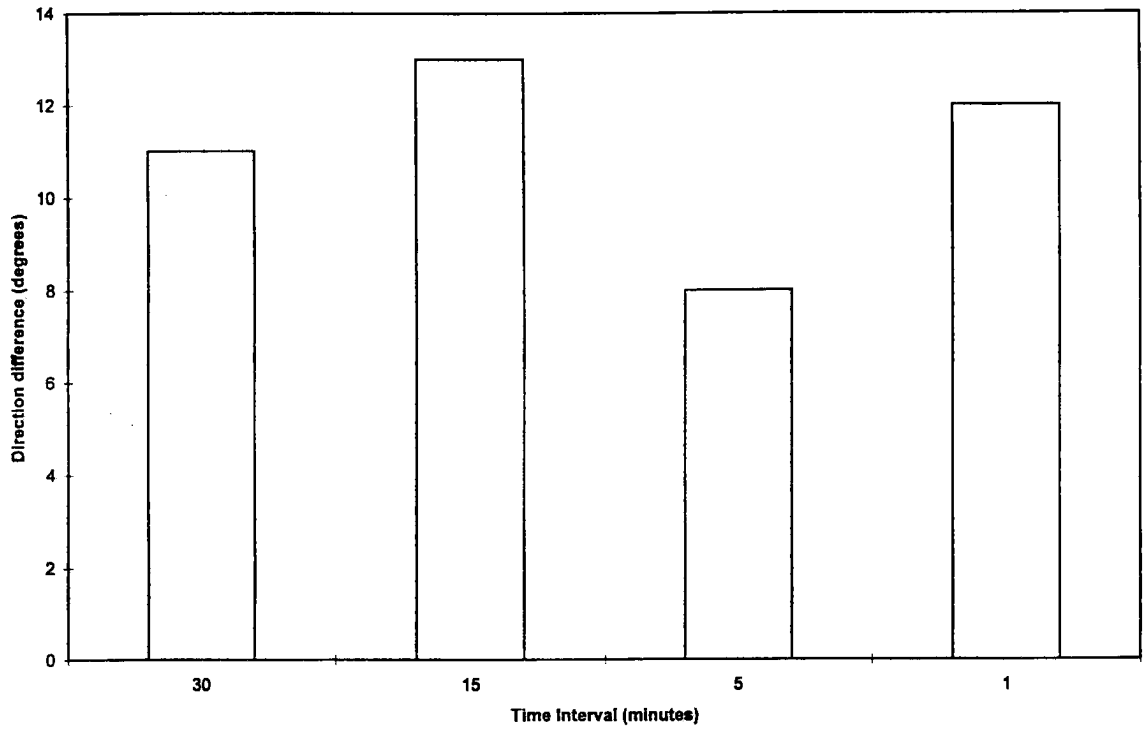

Figure 4-46 Average direction difference (same comparison as above).

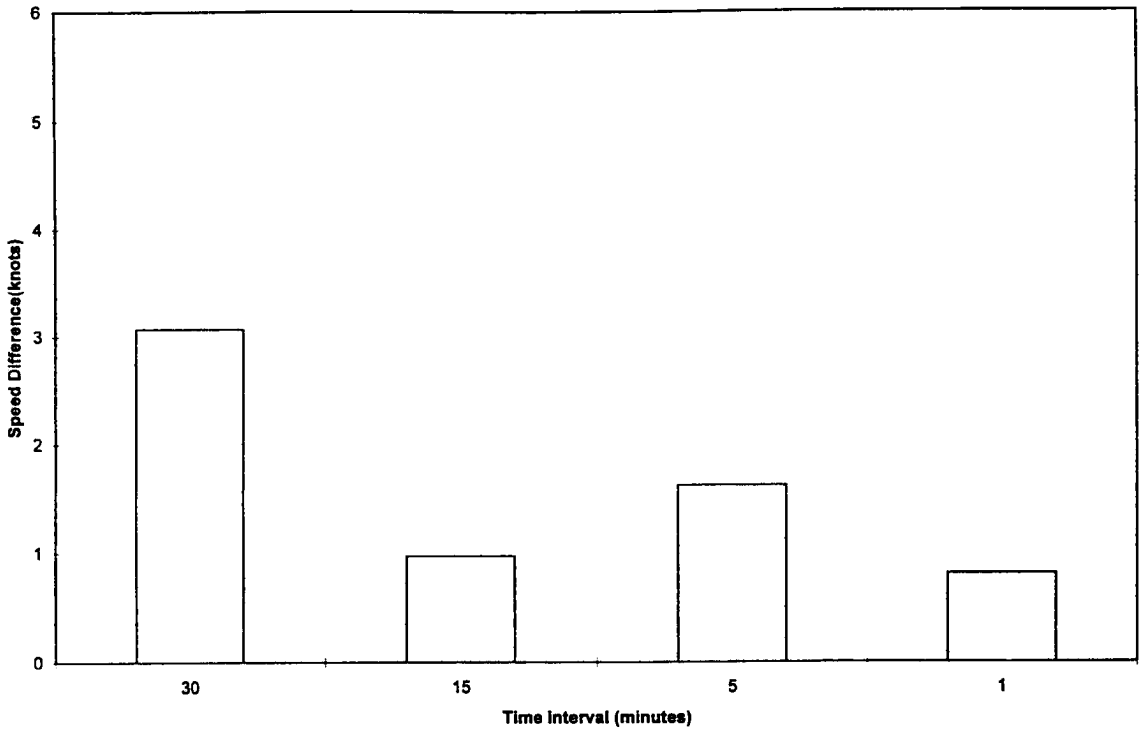

Figure 4-47 Average speed difference of all derived winds when compared to profiler data. Winds derived using 1-minute data are given after five one-minute intervals have elapsed.

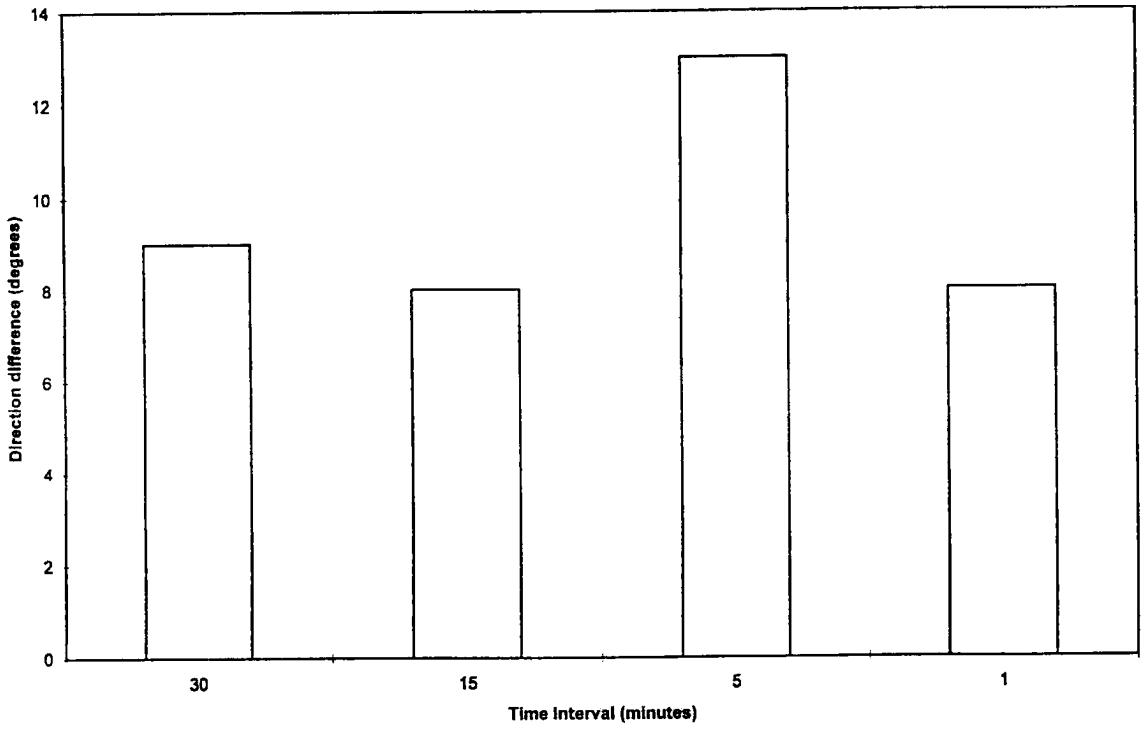

Figure 4-48 Average direction difference (same comparison as above).

5.0 Mesoscale Divergence Fields

5.1 Conventional Computation Scheme

Divergence fields derived from satellite determined wind velocities have an advantage over those derived using surface observations in three ways: the spatial density of the winds is increased greatly, the vectors represent an average of the mean flow instead of an instantaneous observation, and the winds are less likely to be influenced by topography or friction (Negri, et al., 1980). Inability to accurately determine cloud height, however, leads to possible errors in determining divergence. The assumption that the cloud motions tracked were representative of the winds at one level allows an objective analysis of divergence from derived wind fields. This is used to relate divergence/convergence patterns to the formation (or lack thereof) of severe thunderstorms.

Divergence fields were computed for the 31 May Abilene case, the only one for which winds were plotted over a geographical area large enough to create a non-trivial field. Divergence was calculated using one 15-minute data set, consisting of 150 vectors, and two 5-minute data sets of 200-300 vectors each. Divergence is calculated by a program on McIDAS, using vector components from the data files.

Figure 5-1 shows the wind field derived using 5-minute data during the period 2000-05Z. To properly analyze divergence wind vectors were necessary on both sides of the outflow boundary. No cloud targets were available for tracking on the northern side of the boundary, so winds

were approximated and dubbed in based on the 20Z Abilene surface observation of 16 knots. Vectors matching this speed and orthogonal to the boundary approximate the wind field at cloud base level.

A divergence field using 5-minute data is shown in Figure 5-2. The field was computed using intervals of 0.1° between analyzed wind vectors. Contour intervals of $100x10^{-6}$ s^{-1} were used for purposes of clarity. Maximum convergence ($5.0x10^{-4}$ s^{-1}) is noted at the base of the thunderstorm, as expected. Divergence calculated using intervals of 0.3° and 0.5° between vectors are shown in Figures 5-3 and 5-4, respectively. Figure 5-5 shows the wind field derived from 15-minute data for the period 2000-15Z, as well as the same dubbed-in winds north of the boundary. Divergence fields were again calculated using the same intervals described above; results are shown in Figures 5-6 through 5-8. Streamlines were derived for both data sets using McIDAS; the results are shown in Figures 5-9/10. Streamline convergence is occurring south of the central and eastern part of the boundary due to the lack of vectors plotted in close proximity to the southern side. Vorticity fields were also derived; resulting fields are shown in Figures 5-11/12.

Although the data fields used for this study were quite detailed with hundreds of vectors plotted for each interval, useful results could likely be achieved with several tens of vectors plotted over a similar area. The outflow boundary in this case was approximately three degrees longitudinally. A rough divergence field could be produced, for example, using intervals of 0.5° between vectors, with as little as several tens of vectors. This could be done in minimal (~30 minutes) time and would provide a valuable tool for forecasting convergence-enhanced convective activity.

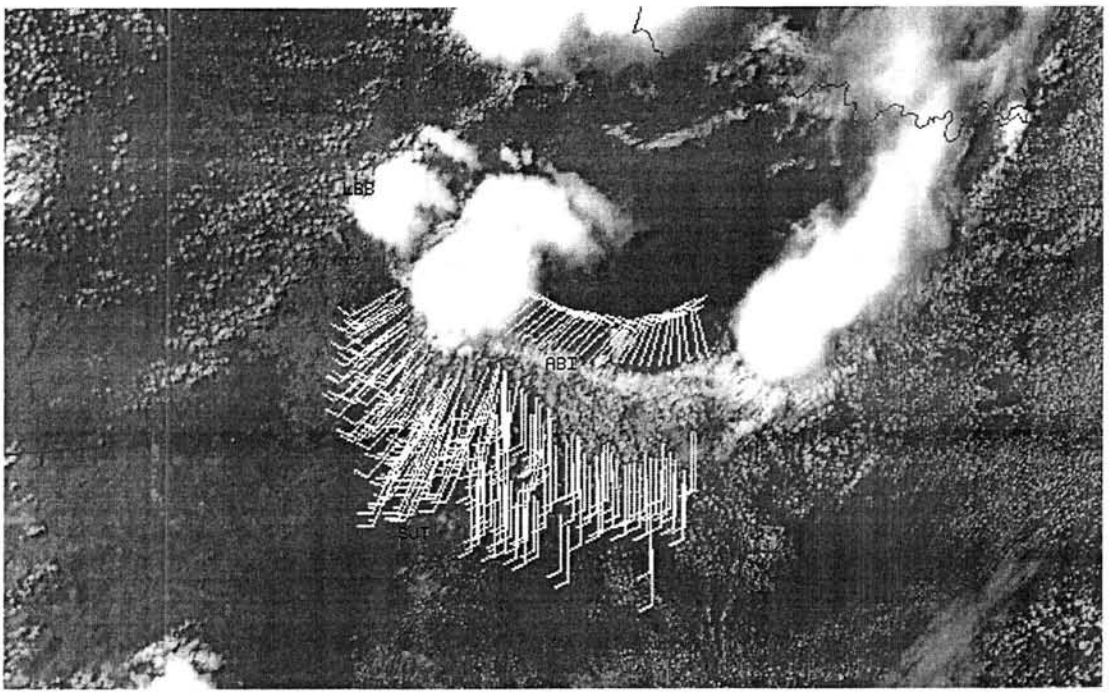

Figure 5-1 Derived 5-minute winds near ABI thunderstorm, 31 May 1995 (1959-2004Z). Winds plotted north of the boundary are dubbed in and are based on surface observations from Abilene, TX at 2000Z.

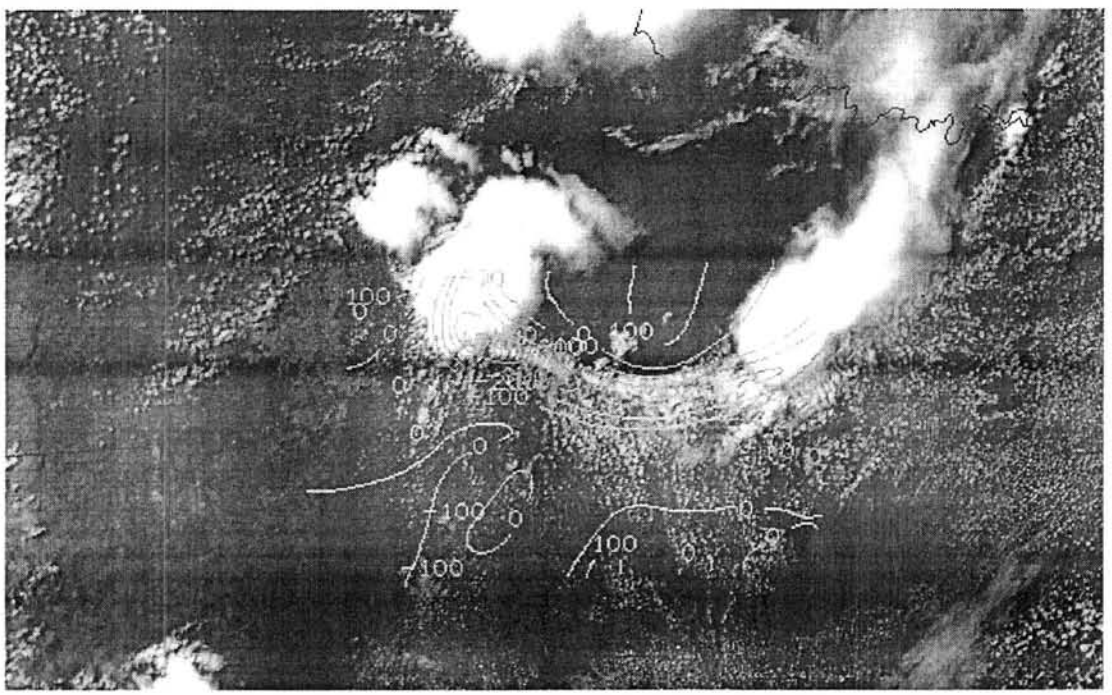

Figure 5-2 Divergence field generated using intervals of 0.1° between analyzed (5-minute) wind vectors. Units are 10^{-6} s^{-1}.

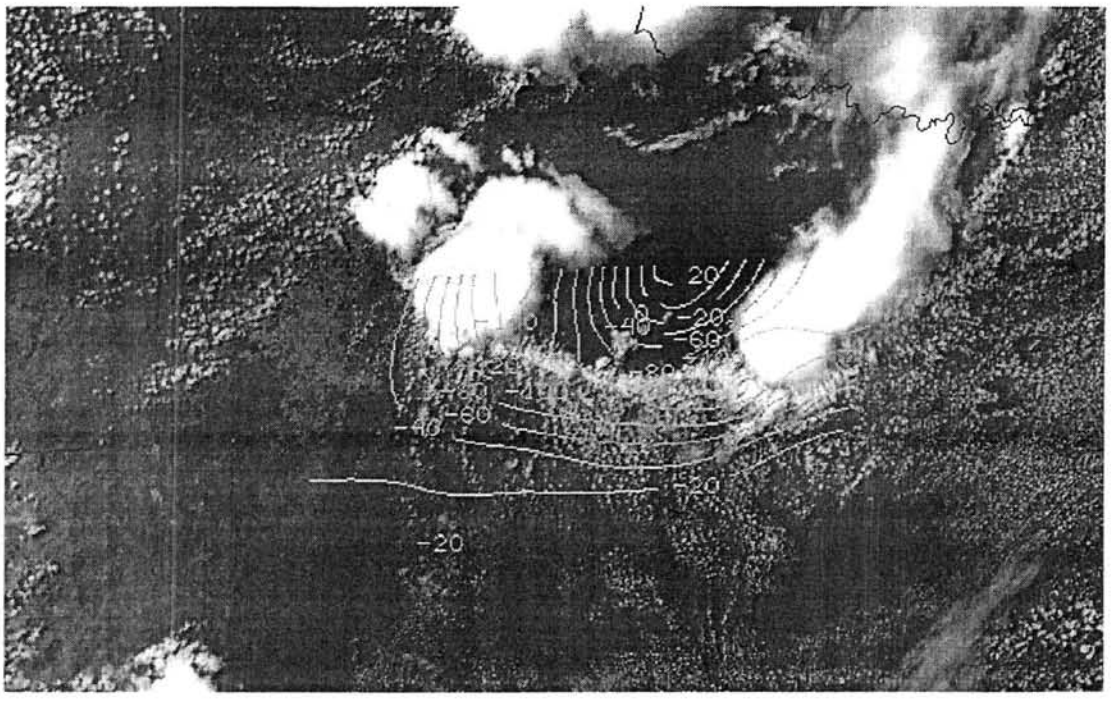

Figure 5-3 Divergence field generated using intervals of 0.3° between analyzed (5-minute) wind vectors. Units are 10^{-6} s^{-1}.

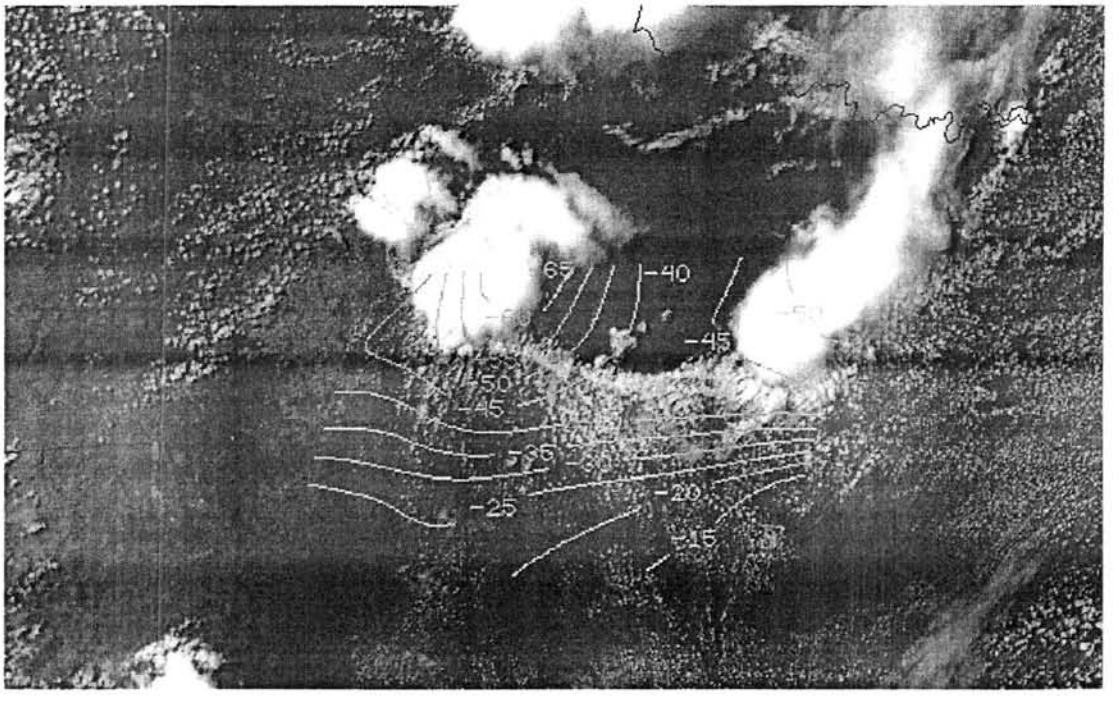

Figure 5-4 Divergence field generated using intervals of 0.5° between analyzed (5-minute) wind vectors. Units are 10^{-6} s^{-1}.

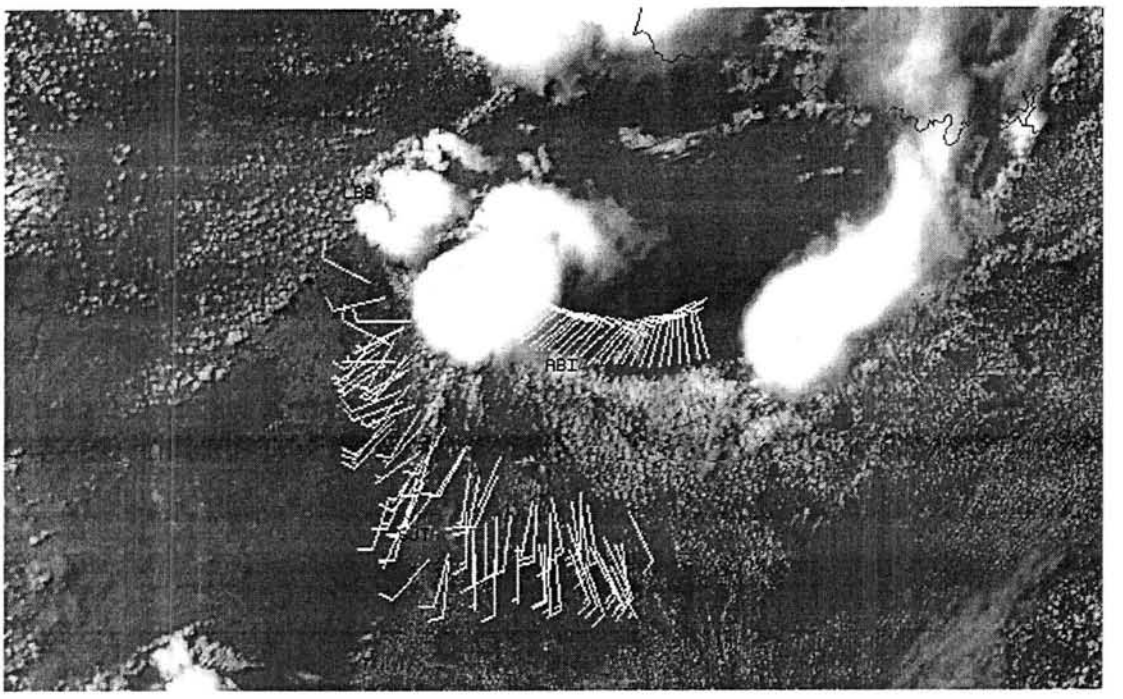

Figure 5-5 Derived 15-minute winds near ABI thunderstorm, 31 May 95 (1959-2015Z). Winds plotted north of the boundary are dubbed in and are based on surface observations from Abilene, TX at 2000Z.

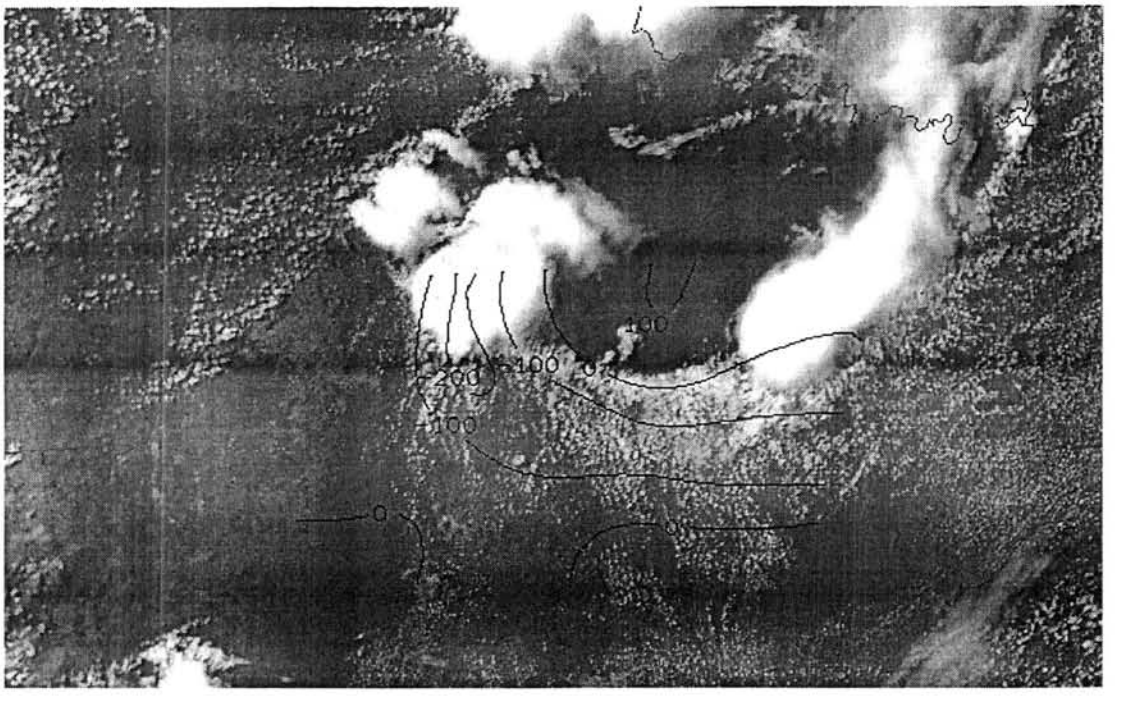

Figure 5-6 Divergence field generated using intervals of 0.1° between analyzed (15-minute) wind vectors. Units are 10^{-6} s^{-1}.

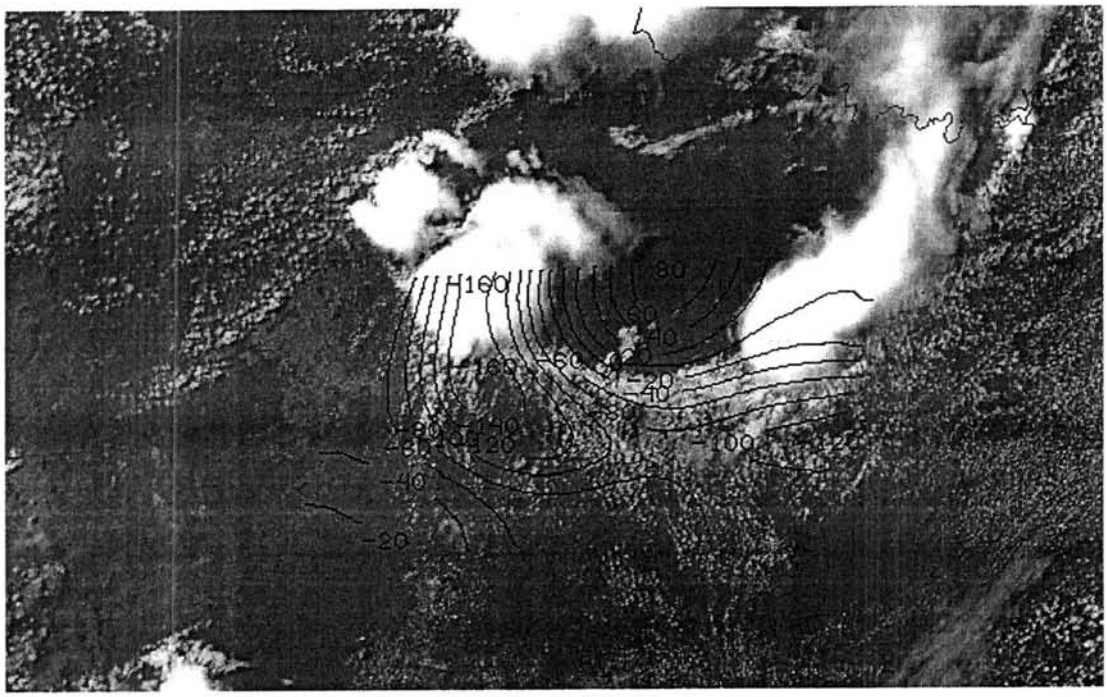

Figure 5-7 Divergence field generated using intervals of 0.3° between analyzed (15-minute) wind vectors. Units are 10^{-6} s^{-1}.

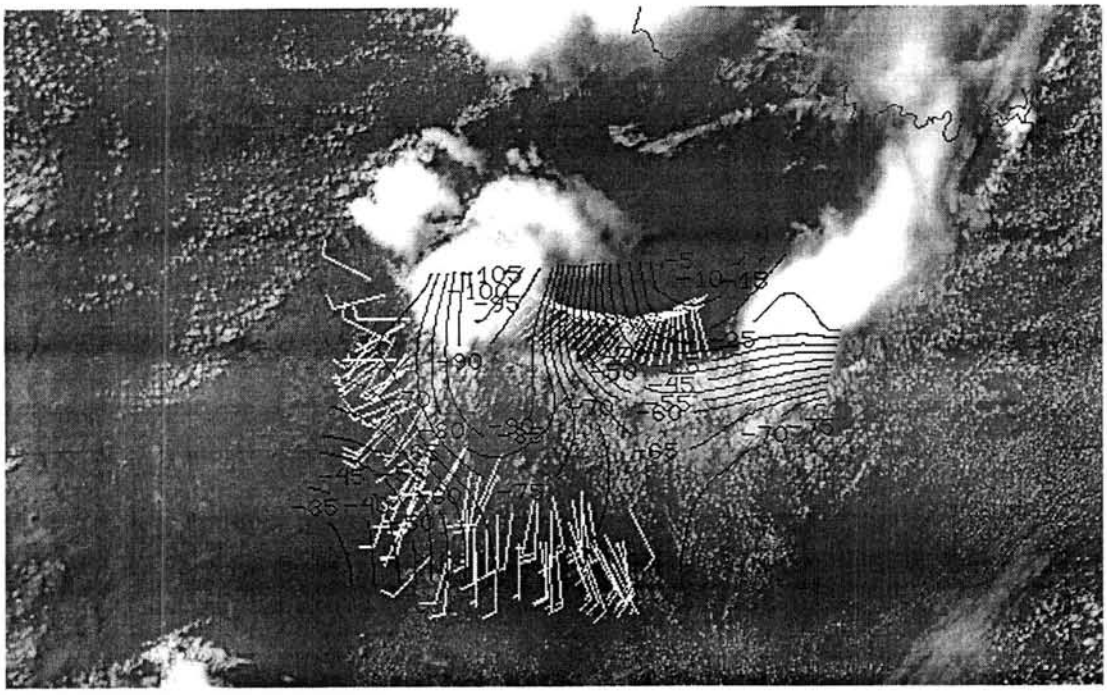

Figure 5-8 Divergence field generated using intervals of 0.5° between analyzed (15-minute) wind vectors. Units are 10^{-6} s^{-1}.

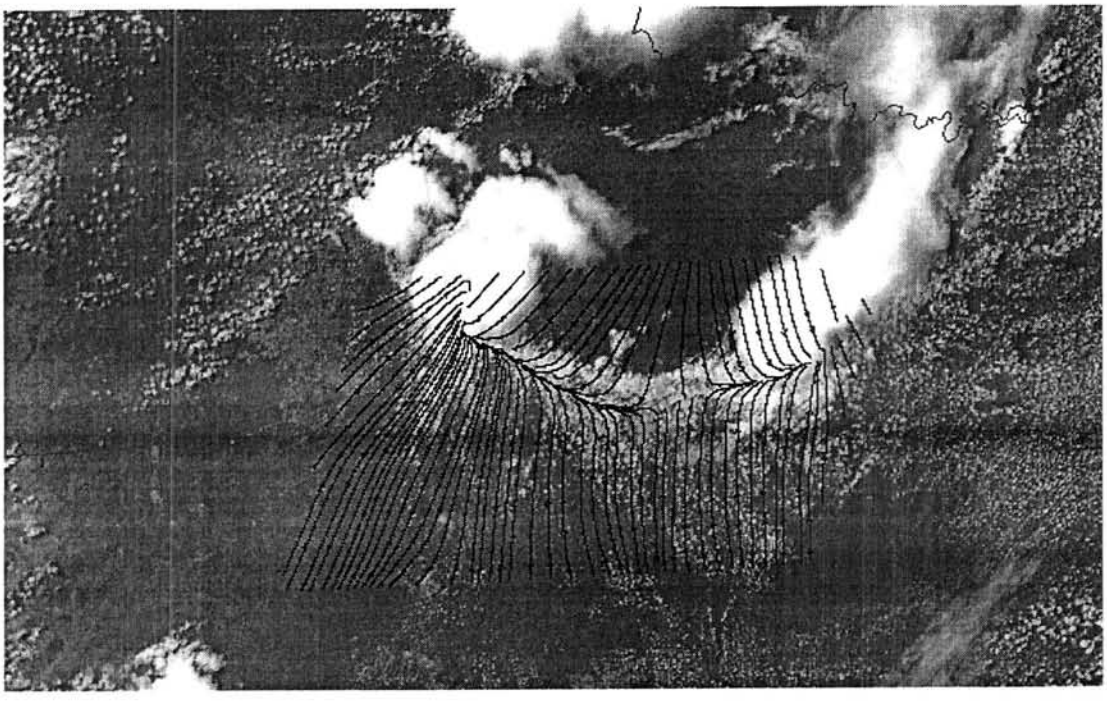

Figure 5-9 Streamline analysis for derived 5-minute winds (1959-2004Z).

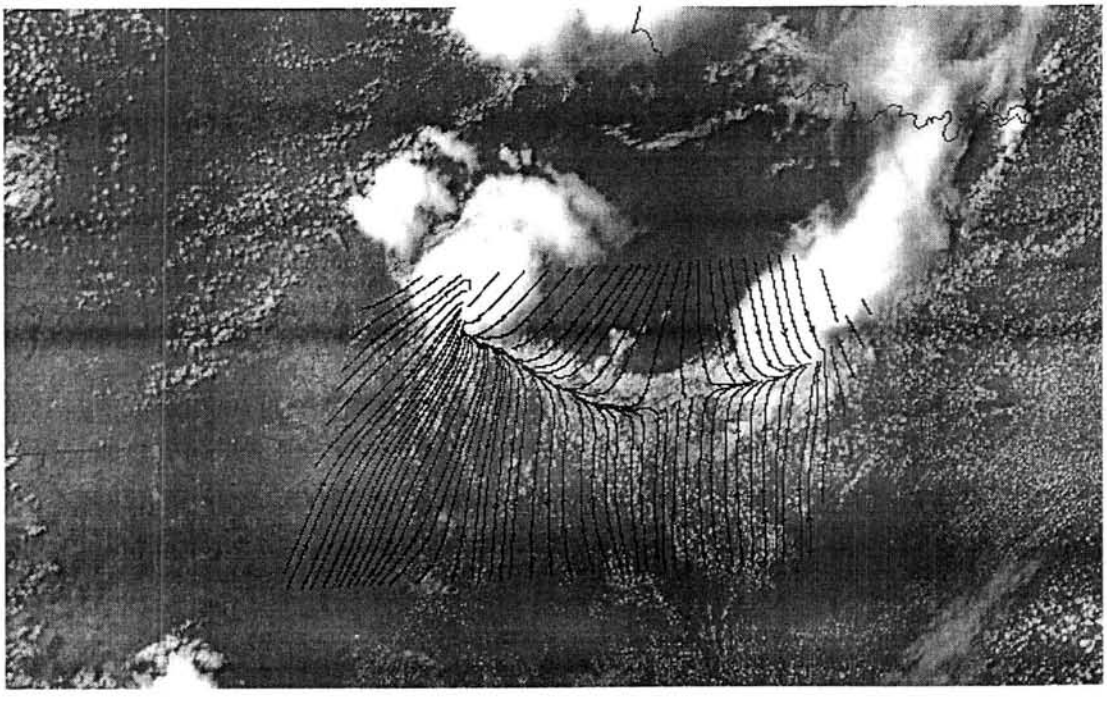

Figure 5-10 Streamline analysis for derived 15-minute winds (1959-2015Z).

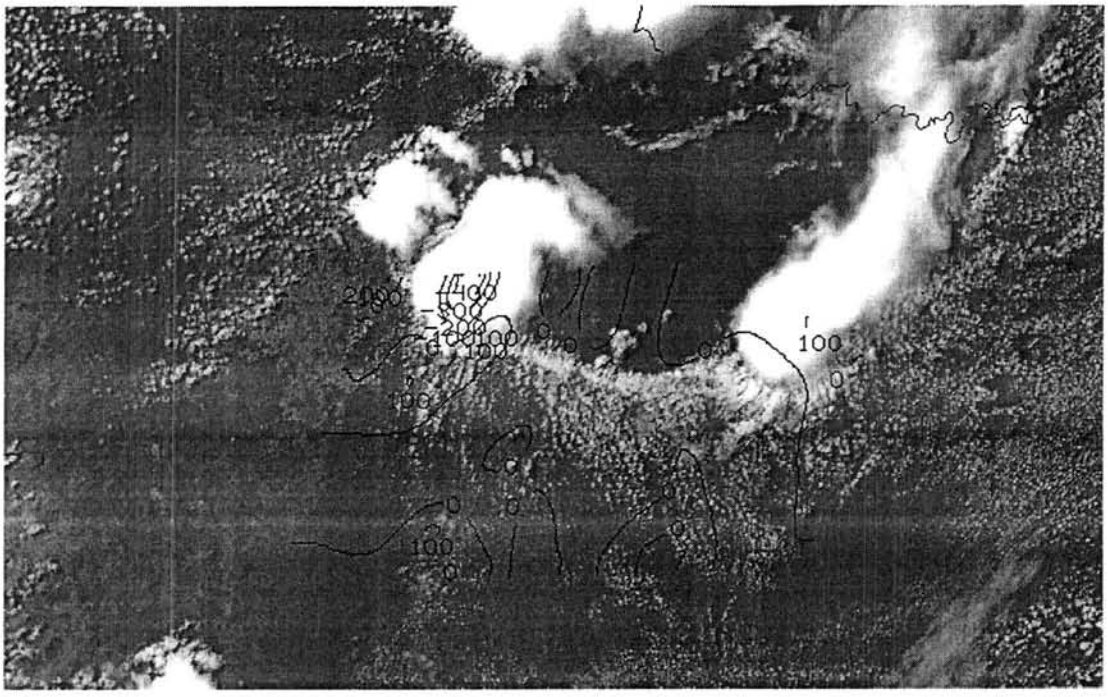

Figure 5-11 Vorticity field generated using intervals of 0.1° between analyzed (5-minute) wind vectors. Units are 10^{-6} s^{-1}.

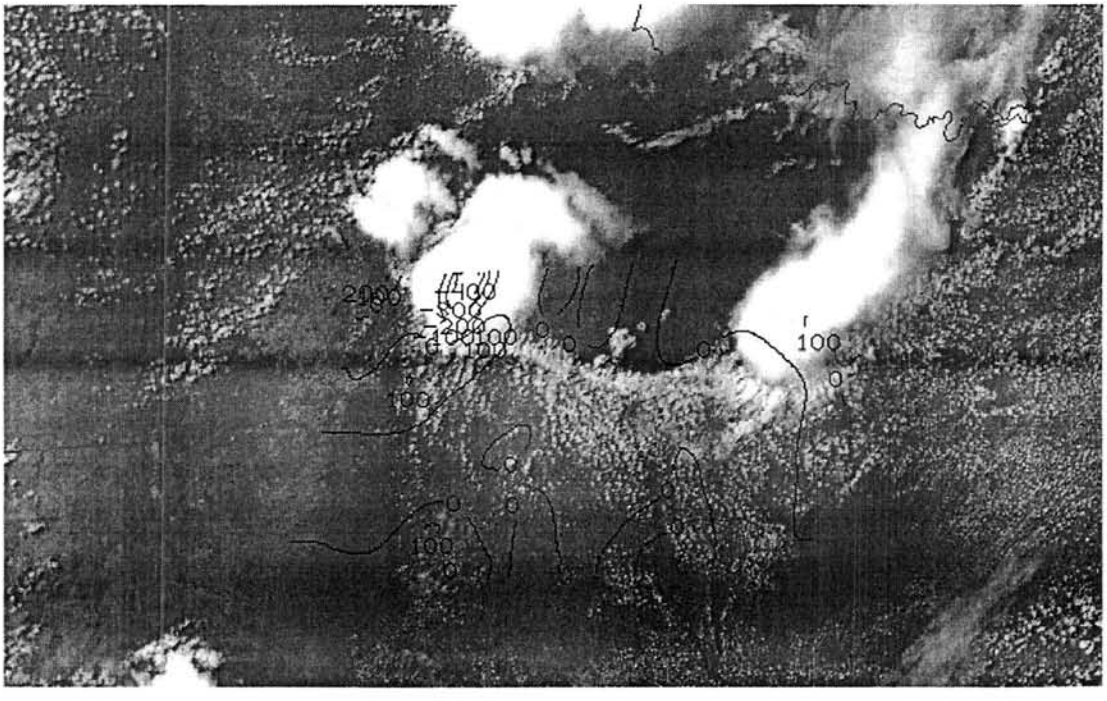

Figure 5-12 Vorticity field generated using intervals of 0.1° between analyzed (15-minute) wind vectors. Units are 10^{-6} s^{-1}.

5.2 Irregular Polygon Method

Another method of computing divergence can be accomplished by calculating the change of area with time, such that:

$$\text{DIV} = \frac{1}{A}\frac{dA}{dt}$$

In this scheme five clouds are chosen as targets, with the area they encircle computed by dividing the area up into three triangles, then computing the area of each triangle. This is done by calculating the distance between each cloud element, then finding the subtended angle by means of the Law of Cosines:

$$\cos\alpha = \frac{b^2 + c^2 - a^2}{2bc}, \quad \text{therefore} \quad \alpha = \cos^{-1}\left(\frac{b^2 + c^2 - a^2}{2bc}\right)$$

The area of the triangle can be found using:

$$\text{Area} = \frac{1}{2}bc(\sin\alpha), \text{ or similarly, } \text{Area} = \frac{1}{2}bc\left\{\sin\left[\cos^{-1}\left(\frac{b^2 + c^2 - a^2}{2bc}\right)\right]\right\}$$

This is repeated for each triangle, and the areas are then added to give the area of the polygon. After a given time interval the area is computed again and divergence values are obtained. Divergence was again calculated using the 31 May 1995 case to compare with values obtained from the McIDAS divergence program. Figures 5-13 and 5-14 show clouds chosen and their respective positions at the initial time (1955Z) and final time (2015Z). Five-minute interval imagery was used for continuity. Total area encompassed at the initial time was 7837 km, shrinking to 6488 km by 2015Z. This resulted in a divergence value of -1.435×10^{-4} s^{-1}, corresponding well with values generated by McIDAS using 0.3° latitude/longitude intervals (-1.4×10^{-4} s^{-1} with five-minute interval data, -1.6×10^{-4} s^{-1} using fifteen-minute).

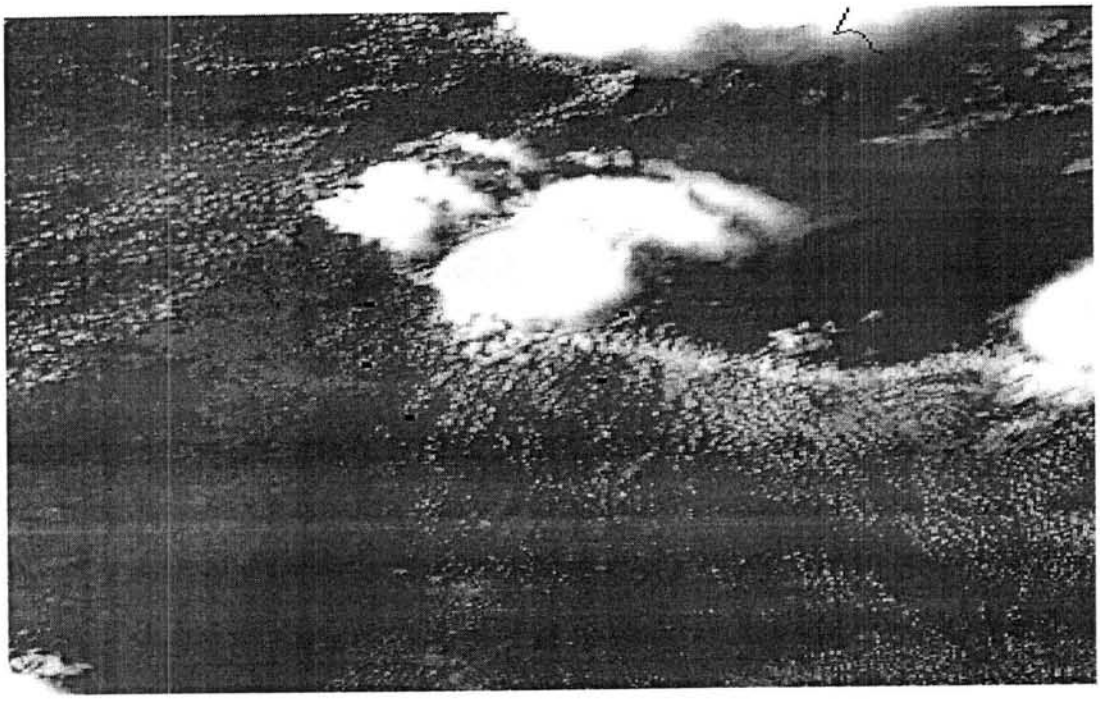

Figure 5-13 Initial position of clouds chosen to compute area using irregular polygon method. Initial time is 1955Z, area encompassed is 7837km.

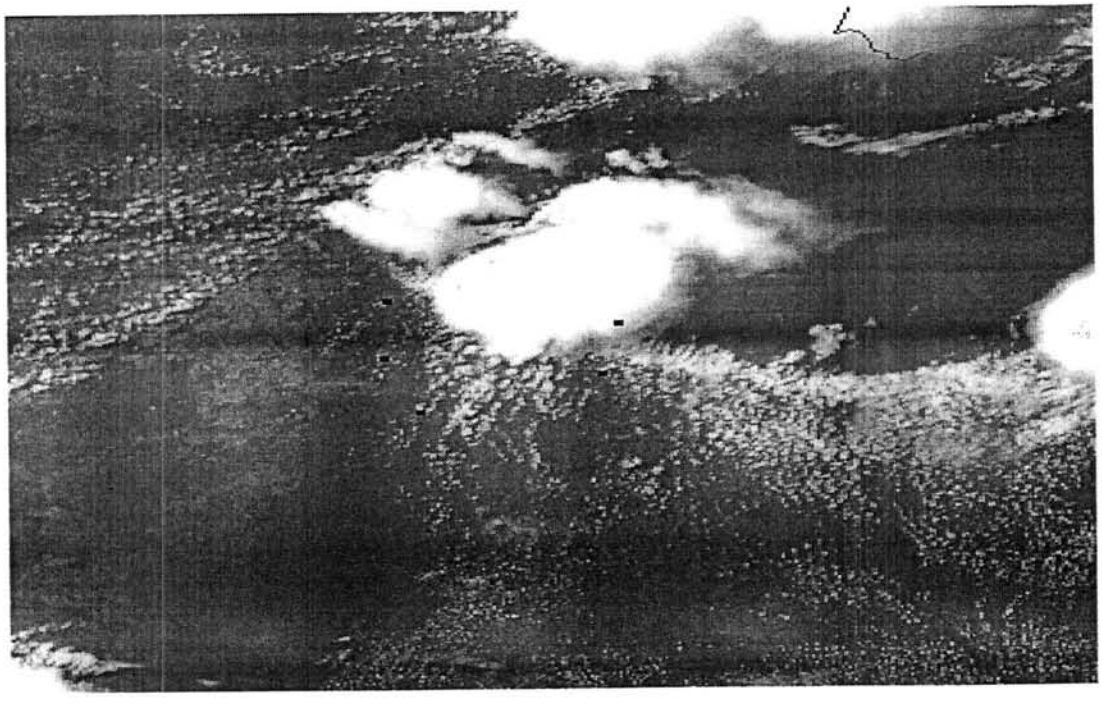

Figure 5-14 Final position of clouds chosen to compute area. Final time is 2015Z, area encompassed is 6488km.

6.0 Conclusion

GOES-8 imagery of varying temporal intervals was used to derive cloud-drift winds in several dynamic and slow-moving flow fields. Cumulus clouds 1-2 km in area with limited vertical development were chosen as targets in each case. Imagery was navigated and winds plotted using McIDAS, an interactive computer system developed at the University of Wisconsin. The single pixel, or manual, method was used to track individual targets. Wind fields were derived for four different cases over the southern and central U.S. These were compared to surface observations and wind profiler data to determine the accuracy of winds derived using GOES-8 imagery. Divergence fields were plotted from derived wind fields to ascertain the effectiveness of using these winds to forecast areas of low-level convergence and enhanced vertical motion.

When compared to surface observations, five-minute interval imagery was found to be the most accurate in both speed and direction. Overall accuracy was noticeably better when winds were compared to profiler data. Heights used to verify winds were determined using surface observations of cloud base height and radiosonde data. Again five-minute interval imagery was best, averaging within one knot of wind speeds recorded by the profiler. Cloud-drift winds derived using low-level cumulus appear most representative of the flow at cloud base, in agreement with earlier studies.

Rapidscan (1-minute) data proved erratic when tracking clouds in slow-moving wind fields for two reasons: round-off error inherent in the

McIDAS software caused large directional errors, and image scintillation due to small navigation errors led to erroneous vector generation. Vector errors decreased rapidly as the number of one-minute intervals used to track a target were increased. Rapidscan imagery offers an excellent source of continuity for tracking clouds at longer intervals. Winds derived from rapidscan imagery after five one-minute intervals have elapsed provide the best representation of low-level wind at cloud base.

Divergence fields were generated over central Texas where an old outflow boundary interacting with warm moist southerly flow was the source of intense convection. Convergence was occurring along the length of the boundary, but strong thunderstorms were forming in just two places. Wind fields derived near the western and central part of the boundary indicated stronger low-level convergence at the western end than along the remainder of the boundary. This was confirmed by computing divergence from derived winds using automated methods and an irregular polygon scheme. Strong convergence in this area at the height measured would help explain the enhanced vertical development in this area as opposed to other sections of the boundary. Figures 6-1 and 6-2 seem to support the fact that the added low-level convergence "trigger" was responsible for the intense convection in that area versus along the central portion of the boundary. While the wind field used was rather detailed (200-300 vectors) and took many hours to generate, forecasting convergence could be accomplished over a meso-β scale (25-250km) area in a short time with several tens of vectors.

Derivation of low-level wind fields using infrared imagery would present difficulties that are not inherent using visible images. Since

satellite resolution is 4 km by 4 km at subpoint, the size of a detectable cloud element would be increased accordingly. Larger cumulus cloud motion can be affected by their own development and dissipation processes. Larger clouds also tend to extend to higher levels, becoming susceptible to effects of vertical wind shear (Fujita, et al., 1975).

Tracking of slow-moving cloud systems also becomes more difficult, especially as the interval between subsequent images becomes shorter. Assuming clouds must move 2.5 km between images to be recognized as moving by the tracking system, then the minimum wind speed necessary for detection at five-minute image intervals would be 16-17 knots. Intervals of fifteen minutes between images require a minimum wind speed of 5-6 knots. To accurately track slow-moving events such as the evening land breeze, which has a normal speed range of 4-10 knots, the shortest image interval usable would be fifteen minutes. The use of shorter intervals would be limited to faster-moving flow fields such as the nocturnal low-level jet.

Manual wind tracking is extremely tedious and a substantial amount of time is required to plot a large wind field. Better automated tracking methods are currently under development at CIRA and elsewhere; faster and more accurate wind field generation will become possible as these methods are employed. Better assignment of cloud height will also be possible using stereographic techniques with GOES-8 and 9, currently being tested by Dr. Garrett Campbell at CIRA. This will improve accuracy of divergence and vorticity fields generated from low-level winds, allowing more insight into the state of the atmosphere at that level. Future studies using these advanced techniques will undoubtedly lead to a better understanding of low-level mesoscale flow.

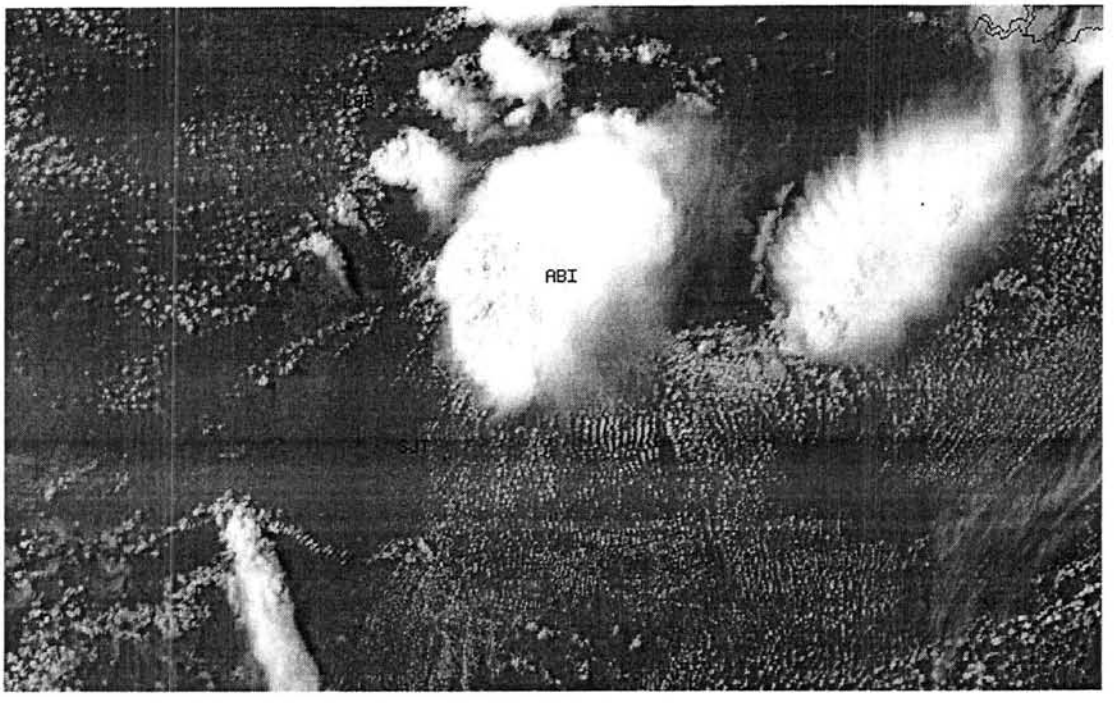

Figure 6-1 Abilene thunderstorm development at 2130Z.

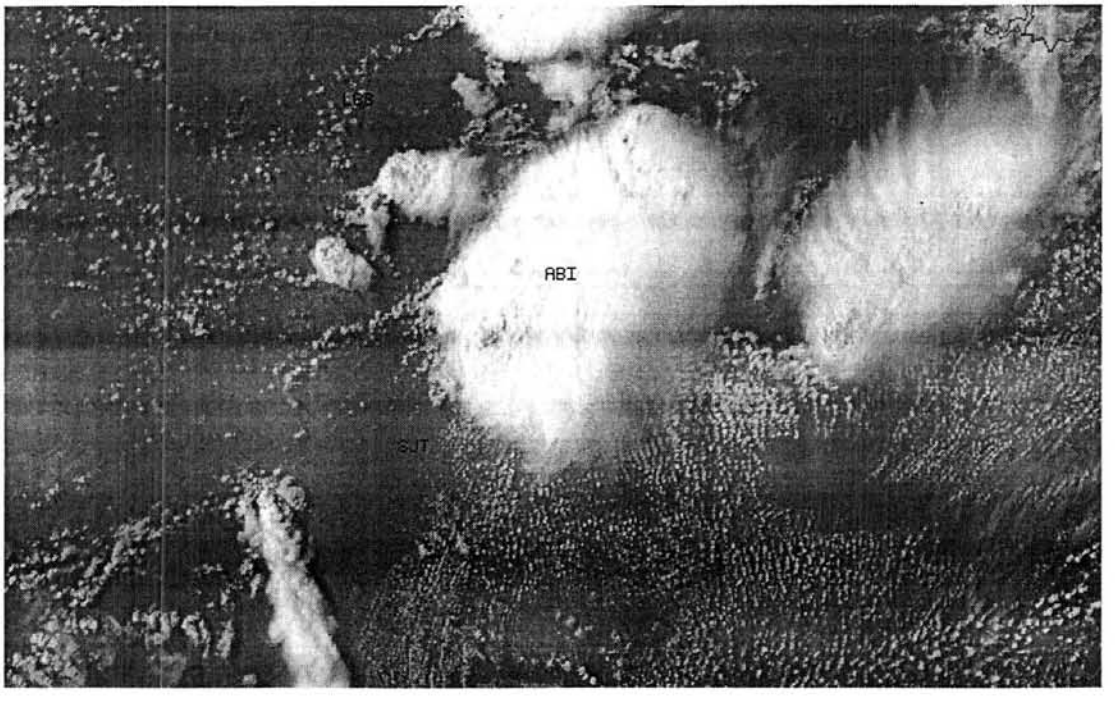

Figure 6-2 Abilene thunderstorm development at 2200Z.

REFERENCES

Fujita, Theodore T. and E.W. Pearl, 1975: Satellite-tracked cumulus velocities. *Journal of Applied Meteorology*, **14**, 407-13.

Chesters, Dennis, 1996: GOES Tech notes. *Goes Internet Web site, http://climate.gsfc.nasa.gof/~chesters/goesproject.html*.

Hasler, A.F., W.C. Skillman, and W.E. Shenk, 1979: In-situ aircraft verification of the quality of satellite cloud winds over oceanic regions. *Journal of Applied Meteorology*, **18**, 1481-1489.

Inoue, Toshiro and W.L. Smith, 1994: The feasibility of extracting low-level wind by tracing low-level moisture observed with GOES-7. *Journal of Applied Meteorology*, **33**, 594-604.

Lee, David H., 1979: Level assignment in the assimilation of cloud motion vectors. *Monthly Weather Review*, **107**, 1055-1074.

Maddox, Robert A. and T.H. Vonder Haar, 1979: Covariance analyses of satellite-derived mesoscale wind fields. *Journal of Applied Meteorology*, **18**, 1327-1334.

Martner, B.E., D.B. Wuertz, B.B. Stankov, R.G. Strauch, E.R. Westwater, K.S. Gage, W.L. Ecklund, C.L. Martin and W.F. Dabberdt, 1993: An evaluation of wind profiler, RASS, and microwave radiometer performance. *Bulletin of the American Meteorological Society*, **74**, 599-613.

Menzel, Paul W. and J.F.W. Purdom, 1994: Introducing GOES-I: the first of a new generation of geostationary operational environmental satellites. *Bulletin of the American Meteorological Society*, 75, 757-781.

Merrill, Robert T., W.P. Menzel, W. Baker, J. Lynch, and E. Legg, 1991: A report on the recent demonstration of NOAA's upgraded capability to derive cloud motion satellite winds. *Bulletin of the American Meteorological Society*, **72**, 372-376.

Negri, Andrew J. and T.H. Vonder Haar, 1980: Moisture convergence using satellite-derived wind fields: a severe local storm case study. *Monthly Weather Review*, **108**, 1170-1182.

Peslen, Cynthia A., 1980: Short-interval SMS wind vector determinations for a severe local storms area. *Monthly Weather Review*, **108**, 1407-1418.

Schlatter, Thomas W. and F.S. Zbar, 1994: Wind profiler assessment report and recommendations for future use 1987-1994. *U.S. Department of Commerce, National Oceanic and Atmospheric Administration publication.*

Schmetz, J., K. Holmlund and A. Ottenbacher, 1993: Developments in operational satellite winds from METEOSAT. *Proceedings of a seminar on Developments in the Use of Satellite Data in Numerical Weather Prediction*, Darmstadt, Germany 6-10 September 1993.

Stewart, Tod R., C.M. Hayden, and W.L. Smith, 1985: A note on water-vapor tracking using VAS data on McIDAS. *Bulletin of the American Meteorological Society*, **66**, 1111-1115.

Suomi, V.E., R. Fox, S.S. Limaye and W.L. Smith, 1983: McIDAS III: A modern interactive data access and analysis system. *Journal of Climate and Applied Meteorology*, **22**, 766-778.

Wilson, Thomas A. and D.D. Houghton, 1979: Mesoscale wind fields for a severe storm situation determined from SMS cloud observations. *Monthly Weather Review*, **107**, 1198-1209.